NAVAL POSTGRADUATE SCHOOL

MONTEREY, CALIFORNIA

THESIS

EASTERN MEDITERRANEAN SEA SPATIAL AND TEMPORAL VARIABILITY OF THERMOHALINE STRUCTURE AND CIRCULATION IDENTIFIED FROM OBSERVATIONAL (T, S) PROFILES

by

Nuri Karaaslan

December 2015

Thesis Advisor: Peter C. Chu
Co-Advisor: Chenwu Fan

Approved for public release; distribution is unlimited

THIS PAGE INTENTIONALLY LEFT BLANK

REPORT DOCUMENTATION PAGE			Form Approved OMB No. 0704–0188
Public reporting burden for this collection of information is estimated to average 1 hour per response, including the time for reviewing instruction, searching existing data sources, gathering and maintaining the data needed, and completing and reviewing the collection of information. Send comments regarding this burden estimate or any other aspect of this collection of information, including suggestions for reducing this burden, to Washington headquarters Services, Directorate for Information Operations and Reports, 1215 Jefferson Davis Highway, Suite 1204, Arlington, VA 22202-4302, and to the Office of Management and Budget, Paperwork Reduction Project (0704-0188) Washington, DC 20503.			
1. AGENCY USE ONLY *(Leave blank)*	**2. REPORT DATE** December 2015	**3. REPORT TYPE AND DATES COVERED** Master's thesis	
4. TITLE AND SUBTITLE EASTERN MEDITERRANEAN SEA SPATIAL AND TEMPORAL VARIABILITY OF THERMOHALINE STRUCTURE AND CIRCULATION IDENTIFIED FROM OBSERVATIONAL (T, S) PROFILES			**5. FUNDING NUMBERS**
6. AUTHOR(S) Nuri Karaaslan			
7. PERFORMING ORGANIZATION NAME(S) AND ADDRESS(ES) Naval Postgraduate School Monterey, CA 93943-5000			**8. PERFORMING ORGANIZATION REPORT NUMBER**
9. SPONSORING /MONITORING AGENCY NAME(S) AND ADDRESS(ES) N/A			**10. SPONSORING / MONITORING AGENCY REPORT NUMBER**
11. SUPPLEMENTARY NOTES The views expressed in this thesis are those of the author and do not reflect the official policy or position of the Department of Defense or the U.S. Government. IRB Protocol number ____N/A____.			
12a. DISTRIBUTION / AVAILABILITY STATEMENT Approved for public release; distribution is unlimited			**12b. DISTRIBUTION CODE**

13. ABSTRACT (maximum 200 words)

In this thesis, the optimal spectral decomposition (OSD) method was used to establish the synoptic monthly varying three-dimensional gridded temperature and salinity data for 54 years on a 0.25°x0.25° grid. The analysis included 164,906 temperature profiles and 53,606 salinity profiles. After the establishment of gridded data, the seasonal and inter-annual variability of thermohaline structure and circulation were investigated. Surface depth shows high seasonal temperature variability through the year. There is almost no seasonal salinity variability in winter and spring seasons, while the summer and fall seasons show slight seasonal variation in the surface depth. P-vector inverse method is used to obtain the sea surface absolute geostrophic velocity. In EOF analyses, intermediate layer heat content anomaly is larger than the surface layer. However, inter-annual variability of heat content anomaly in the deep layer is very weak. Deep layer and intermediate layer show similar freshwater content anomalies, and both of them are larger than the surface layer.

14. SUBJECT TERMS thermohaline, seasonal variability, inter-annual variability, water mass, Levantine Sea, Eastern Mediterranean Sea, absolute geostrophic velocity, Empirical Orthogonal Function, heat content, freshwater content, optimal spectral decomposition, P-vector inverse method			**15. NUMBER OF PAGES** 145
			16. PRICE CODE
17. SECURITY CLASSIFICATION OF REPORT Unclassified	**18. SECURITY CLASSIFICATION OF THIS PAGE** Unclassified	**19. SECURITY CLASSIFICATION OF ABSTRACT** Unclassified	**20. LIMITATION OF ABSTRACT** UU

NSN 7540–01-280-5500 Standard Form 298 (Rev. 2–89) Prescribed by ANSI Std. 239–18

THIS PAGE INTENTIONALLY LEFT BLANK

Approved for public release; distribution is unlimited

EASTERN MEDITERRANEAN SEA SPATIAL AND TEMPORAL VARIABILITY OF THERMOHALINE STRUCTURE AND CIRCULATION IDENTIFIED FROM OBSERVATIONAL (T, S) PROFILES

Nuri Karaaslan
Lieutenant Junior Grade, Turkish Navy
B.S., Turkish Naval Academy, 2009

Submitted in partial fulfillment of the
requirements for the degree of

**MASTER OF SCIENCE IN METEOROLOGY
AND PHYSICAL OCEANOGRAPHY**

from the

**NAVAL POSTGRADUATE SCHOOL
December 2015**

Approved by: Peter C. Chu
Thesis Advisor

Chenwu Fan
Co-Advisor

Peter C. Chu
Chair, Department of Oceanography

THIS PAGE INTENTIONALLY LEFT BLANK

ABSTRACT

In this thesis, the optimal spectral decomposition (OSD) method was used to establish the synoptic monthly varying three-dimensional gridded temperature and salinity data for 54 years on a 0.25°x0.25° grid. The analysis included 164,906 temperature profiles and 53,606 salinity profiles. After the establishment of gridded data, the seasonal and inter-annual variability of thermohaline structure and circulation were investigated. Surface depth shows high seasonal temperature variability through the year. There is almost no seasonal salinity variability in winter and spring seasons, while the summer and fall seasons show slight seasonal variation in the surface depth. P-vector inverse method is used to obtain the sea surface absolute geostrophic velocity. In EOF analyses, intermediate layer heat content anomaly is larger than the surface layer. However, inter-annual variability of heat content anomaly in the deep layer is very weak. Deep layer and intermediate layer show similar freshwater content anomalies, and both of them are larger than the surface layer.

THIS PAGE INTENTIONALLY LEFT BLANK

TABLE OF CONTENTS

LIST OF FIGURES

THIS PAGE INTENTIONALLY LEFT BLANK

LIST OF TABLES

THIS PAGE INTENTIONALLY LEFT BLANK

LIST OF ACRONYMS AND ABBREVIATIONS

AMC	Asia Minor Current
AOU	Apparent Oxygen Utilization
AUVs	Autonomous Underwater Vehicles
AW	Atlantic Water
CLBC	Central Levantine Basin Current
CTD	Conductivity Temperature Depth
DBT	Digital Bathythermograph
EOF	Empirical Orthogonal Function
EMDW	Eastern Mediterranean Deep Water
GLD	Glider
LIW	Levantine Intermediate Water
LSW	Levantine Surface Water
LB	Levantine Basin
MAW	Modified Atlantic Water
MFS	Mediterranean Forecast System
MMA	Mersa-Matruh Anticyclone
MMJ	Mid-Mediterranean Jet
MBT	Mechanical Bathythermograph
NODC	National Oceanographic Data Center
OCL	Ocean Climate Laboratory
OSD	Ocean Station Data
OSD	Optimal Spectral Decomposition
PC	Principal Component
PFL	Profiling Float
POEM	Physical Oceanography of the Eastern Mediterranean
RG	Rhodes Gyre
SMA	Shikmona Anticyclone
SSS	Sea Surface Salinity

SST	Sea Surface Temperature
WMDW	Western Mediterranean Deep Water
WOA94	World Ocean Atlas 1994
WOD	World Ocean Database
WOD98	World Ocean Database 1998
WOD01	World Ocean Database 2001
WOD05	World Ocean Database 2005
WOD09	World Ocean Database 2009
WOD13	World Ocean Database 2013
XBT	Expendable Bathythermograph

ACKNOWLEDGMENTS

I would like to express my sincere gratitude to my thesis advisor, Professor Peter C. Chu, for his undying support and scientific guidance.

I would like to thank to my co-advisor, Mr. Chenwu Fan, for his continuous MATLAB help on my thesis.

Without their help, this thesis could not have been done on time.

I also would like to express my appreciation to the Turkish Navy for giving me this opportunity.

Moreover, I need to thank my classmates and all professors in NPS who helped me in every field during my education.

Of course, my family, who has always supported me, deserves the biggest part of my appreciation.

THIS PAGE INTENTIONALLY LEFT BLANK

I. INTRODUCTION

A. MEDITERRANEAN SEA

The Latin word "Medius Terrae," which means "inland" or "in the middle of land," is known as the origin of the name of the Mediterranean Sea. The Mediterranean region is surrounded by the Europe, Asia and Africa continents (Tanabe, 2013). The Mediterranean region countries are seen in Figure 1.

Figure 1. Mediterranean Sea and Surrounding Countries

Adapted from: WorldAtlas, 2015: Map of the Mediterranean Sea. Accessed 24 August 2015. [Available online at http://www.worldatlas.com/aatlas/infopage/medsea.htm]

The Mediterranean Sea stretches over an area of 2.5 million square kilometers, derived from nearly 3000 kilometers in longitude and 1500 kilometers in latitude. It is a partly-encircled basin that is linked with the Atlantic Ocean through the Strait of Gibraltar; linked with the Black Sea through the Dardanelles Straits and the Turkish Bosphorus. The Mediterranean Sea is divided by the Sicily Channel into two parts. They are: Eastern Mediterranean and Western Mediterranean (Soto-Navarro and Criado-Aldeanueva, 2012).

The Mediterranean Sea extends between the 30° and 46° north latitudes; 5°50′ west and 36° east longitudes (Boxer, 2014). The Western Mediterranean includes the Alboran, Balearic, Tyrrhenian and Ligurian Seas. The Eastern Mediterranean includes the Levantine, Adriatic, Ionian and the Aegean Seas (Theocharis et al., 1998). Major parts of the Mediterranean Sea are seen in Figure 2.

Figure 2. Major Parts and Major Sub-basins of the Mediterranean Sea

Source: Wikipedia contributors, 2015: Mediterranean Sea. Accessed 25 August 2015. [Available online at https://en.wikipedia.org/w/index.php?title=Mediterranean_Sea&oldid=695192772]

The Mediterranean Sea is a quasi-encircled sea nearly landlocked by continents. When correlated to the other oceans' circulation and residence time, that is about 200–1000 years, the Mediterranean Sea is known by its short-lived circulation and residence time, that is about 70 years (Group et al., 2011).

The overall length of the Mediterranean Sea basin is 3,860 kilometers, and the utmost width is 1,600 kilometers. The whole area enclosed by the basin is nearly 2,536,000 kilometers square and the entire volume is almost 3,750,000 kilometers cubic. The Mediterranean Sea has only one link to the Atlantic Ocean through Strait of Gibraltar channel that is 14 kilometers wide and 600 meters mean depth (Papadopoulou et al., 2011). Topographic and bathymetric map of the Mediterranean Sea is seen in Figure 3.

Figure 3. Topographic and Bathymetric Map of the Mediterranean Sea

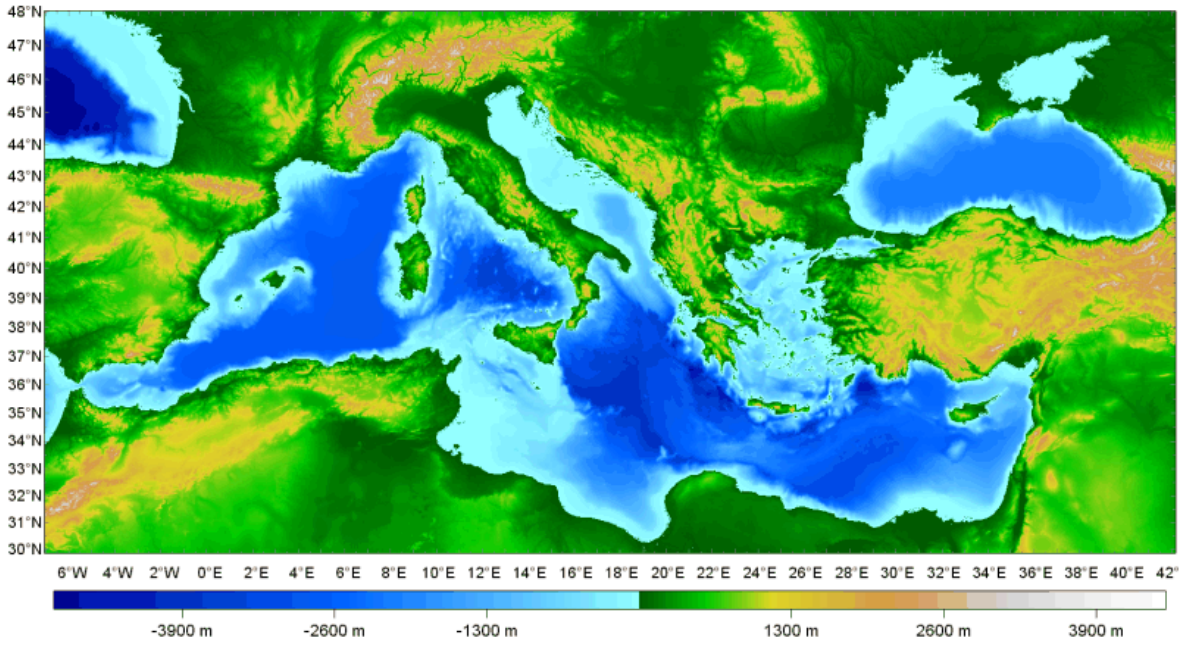

Source: Università degli Studi di Pavia, 2005: The Mediterranean Sea. Accessed 02 September 2015. [Available online at http://www-3.unipv.it/cibra/edu_Mediterraneo_uk]

The average depth of the Mediterranean Sea is nearly 1450 meters; hence it is a shallow basin when it is compared to the mean depth, almost 3850 meters, of all oceans in the world. While the deepest depth is nearly 3733 meters in the Western Mediterranean Sea, the estimated mean depth of it is almost 1612 meters. The deepest depth in the Eastern Mediterranean basin is 5121 meters (Papadopoulou et al., 2011). Depth zones of the Mediterranean Sea are seen in Table 1.

Table 1. Depth Zones by Area of Coverage of the Mediterranean Sea

Depth Zone (meters)	Area (kilometers square)
0-200	578000
200-1000	720000
1000-2000	230000
2000-3500	951000
Over 3500	57000
Total	2536000

Adapted from: Papadopoulou, K. N., V. Markantonatou, and C. J. Smith, 2011: Options for Delivering Ecosystem-based Marine Management. The Mediterranean Sea: Additional information on status of threatened ecological characteristics relevant to the Marine Strategy Framework Directive, 30 pp, [Available online at https://www.liverpool.ac.uk/media/livacuk/odemm/images/ Mediterranean_Sea_Background.pdf]

B. OBJECTIVE

Improvements in the political, military and economic fields in the Mediterranean region, specifically in the Eastern Mediterranean, requires a deeper understanding of the hydrodynamics structure of the Eastern Mediterranean Sea, along with its natural aspects. Thus, the spatial and temporal variations in the Eastern Mediterranean Sea occupy a critical importance, notably in terms of the military based operational objectives. This thesis will scope on analyzing the data obtained from World Ocean Database. Analysis will include inter-annual, seasonal and monthly salinity, temperature and current variation fields from 1960 to 2013. These analyzed salinity, temperature and current

profiles will lead to determine the general current patterns and thermohaline structures. After analyzing the data, results will be compared with the previous studies. Thus, a further understanding of the general circulation patterns of the Eastern Mediterranean Sea will be presented.

C. THESIS ORGANIZATION

In Chapter II, some crucial aspects of the Eastern Mediterranean and Levantine Sea hydrodynamics will be explained. They are; water masses, wind fields, nutrient fields and oceanographic features of the Eastern Mediterranean and Levantine Sea. In Chapter III, information about the dataset used in the thesis will be touched on. The source of the dataset, methods and instruments used for collecting the data will be mentioned. In Chapter IV, methodology for creating the fundamental principles of the study will be explained. In Chapter V, analyses of the data will be conducted. By conducting the analyses, it will be divided into sub sections for deeper understanding. It will mainly focus on the total mean and seasonal variations for the temperature and salinity profiles as well as the current profiles. In Chapter VI, inter-annual variability of the Eastern Mediterranean Sea and first three EOF modes will be studied. In Chapter VII, results that are taken by this study will be summarized and any recommendations for further studies in the future will be pointed out.

THIS PAGE INTENTIONALLY LEFT BLANK

II. OCEANOGRAPHIC FEATURES OF THE EASTERN MEDITERRANEAN AND LEVANTINE SEA

A. EASTERN MEDITERRANEAN AND LEVANTINE SEA

The Eastern Mediterranean Sea includes four important major basins and seas. They are; Ionian basin, Levantine basin, Aegean Sea and Adriatic Sea (Alhammoud et al., 2005). Major sub-basins of the Eastern Mediterranean Sea are seen in Figure 4. The Ionian basin on the west, north-eastern Africa on the south, Middle East on the east, Cretan Archipelago and Asia Minor on the north surround the Levantine basin (Alhammoud et al., 2005).

> The LB communicates with the Ionian Basin through the Cretan passage which is 300 km wide and more than 2000 m deep, on average, between the Cretan and Libyan coasts. To the northwest, it is connected to the Aegean Sea through three passages between the islands of Crete and Karpathos (Kassos Strait, width 67 km, sill depth 350 m), the islands of Karpathos and Rhodes (Karpathos Strait, 43 km and 550 m), and Rhodes and Turkey (17 km and 350 m). The southeastern continental shelf at the Nile delta is separated into two shallow areas: Mersa-Matruh to the west and Shikmona to the east south of Cyprus. (Alhammoud et al., 2005)

Figure 4. Bottom Topography of the Eastern Mediterranean Sea

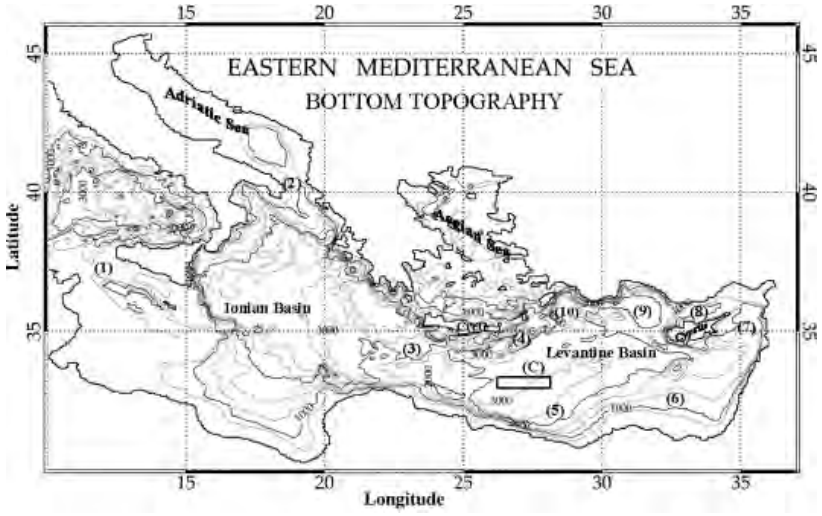

Source: Alhammoud, B., K. Béranger, L. Mortier, M. Crépon, and I. Dekeyser, 2005: Surface circulation of the Levantine Basin: comparison of model results with observations. *Prog.Oceanogr.*, **66**, 299–320.

B. WATER MASSES

The processes of comprehensive pertinence for ocean climate motions cover features of the thermohaline circulations, distribution, water mass formations, mixing and transformation. The Atlantic origin fresh water comes from the Atlantic Ocean to the Mediterranean Sea through the Strait of Sicily. Due to the wind and other forces, this water mass spreads and evaporation surpasses precipitation at the surface. So, the water mass evolves into much saline and dense water mass. The cooling develops in winter season and heating develops in summer season. During storm developments, especially in March, Levantine Intermediate Water (LIW) forms in the Levantine basin. LIW flows and circulates from surface to a few hundred meters depth. Some of LIW masses disperse inside the basin and some leave underneath the Atlantic Water (AW) through the Strait of Sicily (Robinson et al., 1992).

LIW is the most important origin of the Mediterranean water masses in the Atlantic (Robinson et al., 1992). The representation of flow through the Strait of Gibraltar is seen in Figure 5.

Figure 5. Flow Representation through the Strait of Gibraltar

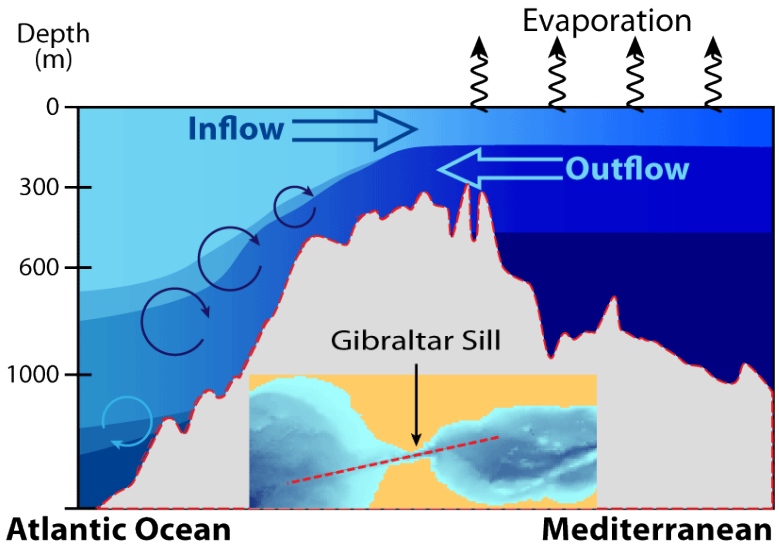

Source: The National Oceanography Centre Southampton, 2015: Mediterranean Outflow Sill. Accessed 04 October 2015. [Available online at http://www.euroargo-edu.org/img/med_outfl_sill.png]

The Mediterranean Sea's thermohaline circulation is mostly described by an open vertical cell covering the whole basin and two closed vertical cells confined by the eastern and western sub-basins (Lascaratos et al., 1999). The open thermohaline cell represents the shift of the AW, which is also known as modified Atlantic Water (MAW), to the LIW. MAW spreads in the surface layer, while the LIW circulates in the intermediate layer. The two closed vertical cells represent the shift of intermediate and surface water to the deep waters, which are Eastern Mediterranean Deep Water (EMDW) and Western Mediterranean Deep Water (WMDW) (Lascaratos et al., 1999). The thermohaline circulation sketch of the Mediterranean Sea is seen in Figure 6.

Figure 6. Thermohaline Circulation of the Mediterranean Sea

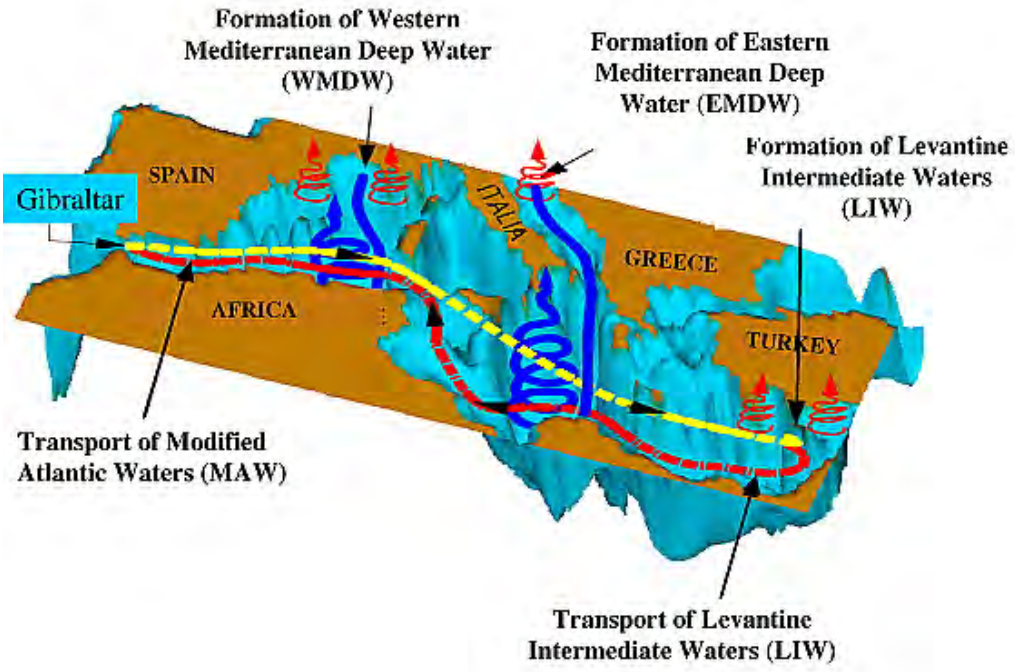

Source: Demirov, E. K., and N. Pinardi, 2007: On the relationship between the water mass pathways and eddy variability in the Western Mediterranean Sea. *Journal of Geophysical Research,* 112, 1–21, doi:10.1029/2005JC003174.

Three main permanent water masses are observed in the Eastern Mediterranean Sea. They are: modified Atlantic Water (MAW), Levantine Intermediate Water (LIW), and Eastern Mediterranean Deep Water (EMDW) (Alhammoud et al., 2005).

1. Modified Atlantic Water (MAW)

Modified Atlantic Water (MAW) spreads towards the Eastern Mediterranean from the Strait of Sicily in the surface layer. It adjusts the mass loss of the Eastern Mediterranean Deep Water by cause of evaporation. As it spreads towards the Eastern Mediterranean, its salinity is intensified and its depth range is declined due to the high evaporation (Alhammoud et al., 2005).

The Modified Atlantic Water is comparably less saline and warmer. The MAW primarily affects the upper thermocline, which is 0–150m (Manca et al., 2004). The MAW is characterized as an extensive homogeneous layer and its signature is seasonal. The minimum salinity of the MAW is nearly 37.2 psu, which is spotted at around 50 meters during summer and its salinity minimum is located near the surface during the winter. The temperature range is between 15 °C and 17 °C and the salinity range is between 37.2 psu and 37.8 psu up to 100 meters depth (Drago et al., 2010).

2. Levantine Intermediate Water (LIW)

Levantine Intermediate Water (LIW) is the most crucial water mass in the Eastern Mediterranean (Alhammoud et al., 2005). It influences not only the whole Mediterranean Sea but also the Atlantic Ocean. It is a homogeneous water mass below the Atlantic Water and circulates nearly between 300 and 700 meters. LIW occurs in the Levantine basin in winter season due to the transformation of the Atlantic Water. As LIW spreads westward, its salinity declines because of the mixing with the bordering water masses (Alhammoud et al., 2005).

LIW is comparably much saline and colder. Its salinity values are between 38.73 psu and 38.78 psu, and temperature values are between 13.75 °C and 13.92 °C at a mean depth of nearly 300 meters at the Strait of Sicily. Its salinity maximum occurs in the

western and south-western of Malta. The recurrence time of LIW in the Strait of Sicily is predicted as 9 months (Drago et al., 2010).

3. Eastern Mediterranean Deep Water (EMDW)

Eastern Mediterranean Deep Water circulates nearly below 800 meters depth. It is dense water mass and relatively less saline and colder. It forms in the northern section of the eastern basin due to the strong cooling. Its mean salinity value is around 38.7 psu and its mean temperature value is nearly 13.6 °C (Alhammoud et al., 2005). Vertical distribution of the water masses in the Mediterranean Sea is seen in Figure 7.

Figure 7. Vertical Distribution of Water Masses in the Mediterranean Sea

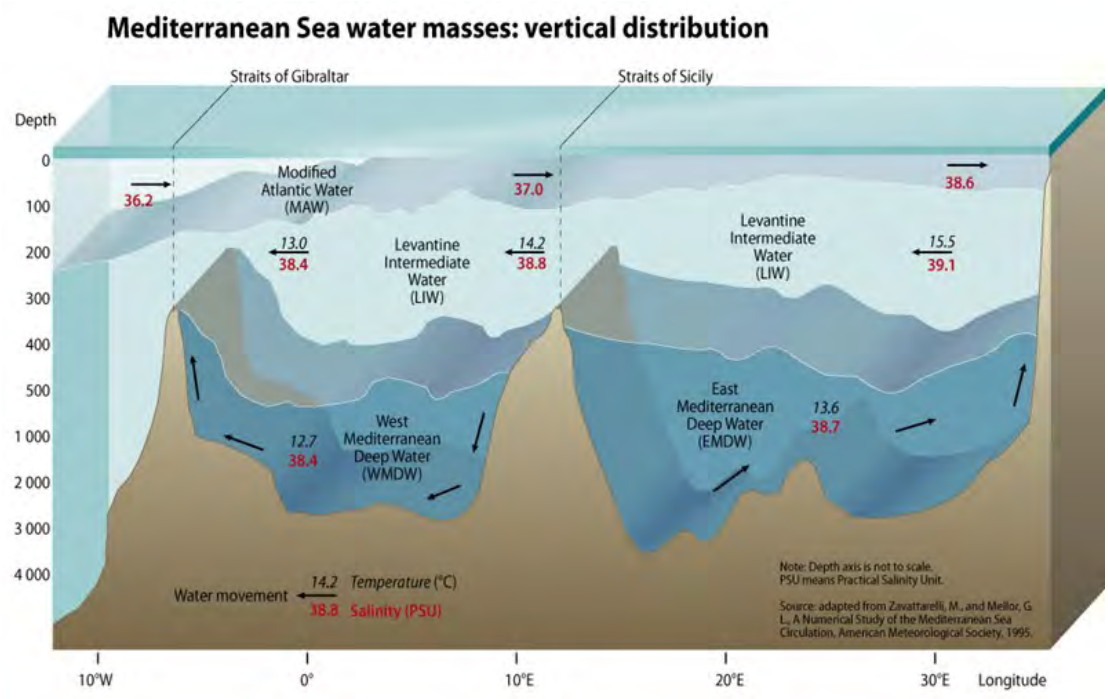

Source: GRID-Arendal, 2013: Mediterranean Sea water masses: vertical distribution. Accessed 08 October 2015. [Available online at http://www.grida.no/graphicslib/detail/mediterranean-sea-water-masses-vertical-distribution_d84b]

C. WIND FIELDS

The Mediterranean basin is nearly bounded by mountains. The meteorological events in this area are affected by mountain chains and defined by the other sub-basins. The importance of the sub-basins comes from the synoptic-scale airflow, which usually communicates with the surrounding orography (Zecchetto and De Biasio, 2007). Spatial distribution of the annual mean wind speed and wind direction of the Mediterranean Sea is seen in Figure 8.

Figure 8. Spatial Distribution of the Annual Mean Wind Speed (Upper) and Wind Direction (Lower) of the Mediterranean Sea

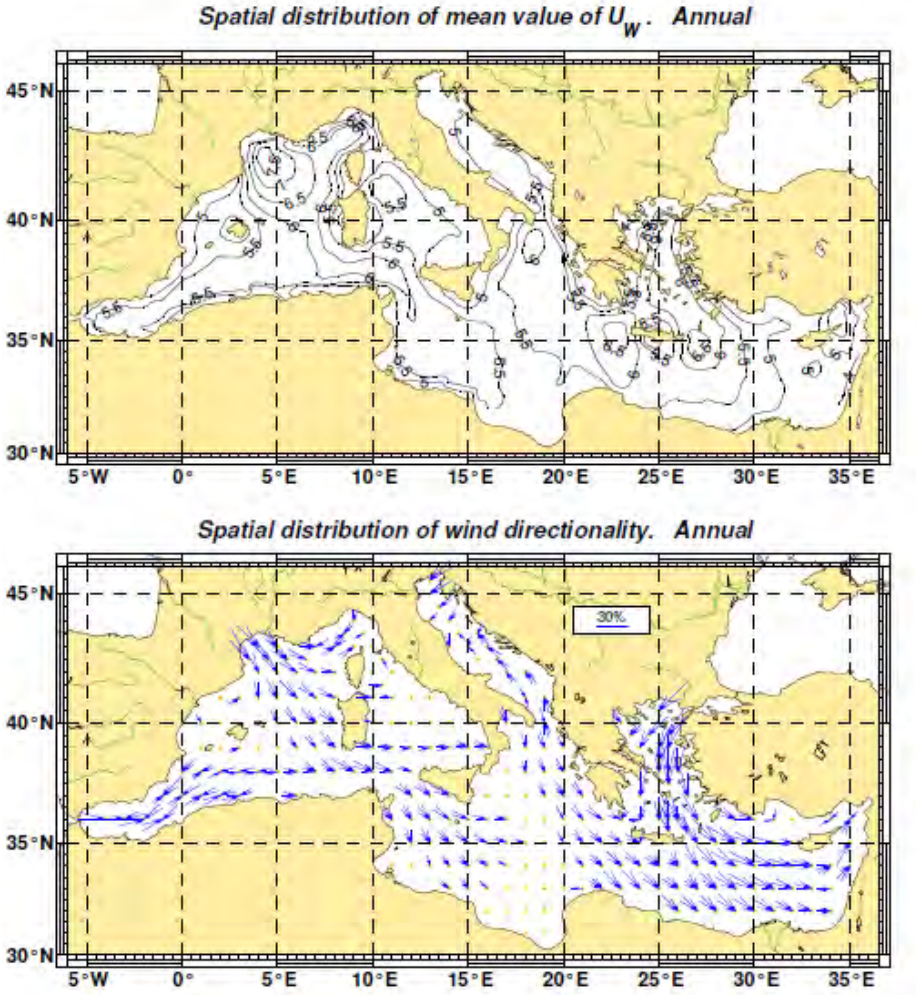

Source: Gaillard, P., and Coauthors, 2004: Wind and wave atlas of the Mediterranean Sea. Accessed 15 October 2015. [Available online at http://users.ntua.gr/mathan/pdf/Pages_from%20_WIND_WAVE_ATLAS_MEDITERRANEAN_SEA_2004.pdf].

The regional prevailing winds in the Mediterranean region are westerlies with a northwesterly tilt and cross over the Mediterranean Sea longitudinally. The Mediterranean region is characterized by the mountain ranges and this also assists to describe the wind climate of the basin and its sub-basins. During the winter months, cyclonic storms are leading systems in the Mediterranean region (Heidorn, 2007).

Mediterranean region is the center place for the cyclogenesis, beginning of low pressure systems during the winter season. It is believed that the highest consolidation of regionally grown cyclones on the globe occurs in the Mediterranean region, partly during the winter season (Heidorn, 2007). Infrequently, some of these cyclones grow into giant storms looking like Atlantic hurricanes; however, they are not actual tropical storms. Although the Mediterranean cyclones are tinier and mostly less damaging than the Atlantic and Pacific tropical storms, these Mediterranean cyclones are very much alike to the tropical cyclones and polar lows in terms of the properties in the structure. Some of the important Mediterranean cyclones developed into hurricane-like conditions in the region during the last sixty years (Heidorn, 2007). The Mediterranean Storm, which occurred in the Mediterranean region in 15 January 1995, is seen in Figure 9.

Figure 9. Hurricane-like Cyclone System Occurred in 15 January 1995 in the Mediterranean Region

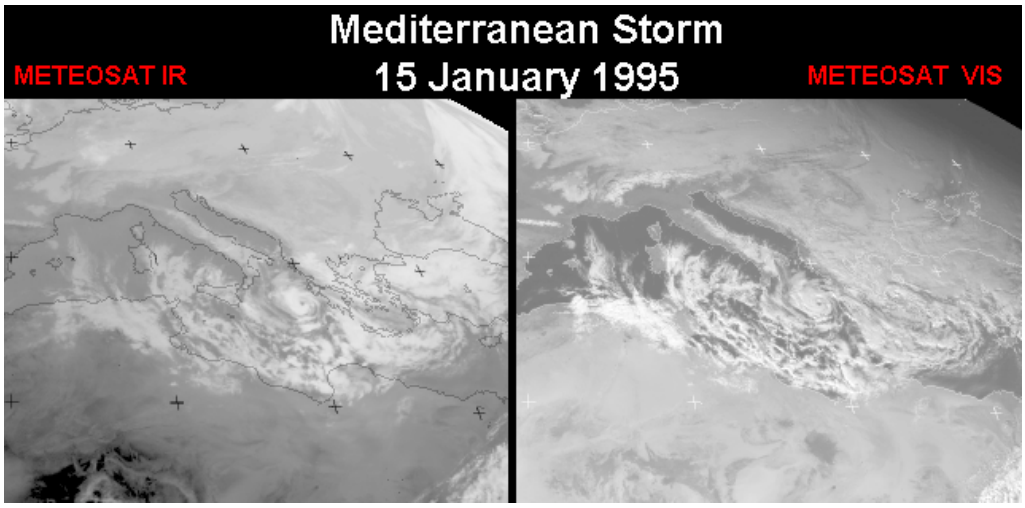

Source: Heidorn, K. C., 2007: The Mediterranean: Birthplace of the Winds. Accessed 24 October 2015. [Available online at http://www.islandnet.com /~see/weather/almanac/ arc2007/alm07mar.htm]

The general wind directionality in the Mediterranean Sea is from north and north-west as seen in Figures 8,10,11,12 and 13, respectively.

The ocean waves occur on the region from north-west to south-east due to winds in the Mediterranean region. Thus, large waves are observed at the north shores of Algeria, Tunisia, and Egypt. These areas are needed to be surveyed carefully for the safety concerns of the coastal structures (Ancient Ports, 2015).

During the winter, winds are generally westerlies and north westerlies with average velocities of 12 to 17 knots. While the south-west winds predominate in the Adriatic Sea, both east and west winds are common between the Strait of Gibraltar and Sardinia. Generally, the north and north-east winds are observed around the Cyprus and the northeastern Mediterranean Sea. The Aegean Sea departs from the general pattern in the Eastern Mediterranean Sea, and north winds dominate in all seasons whereas both north and sound winds are recurrent in the winter (National Geospatial-Intelligence Agency, 2011). Spatial distribution of the winter season wind direction of the Mediterranean Sea is seen in Figure 10.

Figure 10. Spatial Distribution of Winter Season Wind Direction of the Mediterranean Sea

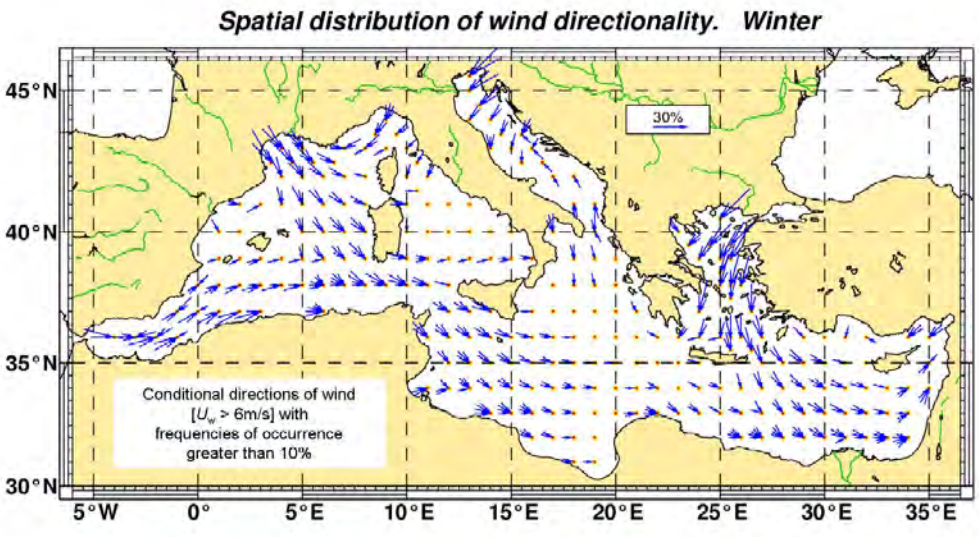

Source: Gaillard, P., and Coauthors, 2004: Wind and wave atlas of the Mediterranean Sea. Accessed 15 October 2015. [Available online at http://users.ntua.gr/mathan/pdf/Pages_from%20_WIND_WAVE_ATLAS_MEDITERRANEAN_SEA_2004.pdf].

Apart from the northeastern Mediterranean Sea, the general wind pattern has slight variation in the spring season, where south-west winds are noticeable at this time with average wind velocities 9 to 13 knots in the spring season. Spatial distribution of the spring season wind direction of the Mediterranean Sea is seen in Figure 11.

Figure 11. Spatial Distribution of Spring Season Wind Direction of the Mediterranean Sea

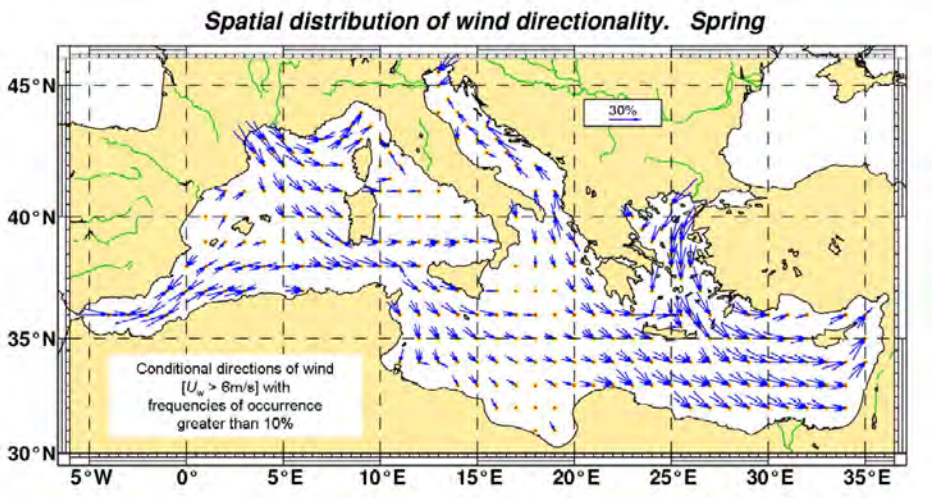

Source: Gaillard, P., and Coauthors, 2004: Wind and wave atlas of the Mediterranean Sea. Accessed 15 October 2015. [Available online at http://users.ntua.gr/mathan/pdf/Pages_from%20_WIND_WAVE_ATLAS_MEDITERRANEAN_SEA_2004.pdf].

The average wind velocities are 5 to 9 knots over the area in the summer season. The general wind pattern stays unchanging other than the Aegean Sea, where south winds are infrequent (National Geospatial-Intelligence Agency, 2011). Fall season shows little difference in the general wind pattern excluding the southeastern Mediterranean Sea, where winds are fluctuating. The average wind velocities grow to 7 to 10 knots in this season (National Geospatial-Intelligence Agency, 2011). Spatial distributions of the wind directionality for summer and autumn seasons are depicted in Figure 12 and Figure 13, respectively.

Arrows, which represent the direction of the winds, only resemble the winds larger than 6 meter per second and frequent larger than 10%. The arrow lengths are relative to the occurrence frequency (Gaillard et al., 2004).

Figure 12. Spatial Distribution of Summer Season Wind Direction of the Mediterranean Sea

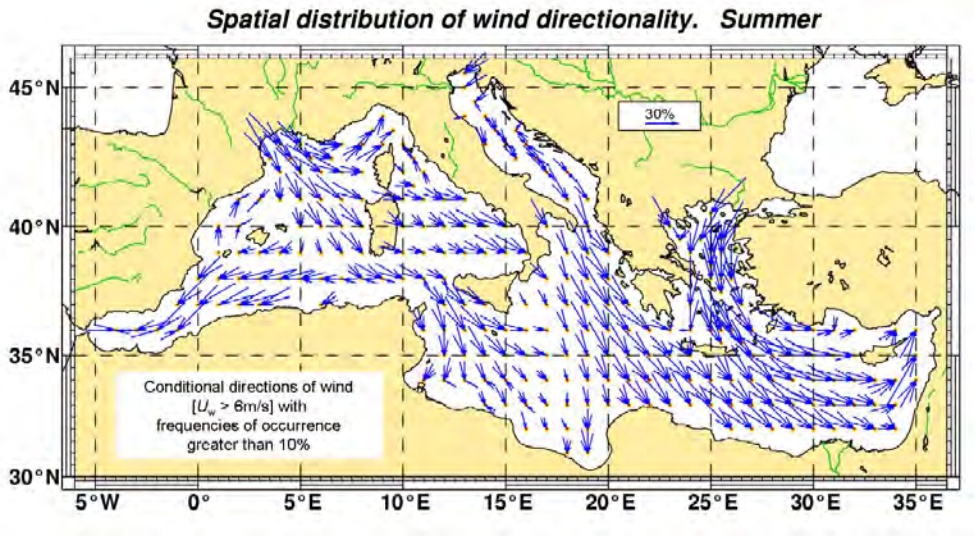

Source: Gaillard, P., and Coauthors, 2004: Wind and wave atlas of the Mediterranean Sea. Accessed 15 October 2015. [Available online at http://users.ntua.gr/mathan/pdf/Pages_from%20_WIND_WAVE_ATLAS_MEDITERRANEAN_SEA_2004.pdf].

Figure 13. Spatial Distribution of Autumn Season Wind Direction of the Mediterranean Sea

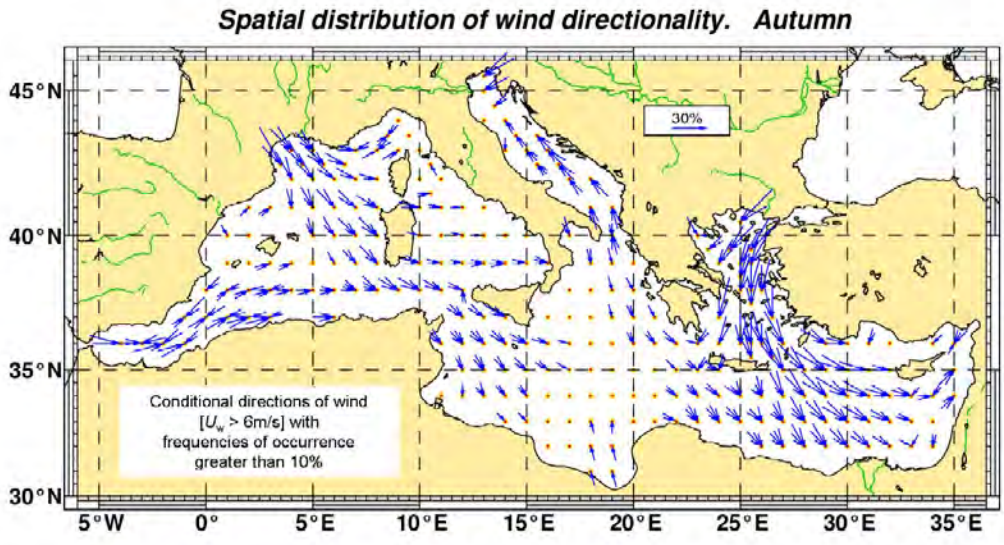

Source: Gaillard, P., and Coauthors, 2004: Wind and wave atlas of the Mediterranean Sea. Accessed 15 October 2015. [Available online at http://users.ntua.gr/mathan/pdf/Pages_from%20_WIND_WAVE_ATLAS_MEDITERRANEAN_SEA_2004.pdf].

The differential heating of the land and sea, which is observed in the warm season and occasionally apparent in the cool season, leads to day-to-day shift of the land and sea breezes. The typical sea breezes dominate from April to October, onset at 0700 or 0800, extending to a maximum around 1300 or 1400, and lasting until around 1800 or 1900. The sea breeze appears later in the morning in the spring and autumn; while its beginning may be postponed until noon in the winter season. The land and sea breezes extend around 10 to 20 miles from the coast. While the mean magnitudes of the land breezes are 5 to 9 knots, the sea breezes are stronger, reaching to 11 to 16 knots (National Geospatial-Intelligence Agency, 2011).

1. Etesian Winds

The most widespread regional wind in the Levantine basin of the Eastern Mediterranean Sea is the Etesian winds. The name comes from the Greek origin "etos," which meaning "yearly" to indicate the Etesian winds' annual endurance (Zecchetto and De Biasio, 2007).

The regular directions of the Etesian winds are from north and northwestern. The cold air and clear skies are observed as a result effect of Etesian winds between the late May and early October. Although they are generally dry, cool and moderate; they may turn into a windstorm over off-shore areas, extending maximum wind speed early afternoon (WeatherOnline, 2015).

The high pressure system over the Balkans and southeastern Europe, low pressure system over Turkey, and evolution of the south Asian warmth over the Anatolian plateau causes the occurrence of the Etesian winds (WeatherOnline, 2015). They are a component of the Asian monsoon system. Thermal lows deepening over Turkey may cause windstorm type Etesian winds. They can generate important seas along the Egyptian and Israeli shores due to the lengthened span of these winds (WeatherOnline, 2015). Location of Etesian winds is seen in Figure 14.

Figure 14. Location of the Etesian Winds

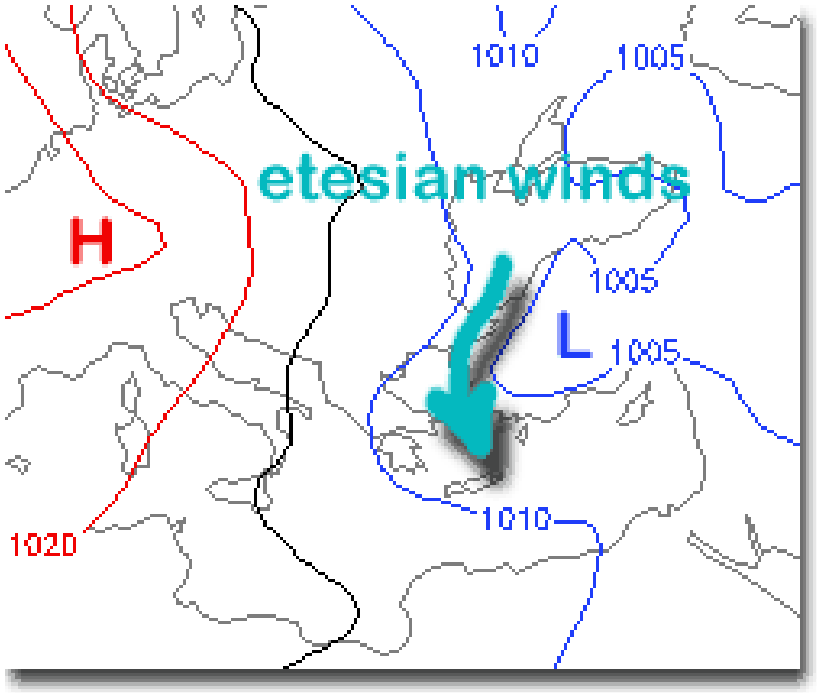

Source: WeatherOnline, 2015: Etesian Winds. Accessed 12 November 2015. [Available online at http://www.weatheronline.co.uk/reports/wind/The-Etesian-Winds.htm]

2. Khamsin Winds

The Khamsin winds develop in north of Africa and around the Eastern Mediterranean region periodically between the end of winter and the beginning of summer. They are overwhelming, warm, dry, and sandy south / south-east winds. The name "Khamsin" comes from the Arabic originated "Khamsun" or "Hamsin," which means "fifty" referring to the duration time of the wind. The Khamsin winds appear advance of depressions, which maneuver to eastward or north-eastward in the Mediterranean Sea or over north of Africa (WeatherOnline, 2015). Settlement of the Khamsin winds in the Eastern Mediterranean Sea is seen in Figure 15.

Figure 15. Settlement of the Khamsin Winds in the Eastern Mediterranean Sea

Source: Met Office, 2015: Winds of the world. Accessed 12 November 2015. [Available online at http://www.metoffice.gov.uk/learning/wind/wind-names]

D. NUTRIENTS

The Mediterranean Sea is generally distinguished by low nutrient concentration, especially in the Eastern Mediterranean (Tanhua et al., 2013). The surface layers are mostly quite nutrient exhausted. Due to low nutrient concentration, Mediterranean can be classified as oligotrophic or indeed ultra-oligotrophic sea. The nutrient exhausted surface layer of the Eastern Mediterranean is thicker and the deeper comparing to the Western Mediterranean (Tanhua et al., 2013).

Deep water with greater nutrient values flows towards the Atlantic Ocean, while the Atlantic Water with lower nutrient values flows towards the Mediterranean Sea. This circulation pattern, known as anti-estuarine circulation, is one of the main reasons for lower nutrient concentration in the Mediterranean Sea (Tanhua et al., 2013).

The apparent oxygen utilization (AOU) rate is nearly 70–80 $\mu mol\ kg^{-1}$. Even at the oxygen minimum layer of the intermediate depths, the oxygen concentration rate is nearly 180 $\mu mol\ kg^{-1}$. Considering this rate difference, the Mediterranean is known as a

well oxygenated sea. This high oxygen concentration in the Mediterranean Sea is due to the dynamic and quick circulation of the Mediterranean Sea (Tanhua et al., 2013).

The dissolved oxygen and nutrient concentrations in the Eastern Mediterranean Sea show largely homogenous distribution in the upper layer. The surface waters are almost saturated with the dissolved oxygen. The distribution of nutrients in the Levantine basin is seen in Figure 16 (Krom et al., 2014).

Figure 16. Vertical Sections of Dissolved Oxygen and Nutrients along West-East Cross Section of the Levantine Basin

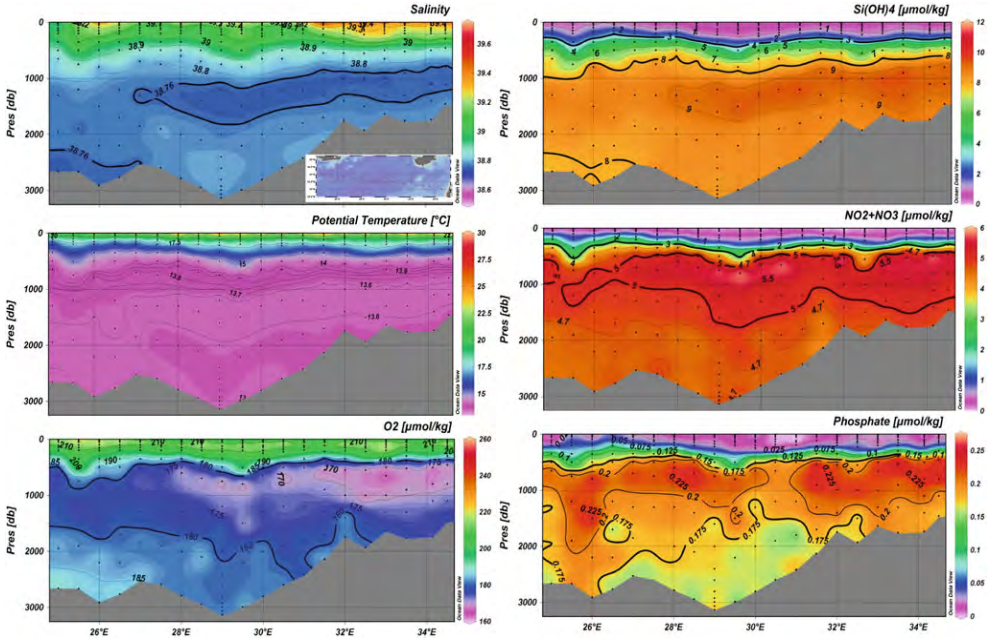

Source: Krom, M., N. Kress, I. Berman-Frank, and E. Rahav, 2014: Past, Present and Future Patterns in the Nutrient Chemistry of the Eastern Mediterranean. *The Mediterranean Sea Its history and present challenges,* S. Goffredo, and Z. Dubinsky, Eds., Springer, 49–68.

The distribution of the dissolved oxygen concentrations is large at the surface. As depth increases, the dissolved oxygen concentration reaches to the slightest values at the 500–1500m layer. Then, it rises towards the bottom of the Levantine basin, or down to 2500m (Krom et al., 2014). Composite depth profiles of dissolved oxygen and nutrients in the Levantine basin are seen in Figure 17.

The nitrate depth profile is nearly opposite of the dissolved oxygen profile. The nitrate concentration is small at the surface. It reaches to the greatest values at the 500–1500m layer, and then it reduces towards the bottom of the Levantine basin, or down to 2500m. The silicic acid depth profile shows a similar pattern with the nitrate depth profile (Krom et al., 2014).

Figure 17. Composite Depth Profiles of Dissolved Oxygen and Nutrients in the Levantine Basin

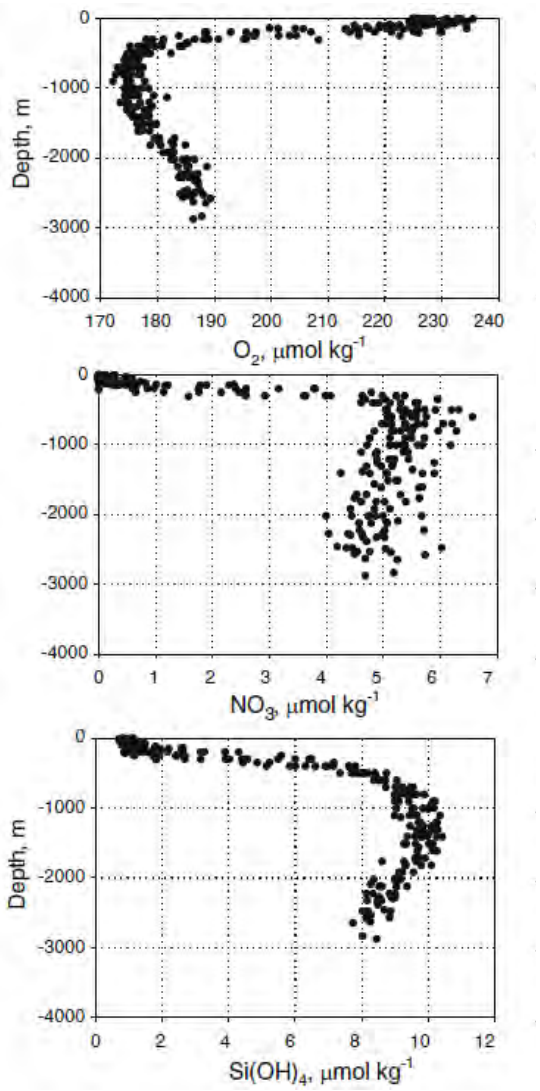

Source: Krom, M., N. Kress, I. Berman-Frank, and E. Rahav, 2014: Past, Present and Future Patterns in the Nutrient Chemistry of the Eastern Mediterranean. *The Mediterranean Sea Its history and present challenges,* S. Goffredo, and Z. Dubinsky, Eds., Springer, 49–68.

THIS PAGE INTENTIONALLY LEFT BLANK

III. DATA

A. HISTORICAL BACKGROUND OF THE DATASETS

The data used in this study were obtained from the World Ocean Database 2013 (WOD13), which was developed by the Ocean Climate Laboratory (OCL) at the National Oceanographic Data Center (NODC), Silver Spring, Maryland, USA. The scientifically quality-controlled in-situ sub-surface and surface measurements were included in the WOD13 (Johnson et al., 2013).

The first release of these dataset series was the World Ocean Atlas 1994 (WOA94). It was comprised of temperature, salinity, oxygen, phosphate, nitrate, and silicate profiles. The second release of the dataset was World Ocean Database 1998 (WOD98). This release renewed the previous one by adding new data as well as new variables. The third release of the dataset was World Ocean Database 2001(WOD01). The data, which were collected from new instruments types such as Undulating Ocean Recorders and profiling floats, were covered in WOD01.

The fourth release of the dataset was World Ocean Database 2005 (WOD05). This dataset updated the previous one by containing data from new variables and from one new instrument that is gliders. The fifth update of the dataset was World Ocean Database 2009 (WOD09). It added a new feature that was quality control. The data in this release were updated every three months (Boyer et al., 2013).

The newest release of these series is World Ocean Database 2013 (WOD13). In this release, the standard depth levels were expanded from 40 to 138 to have better resolution. The comparison of amount of the data in WOD13 with the previous versions of World Ocean Database (WOD) and standard depth levels are seen in Table 2 and Table 3, respectively (Boyer et al., 2013).

Table 2. Comparison of amount of Data in WOD13 with Previous Versions of WOD

Dataset	NODC (1974)[1]	NODC (1991)[2]	WOA94	WOD98	WOD01	WOD05	WOD09	WOD13
OSD [3]	425,000	783,912	1,194,407	1,373,440	2,121,042	2,258,437	2,541,298	3,115,552
CTD [4]	na	66,450	89,000	189,555	311,943	443,953	641,845	848,911
MBT [5]	775,000	980,377	1,922,170	2,077,200	2,376,206	2,421,940	2,426,749	2,425,607
XBT	290,000	704,424	1,281,942	1,537,203	1,743,590	1,930,413	2,104,490	2,211,689
MRB	na	na	na	107,715	297,936	445,371	566,544	1,411,762
DRB	na	na	na	na	50,549	108,564	121,828	251,712
PFL	na	na	na	na	22,637	168,988	547,985	1,020,216
UOR	na	na	na	na	37,645	46,699	88,190	88,190
APB	na	na	na	na	75,665	75,665	88,583	1,713,132
GLD	na	na	na	na	na	338	5,857	103,798
Total Stations	**1,490,000**	**2,535,163**	**4,487,519**	**5,285,113**	**7,037,213**	**7,900,368**	**9,155,099**	**13,190,569**
Plankton	na	na	na	83,650	142,900	150,250	218,695	242,727
SUR [6]	na		na	na	4,743	9,178	9,178	9,289

Source: Johnson, D., T. Boyer, H. Garcia, R. Locarnini, O. Baranova, and M. Zweng, 2013: World Ocean Database 2013 User's Manual. NODC Internal Report 22, 163 pp, [Available online at http://www.nodc.noaa.gov/OC5/WOD13/docwod13.html]

Table 3. Standard Levels and Depths in Meters

Depth	Level #	Depth	Level #	Depth	Level #	Depth	Level #
0	1	475	36	2400	71	5900	106
5	2	500	37	2500	72	6000	107
10	3	550	38	2600	73	6100	108
15	4	600	39	2700	74	6200	109
20	5	650	40	2800	75	6300	110
25	6	700	41	2900	76	6400	111
30	7	750	42	3000	77	6500	112
35	8	800	43	3100	78	6600	113
40	9	850	44	3200	79	6700	114
45	10	900	45	3300	80	6800	115
50	11	950	46	3400	81	6900	116
55	12	1000	47	3500	82	7000	117
60	13	1050	48	3600	83	7100	118
65	14	1100	49	3700	84	7200	119
70	15	1150	50	3800	85	7300	120
75	16	1200	51	3900	86	7400	121
80	17	1250	52	4000	87	7500	122
85	18	1300	53	4100	88	7600	123
90	19	1350	54	4200	89	7700	124
95	20	1400	55	4300	90	7800	125
100	21	1450	56	4400	91	7900	126
125	22	1500	57	4500	92	8000	127
150	23	1550	58	4600	93	8100	128
175	24	1600	59	4700	94	8200	129
200	25	1650	60	4800	95	8300	130
225	26	1700	61	4900	96	8400	131
250	27	1750	62	5000	97	8500	132
275	28	1800	63	5100	98	8600	133
300	29	1850	64	5200	99	8700	134
325	30	1900	65	5300	100	8800	135
350	31	1950	66	5400	101	8900	136
375	32	2000	67	5500	102	9000	137
400	33	2100	68	5600	103		
425	34	2200	69	5700	104		
450	35	2300	70	5800	105		

Source: Johnson, D., T. Boyer, H. Garcia, R. Locarnini, O. Baranova, and M. Zweng, 2013: World Ocean Database 2013 User's Manual. NODC Internal Report 22, 163 pp, [Available online at http://www.nodc.noaa.gov/OC5/WOD13/docwod13.html]

B. THE FEATURES OF THE DATASETS IN WOD13

The data in WOD13 are comprised of eleven datasets, each of which is characterized by the instruments that collect the data. Moreover, the variables in the WOD13 database were measured both at observed depth levels and at 138 standard depth levels. The datasets in WOD13 are listed in Table 4.

Table 4. Datasets in the WOD13

DATASETS	DATASETS INCLUDES
OSD	Ocean Station Data, Low-resolution CTD/XCTD, Plankton data
CTD	High-resolution Conductivity-Temperature-Depth / XCTD data
MBT	Mechanical / Digital / Micro Bathythermograph data
XBT	Expendable Bathythermograph data
SUR	Surface-only data
APB	Autonomous Pinniped data
MRB	Moored buoy data
PFL	Profiling float data
DRB	Drifting buoy data
UOR	Undulating Oceanographic Recorder data
GLD	Glider data

Source: Johnson, D., T. Boyer, H. Garcia, R. Locarnini, O. Baranova, and M. Zweng, 2013: World Ocean Database 2013 User's Manual. NODC Internal Report 22, 163 pp, [Available online at http://www.nodc.noaa.gov/OC5/WOD13/docwod13.html]

1. Ocean Station Dataset (OSD)

Ocean Station Data includes measurements that are conducted via research vessels. The reversing thermometers are used to measure the temperature and special bottles are used to gather the seawater samples (Boyer et al., 2013). The salinity, oxygen, nutrient and chlorophyll are the variables that are measured via collected water samples (Boyer et al., 2013).

2. Conductivity Temperature Depth (CTD) Dataset

a. High-Resolution CTD Data

CTD dataset are comprised of oxygen, chlorophyll, temperature and salinity profiles (Boyer et al., 2013). If the depth increment of the data is less than two meters, it is classified as high-resolution CTD (Boyer et al., 2013).

b. Low-Resolution CTD Data

The pressure sensor, which is used to convert the measured pressure to depth; a temperature device; and a conductivity sensor, which is used to evaluate the salinity measurements, is the combination to refer the Conductivity-Temperature-Depth (CTD) instruments. If the depth increment is more than two meters, it is classified as low-resolution CTD (Johnson et al., 2013).

3. Mechanical/Digital/Micro Bathythermograph (MBT) Dataset

The MBT data provides temperature information as a function of depth. The MBT data is collected by using Mechanical Bathythermograph (MBT), Digital Bathythermograph (DBT) and Micro Bathythermograph (micro BT) instruments (Johnson et al., 2013).

4. Expendable Bathythermograph (XBT) Dataset

The deployment of the XBTs dates back to the 1966. The expendable bathythermograph is generally used instead of MBT in most measurements. It has a thermistor, which measures temperature versus depth. This instrument can be submerged from ship, airplane, or submarine. There is a command unit for recoding the temperature information over the copper wire (Boyer et al., 2013).

5. Profiling Float (PFL) Dataset

Temperature, salinity, and pressure data, which is gathered from the drifting profiling floats such as Profiling Autonomous Lagrangian Circulation Explorer, free-drifting hydrographic profiler, Sounding Oceanographic Lagrangian Observer and Autonomous Profiling Explorer, is included in PFL dataset (Johnson et al., 2013). The Argo Project is the main contributor to the PFL dataset in the WOD13 (Johnson et al., 2013).

6. Glider (GLD) Dataset

Data, from reusable autonomous underwater vehicles (AUVs), is included in the Glider dataset. AUVs are designed to reach to certain depths and measure the temperature, salinity, current and other quantities (Boyer et al., 2013). Different types of gliders are seen in Figure 18.

Figure 18. Different Types of Gliders

Source: Integrated Ocean Observing System, 2014: Gliders/Autonomous Underwater Vehicles. Accessed 15 November 2015. [Available online at http://www.ioos.noaa.gov/glider/welcome.html]

C. CHARACTERISTICS OF THE DATA USED IN THE THESIS

The data used in the thesis are from 1960 to 2013. The data obtained from WOD13 are re-organized according to the geographical area of interest, which is Eastern Mediterranean Sea. According to the annual distribution of temperature profiles, temporal distribution of temperature in the Eastern Mediterranean Sea, seen in Figure 19, shows that the maximum number of temperature profiles, which was gathered in 1968, is almost 8,000; while the minimum number of the temperature profiles, which was gathered in 1960, is almost 900. According to the monthly distribution of temperature profiles, May and October have the maximum number of temperature profiles, almost 18,000; while December has the minimum number of the temperature profiles, nearly 10,000.

Figure 19. Temporal Distribution of Temperature Profiles in the Eastern Mediterranean Sea

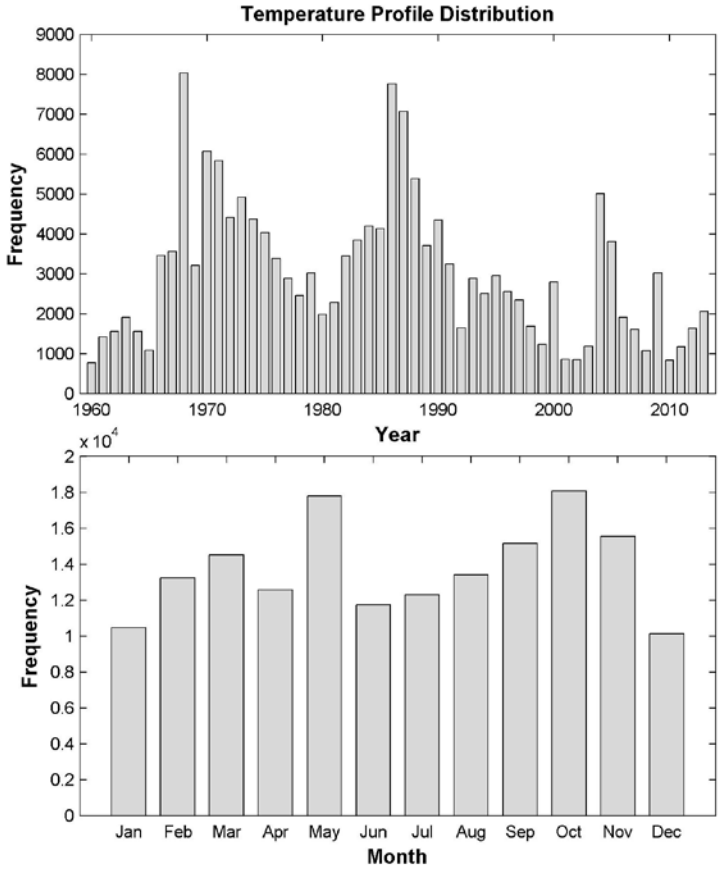

It is clear that the amount of temperature profile data collected along the African coast is less compared to other regions in the Eastern Mediterranean. The reliability of the study depends on how frequently the data were collected, which is one of the crucial aspects in determining the circulation patterns. The analyses included a total of 164,906 temperature profiles. The spatial distribution of the temperature profiles in the Eastern Mediterranean region is seen in Figure 20.

Figure 20. Spatial Distribution of Temperature Profiles in the Eastern Mediterranean

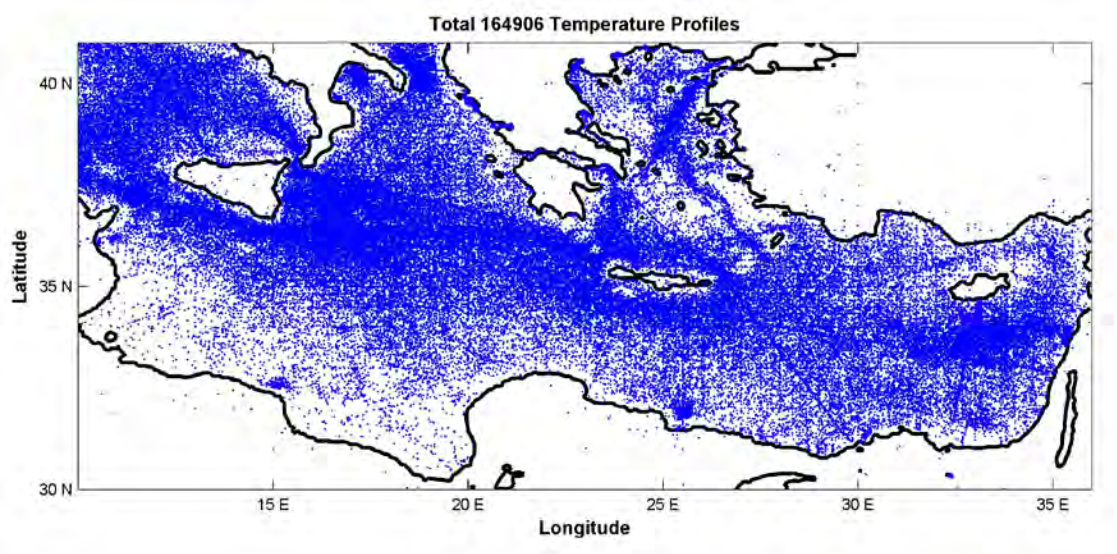

According to the temporal distribution of the salinity, 2005 has the maximum number of salinity profiles, nearly 3,700; whereas the minimum number of salinity profiles, nearly 250, was obtained in 1964. The temporal distribution histogram of the salinity profiles and the spatial distribution histogram of the salinity profiles are shown in Figure 21 and Figure 22, respectively. October has the maximum number of salinity profiles, nearly 6,000; while the minimum number of the salinity profiles, nearly 2,900, was produced in January. The analyses included a total of 53,606 salinity profiles.

Figure 21. Temporal Distribution of Salinity Profiles in the Eastern Mediterranean

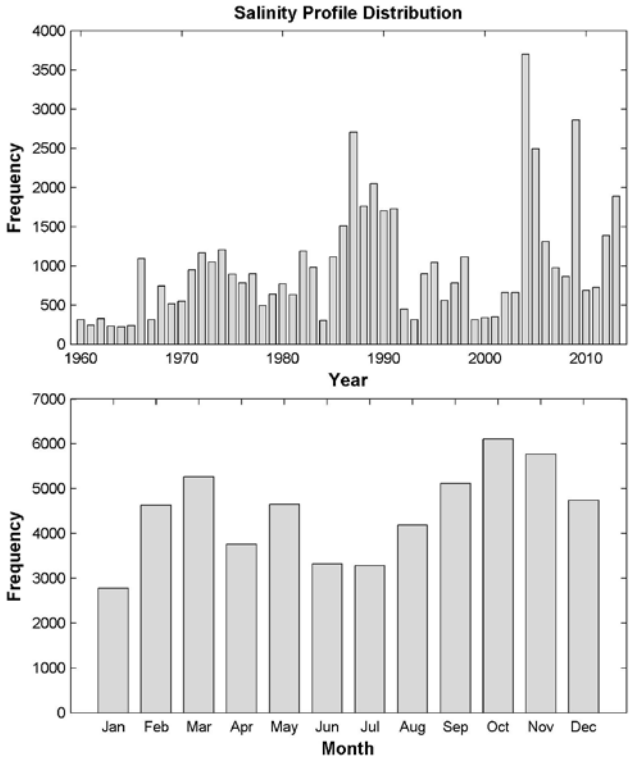

Figure 22. Spatial Distribution of Salinity Profiles in the Eastern Mediterranean

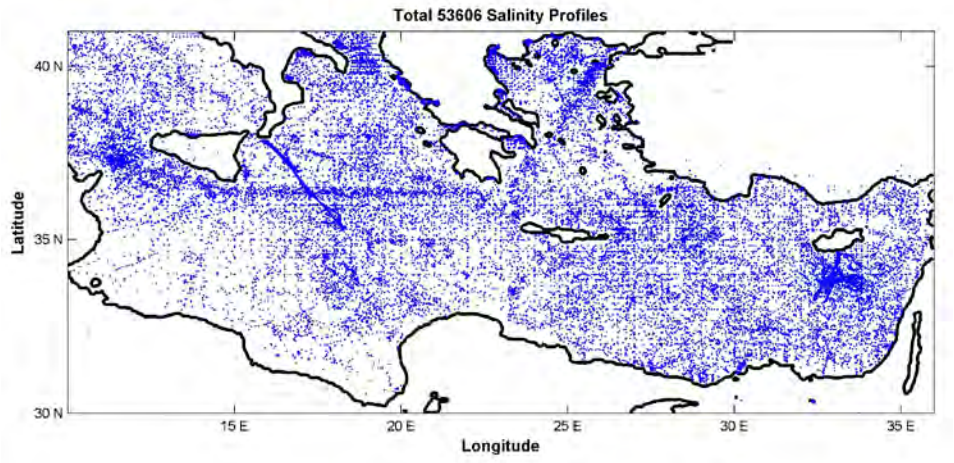

The data in the WOD13 were collected via many oceanographic instruments and WOD13 included many datasets. Types of the datasets, used for salinity analyses, are: Conductivity-Temperature-Depth (CTD) data, Glider (GLD) data, and Ocean Station Data (OSD) and Profiling Float (PFL) data. The number of the monthly and annually salinity profiles and their distribution according to the different type of datasets are presented in Figure 23, and Figure 24, respectively.

Figure 23. Monthly Distribution of the Different Datasets for Salinity Profiles in the Eastern Mediterranean

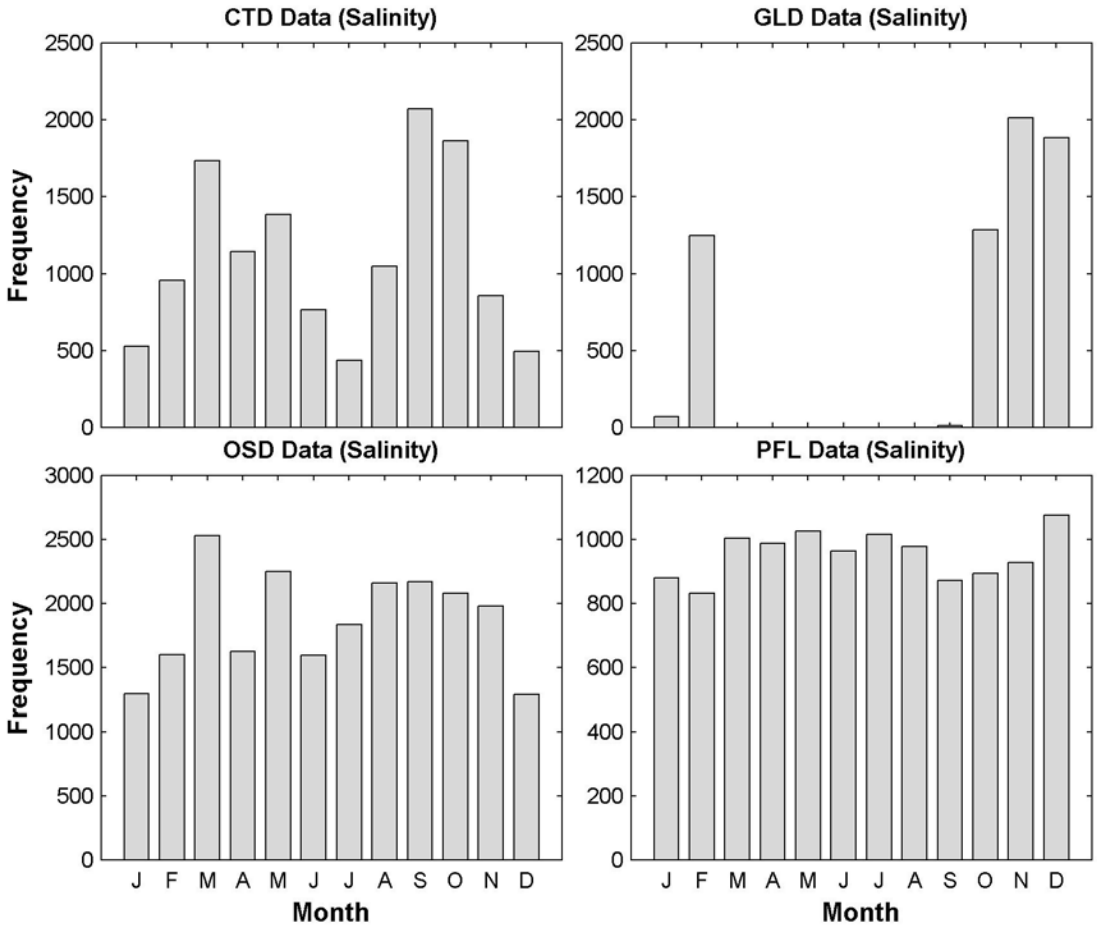

Figure 24. Annually Distribution of the Different Datasets for Salinity Profiles in the Eastern Mediterranean

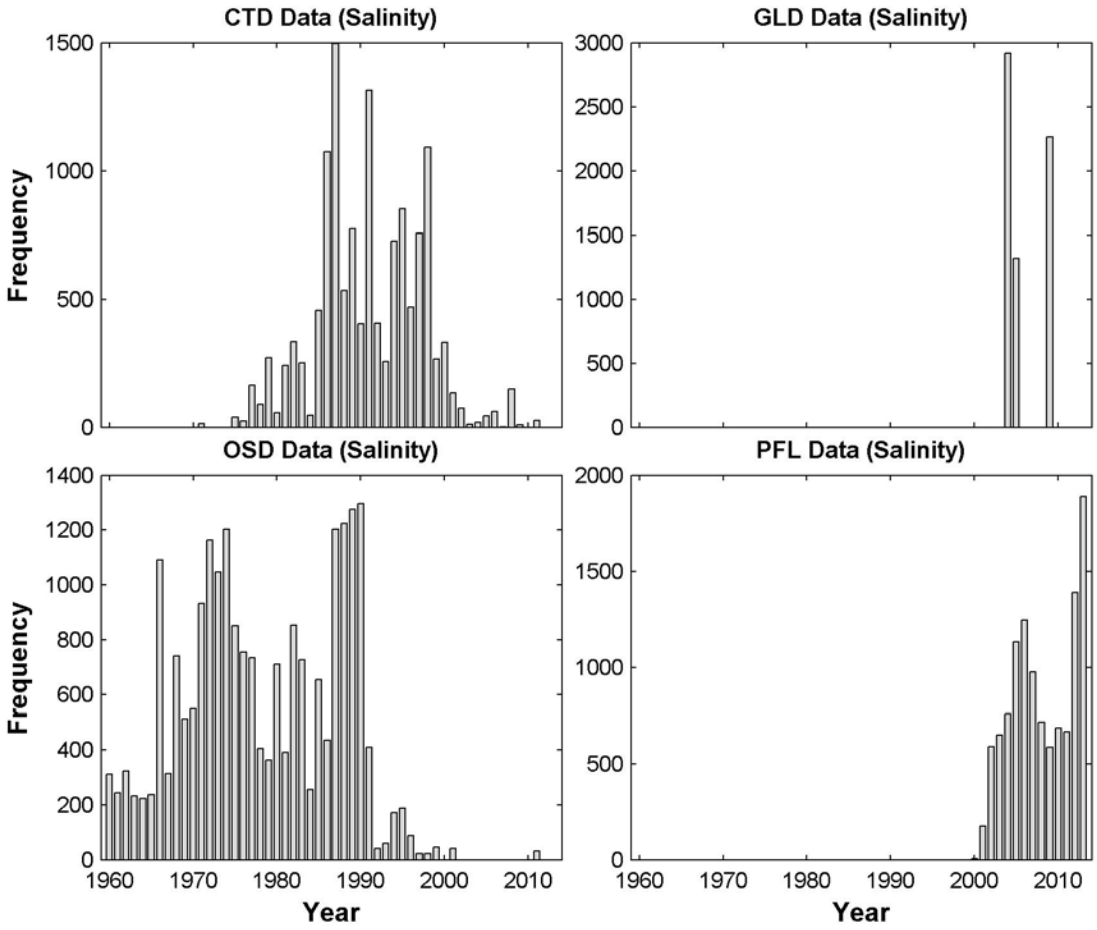

Types of the datasets, used for temperature analyses, are: Conductivity-Temperature-Depth (CTD) data, Glider (GLD) data, Ocean Station Data (OSD), Profiling Float (PFL) data, Expendable Bathythermograph (XBT) data and Mechanical Bathythermograph (MBT) data. The number of the monthly and annually temperature profiles and their distribution according to the different type of datasets are presented in Figure 25, and Figure 26, respectively.

Figure 25. Monthly Distribution of the Different Datasets for Temperature Profiles in the Eastern Mediterranean

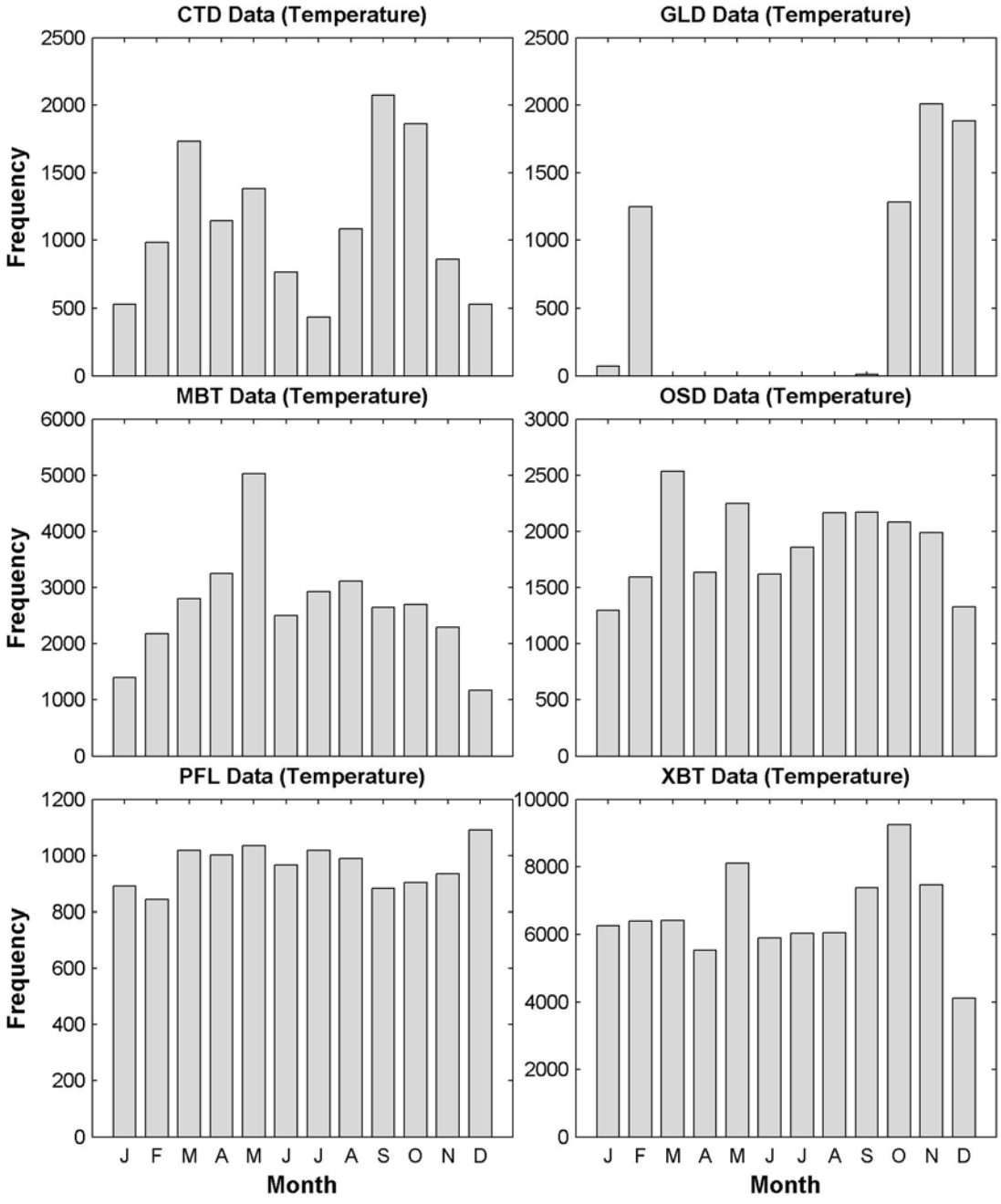

Figure 26. Annually Distribution of the Different Datasets for Temperature Profiles in the Eastern Mediterranean

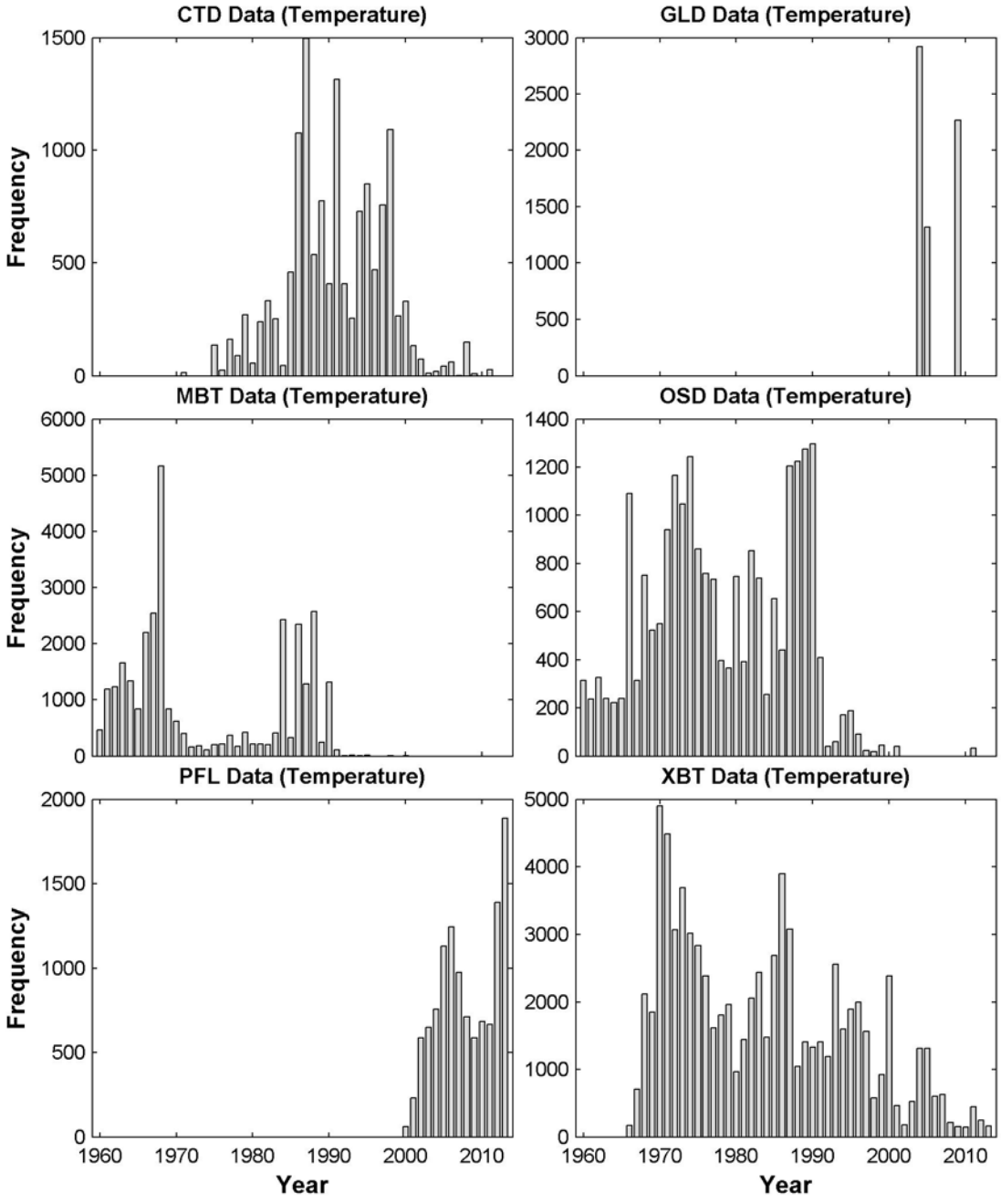

IV. METHODOLOGY

A. OPTIMAL SPECTRAL DECOMPOSITION (OSD) METHOD

Data assimilation is a necessary method for ocean studies. Moreover, it is very significant to provide the realization of ocean modeling and prediction. The Optimal Spectral Decomposition (OSD) method is an effective approach for data analysis. The OSD method has been developed for ocean data analysis to establish temporally varying 3-D gridded (T, S) fields from the WOD13 profiles (Chu et al., 2015). First nine basis functions of the Eastern Mediterranean Sea are seen in Figure 27.

> The basis functions, depending only on the topography of the ocean basin, are the eigenvectors of the Laplacian operator with the same lateral boundary conditions as the assimilated variable anomalies. (Chu et al., 2015)

Figure 27. First Nine Basis Functions of the Eastern Mediterranean Sea

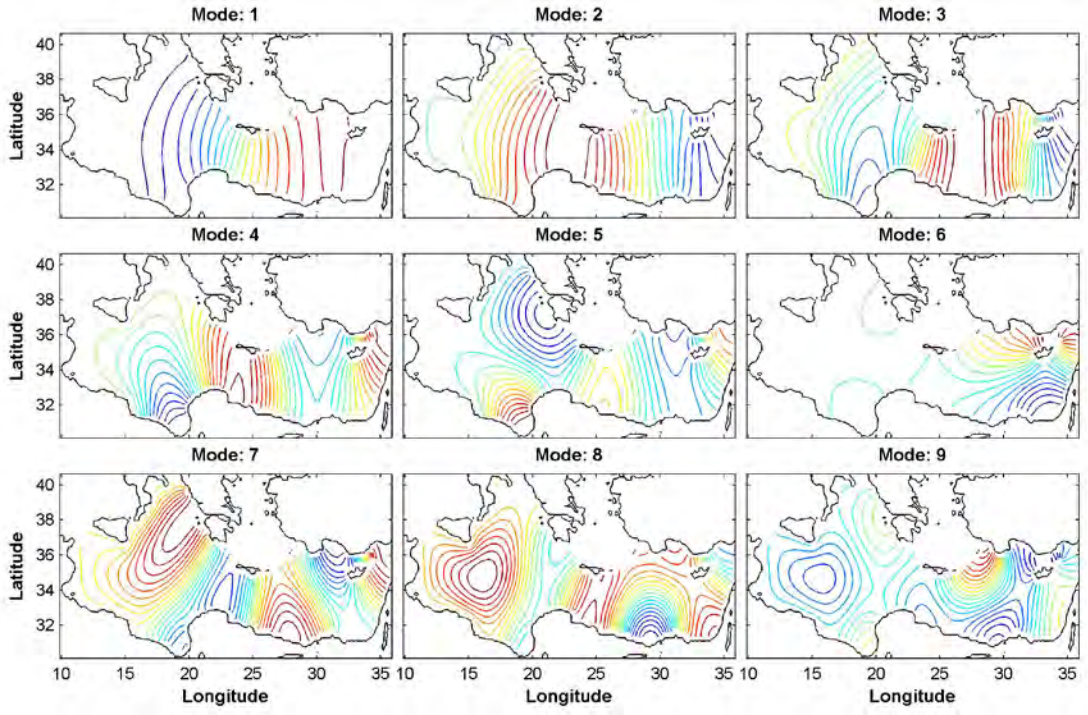

Selection of basis functions $\{\varnothing k(x,z)\}$ needs to satisfy three necessary conditions: (i) satisfaction of the same homogeneous boundary condition of the assimilated variable anomaly, (ii) orthonormal, and (iii) independence of the assimilated variable. (Chu et al., 2015)

K shows the number of basis functions and N shows the number of grid points, so orthonormal can be expressed as;

$$\sum_{n=1}^{N} \varnothing_k(x_n)\varnothing_{k'}(x_n) = \delta_{kk'} \tag{0.1}$$

$$\delta_{kk'} = \begin{cases} 0 & if \quad k \neq k' \\ \\ 1 & if \quad k = k' \end{cases} \tag{0.2}$$

Horizontal grid points are represented by xn = (xi, yj), n = 1, 2,…, N. The following matrix represents the first K discrete basis functions for all grid points.

$$G = \{g_{nk}\} = \begin{bmatrix} \varnothing_1(x_1) & \varnothing_1(x_2) & \cdots & \varnothing_1(x_N) \\ \varnothing_2(x_1) & \varnothing_2(x_2) & \cdots & \varnothing_2(x_N) \\ \cdots & \cdots & \cdots & \cdots \\ \varnothing_k(x_1) & \varnothing_k(x_2) & \cdots & \varnothing_k(x_N) \end{bmatrix} \tag{0.3}$$

B. EMPIRICAL ORTHOGONAL FUNCTION (EOF) METHOD

Empirical Orthogonal Function (EOF) method has been used in meteorology and oceanography in order to interpret the spatial and temporal analysis related to the instability of variables such as currents, winds, temperature and to be able to figure out the mechanisms behind those variables (Kaihatu et al., 1998).

> The empirical orthogonal eigenfunction (EOF) method, first introduced to geophysics by Lorenz (1956), has subsequently been used to enable analysis of data with complex spatial/temporal structures. Using this method, the most efficient decomposition of the data into representative modes is determined by empirically finding the eigenfunctions that best describe the information. (Kaihatu et al., 1998)
>
> Retention of only the first few modes may contain a significant portion of the total variance, leading to potentially significant storage savings if not all the variance is required. Additionally, each mode contains phenomena with differing spatial/temporal scales and thus can be isolated. (Kaihatu et al., 1998)

In this thesis, EOF method allows us to analyze the long term anomaly of the heat content and freshwater content. Temperature anomaly field $\hat{T}$ is obtained by subtracting the monthly mean $\overline{T}$ from temperature data *T*.

$$\hat{T}\left(x_i, y_j, z_k, \tau_l, t_m\right) = T\left(x_i, y_j, z_k, \tau_l, t_m\right) - \overline{T}\left(x_i, y_j, z_k, t_m\right) \tag{0.4}$$

$\hat{T}$ is modified into a N×P matrix as $\hat{T}\left(r_n, \tilde{t}_p\right)$. N represents the number of grid points and P represents the number of the time points. In this study, a total of 648 (54 years by 12 months) time points were used for P value. N is dependent on the area that is used for analysis. After some modifications of the equation (1.4), $\hat{T}\left(r_n, \tilde{t}_p\right)$ anomaly field can be written as,

$$\hat{T}\left(r_n, \tilde{t}_p\right) = \sum_{\alpha} PC_{\alpha}\left(\tau_l, t_m\right)\Phi_{\alpha}\left(x_i, y_j, z_k\right) \tag{0.5}$$

where temporal variation is represented by $PC_{\alpha}\left(\tau_l, t_m\right)$, and spatial variation is represented by $\Phi_{\alpha}\left(x_i, y_j, z_k\right)$.

Table 5 and Table 6 show the variances of first four EOF modes of freshwater content and heat content, respectively. According to tables, first four modes represent the nearly 50% of the total variances, whereas the remaining 26 modes represent the other 50% of the total variance. Thus, it is clear that the first few modes are much noteworthy to understand the general distribution of variation.

Table 5. Freshwater Content Variances of First Four EOFs Modes

EOFs	Variance (%)	Total Variance (%)
1	25.2	25.2
2	11.9	37.1
3	8.47	45.57
4	6.3	51.87

Table 6. Heat Content Variances of First Four EOFs Modes

EOFs	Variance (%)	Total Variance (%)
1	27.8	27.8
2	11	38.8
3	6.02	44.82
4	4.65	49.47

C. P-VECTOR INVERSE METHOD

P-vector inverse method is used to obtain the absolute geostrophic velocity from temperature and salinity (T, S) data. There are three required physical basis for the P-vector inverse method. They are: mass conservation, geostrophic balance, and no major cross-isopycnal mixing except water masses in contact with the atmosphere (Chu et al., 1998).

The conservation of mass is represented by the equation,

$$\vec{V} \cdot \nabla \rho = 0 \tag{0.6}$$

where ρ represents the potential density, by differentiating this equation with respect to z and multiplying with the coriolis parameter f, conservation of potential vorticity equation can be produced as,

$$q = f \frac{\partial \rho}{\partial z}, \ \vec{V} \cdot \nabla q = 0 \tag{0.7}$$

Equations (1.6) and (1.7) indicate that $\vec{V}$ is perpendicular to both $\nabla \rho$ and ∇q therefore, the velocity $\vec{V}$ is parallel to $\nabla q \times \nabla p$. (Chu et al., 1998)

So, the unit vector $\vec{P}$ is parallel to the velocity $\vec{V}$, and unit vector $\vec{P}$ can be produced as,

$$\vec{P} = \frac{\nabla \rho \times \nabla q}{\left| \nabla \rho \times \nabla q \right|} \tag{0.8}$$

As a result, velocity $\vec{V}$ can be obtained as,

$$\vec{V} = r\left(x, y, z\right)\vec{P} \tag{0.9}$$

where r represents the proportionality factor and can be determined by set of algebraic equations by using the thermal wind relation (Chu et al., 1998).

THIS PAGE INTENTIONALLY LEFT BLANK

V. SEASONAL VARIABILITY

A. TEMPERATURE FIELD

Figure 28 shows the total mean temperature of the Eastern Mediterranean Sea at different depths between 1960 and 2013. The sea surface temperature changes from 23 ^{o}C in the east coast of the Levantine Sea to 18 ^{o}C in the entrance of the Adriatic Sea. The temperature values have slight variation from surface to 20m depth. Until 20m depth, the temperature variation is nearly 1 - 2 ^{o}C. The mean temperature in the 50m depth shows a little much variation comparing to 20m depth. The 50m depth shows transition zone characteristics between the surface depth and the 150m depth. In 100m depth, the warmest section of the Eastern Mediterranean is at the very east coast of the Levantine Sea with a temperature of almost 17 ^{o}C, while the coldest section of the Eastern Mediterranean is at the Gulf of Taranto and Strait of Otranto with a temperature of almost 14.5 ^{o}C. The 16 ^{o}C isothermal line runs from Cretan passage to Sfax, passing through the north coast of the Egypt and Libya. The 16 ^{o}C and 15 ^{o}C isothermal lines nearly cover all the Central Ionian Sea. The 150m depth is the beginning of the intermediate layer of the Eastern Mediterranean Sea. From 150m to 400m depth, the temperature difference between the east part of the Eastern Mediterranean and the west part of the Eastern Mediterranean decreases as the depth goes down. In 400m depth layer, temperature distribution is almost uniform through the basin and the temperature is almost 15 ^{o}C. Seemingly, there is no another isothermal line in the 400m depth layer except the very west border of the basin. The deep layer of the Eastern Mediterranean Sea begins at the 600m depth. There is nearly no temperature change at 600m depth layer with a temperature of almost 14 ^{o}C. Below 600m, temperature remains nearly uniform down to the bottom.

Figure 28. Total Mean Temperature (^{o}C) at Different Depths

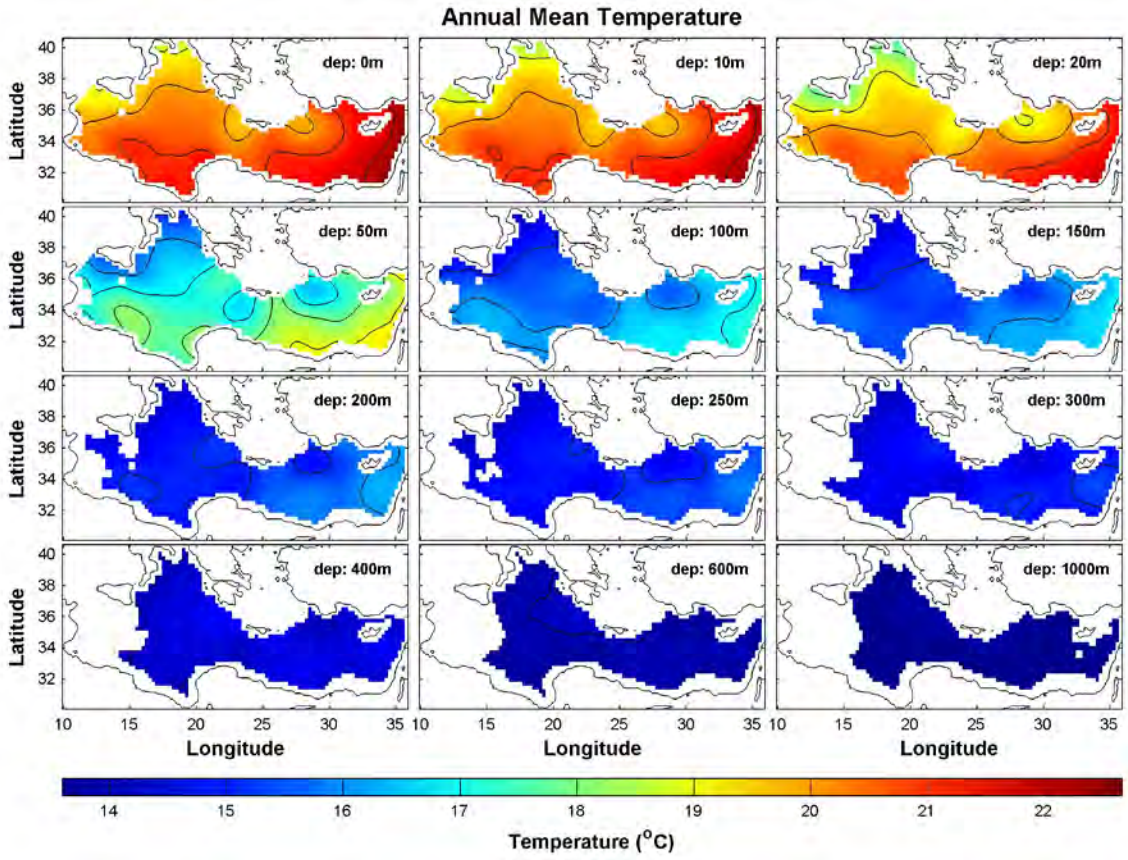

Figure 29 shows the climatological monthly mean temperature at the surface. Temperature drastically drops almost 3 ^{o}C from December to January. As time goes by, temperature continues to decline in the winter season. The coldest part in the Eastern Mediterranean is the entrance of the Adriatic with a temperature of 13 ^{o}C. Also, February is the coldest month through the year. In the spring season, March draws attention with a highly similar temperature characteristic of February. May is like a transition month between spring and summer seasons. Temperature increases to 19 ^{o}C in the western part and to 22 ^{o}C in the eastern part of the basin in May.

Relatively colder part, with a temperature of almost 19.5 ^{o}C, is the entrance of the Strait of Gibraltar for June in summer season. Relatively warmer part, with a temperature of almost 24.5 ^{o}C, is the coast of Syria. Temperature increases nearly from 24 ^{o}C to 27 ^{o}C throughout the whole basin in July and increases to almost 29 ^{o}C in August. August is the warmest month through the year. East part of the basin and north coasts of the Africa are the warmest areas that are spotted in August. With the beginning of the fall season, temperature reduces slowly until December.

Figure 29. Climatological Monthly Mean Temperature at the Surface

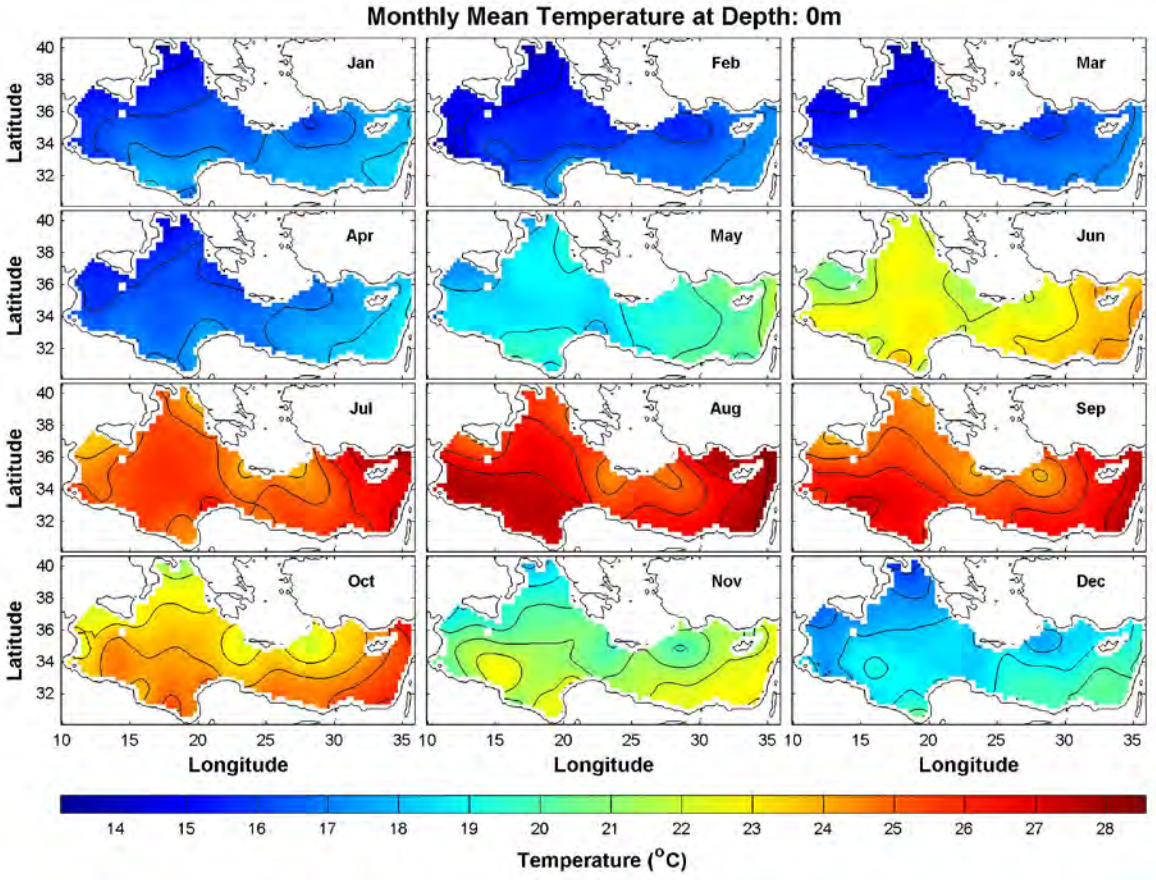

Figure 30 shows the climatological monthly mean temperature at the 150m depth. The mean temperature varies almost from 14.5 ^{o}C to 17 ^{o}C through the basin. As observed at the surface, the warmer spots are detected in the eastern part and the colder spots are detected in the western and northern part of the basin.

Figure 30. Climatological Monthly Mean Temperature at 150m Depth

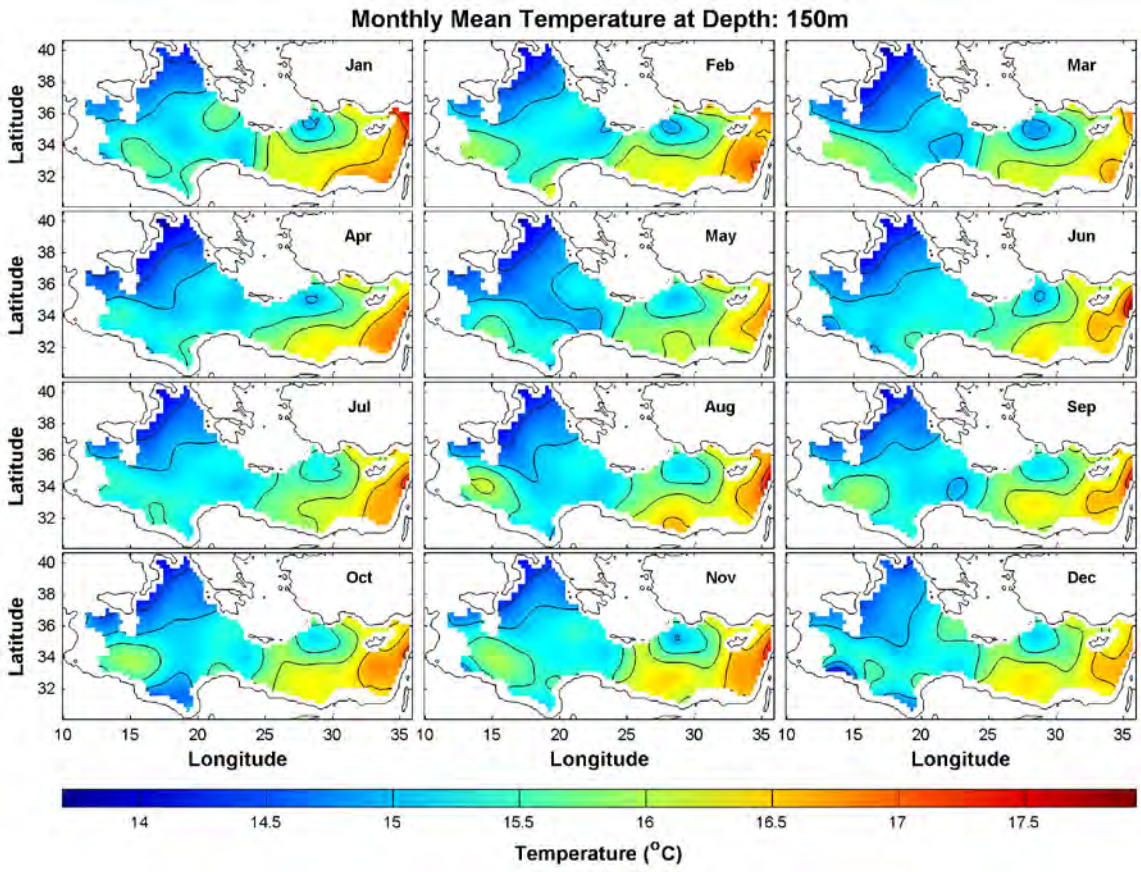

Figure 31 shows the climatological monthly mean temperature at the 600m depth. The temperature distribution is almost same for all months. Temperature varies from 13.5 ^{o}C to 14.5 ^{o}C. While the eastern part of the basin and north coasts of Africa are the warmer spots at the surface and 150m depth, they are colder spots at 600m depth. Even though a significant seasonal variation is observed at the surface depth, there is almost no seasonal temperature variation at 600m depth.

Figure 31. Climatological Monthly Mean Temperature at 600m Depth

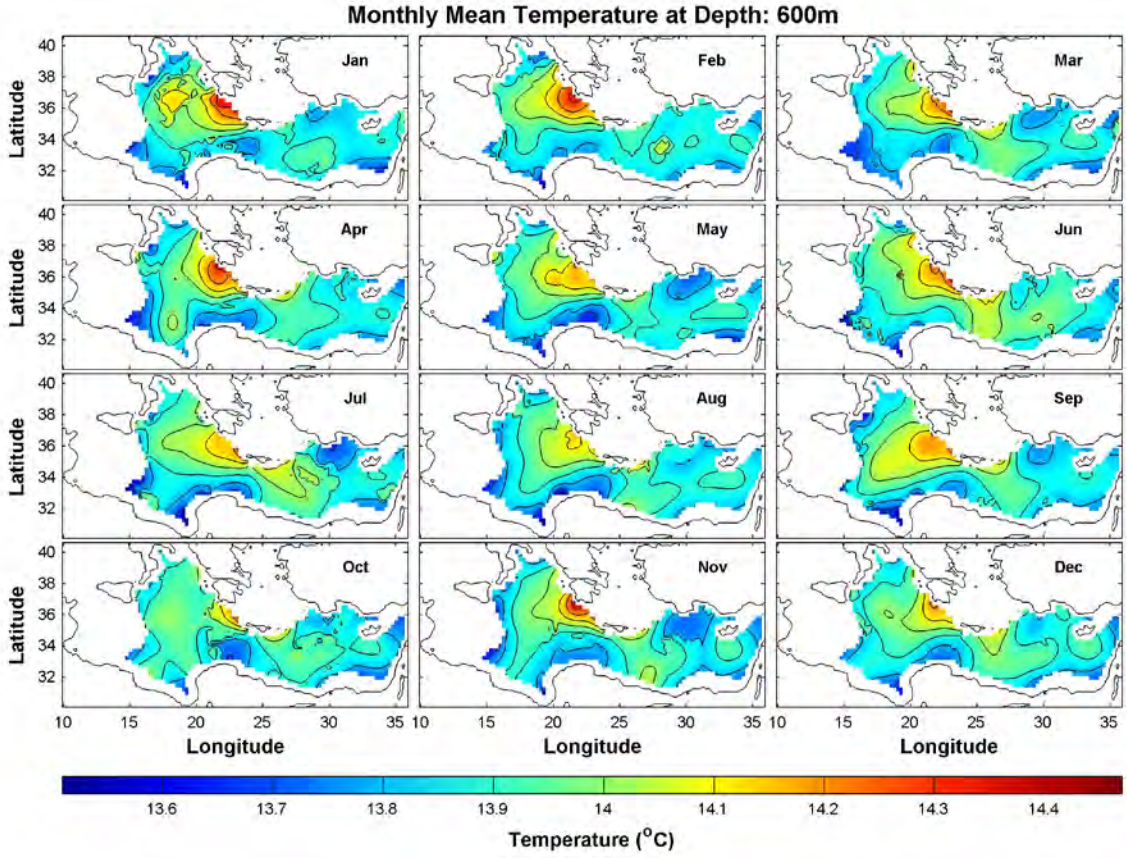

B. SALINITY FIELD

Figure 32 shows the total mean salinity, which is almost uniformly distributed through the basin until 100m depth with a salinity value of nearly 37 psu in the entrance of Strait of Gibraltar and with a salinity value of nearly 39 psu in the Levantine Basin north-east corner, where Turkey south coast and Syria west coast intersects.

Figure 32. Total Mean Salinity (psu) at Different Depths

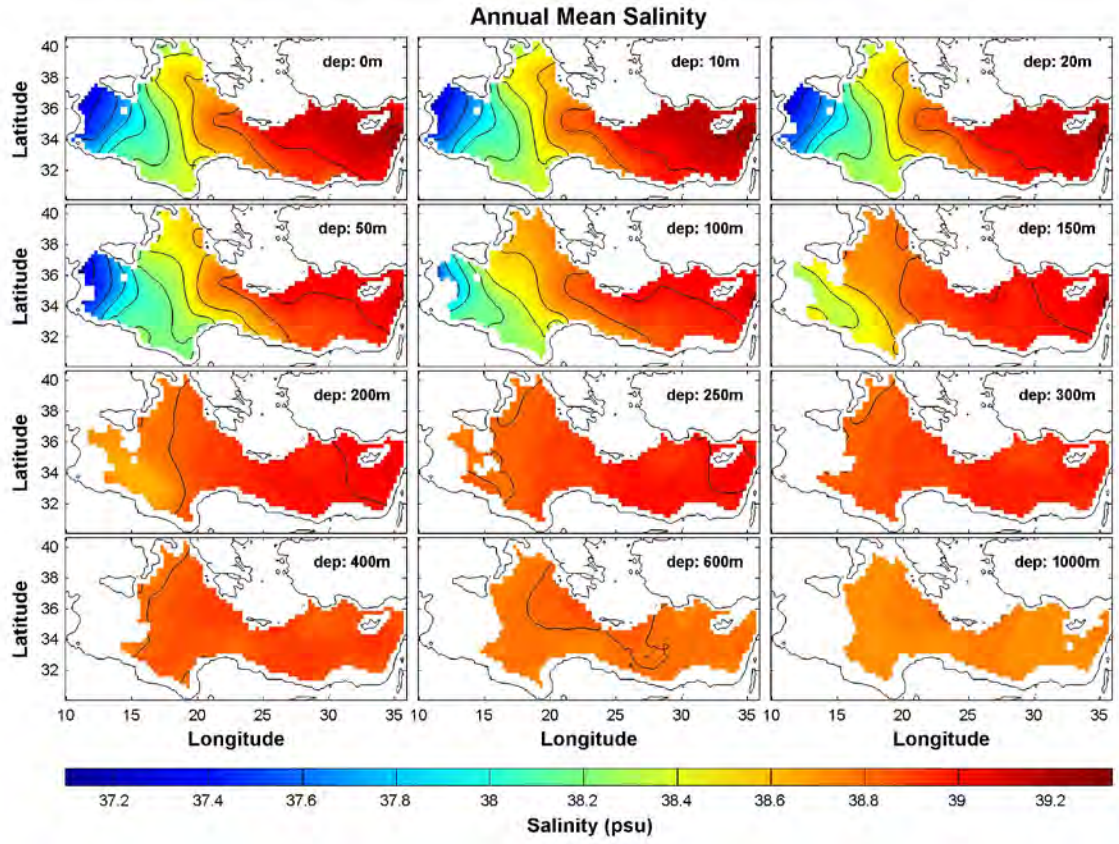

Between 100m and 200m, western part of the basin around Strait of Sicily and Malta becomes much saline with a salinity value of 38 to 38.8 psu, while the eastern part of the basin stays same with a salinity value of nearly 39 psu. From 200m to 600m depth, the salinity variation is very slight through the basin. Both eastern and western parts of the basin become almost equally salted with a mean salinity value of nearly 38.8 psu.

Below 600m depth, there is almost no variation in the salinity distribution through the basin.

Figure 33 shows the climatological monthly mean salinity at the surface. There is no significant seasonal salinity variation for winter and spring seasons. From December to June, western part and eastern part of the basin stay nearly constant with a salinity value of almost 37 psu and almost 39.2 psu, respectively. With the beginning of July, eastern part of the basin becomes much saline, while the western part stays nearly stable. Maximum salinity is observed in October with a salinity value of almost 39.8 psu at the eastern part of the basin.

Figure 33. Climatological Monthly Mean Salinity (psu) at the Surface

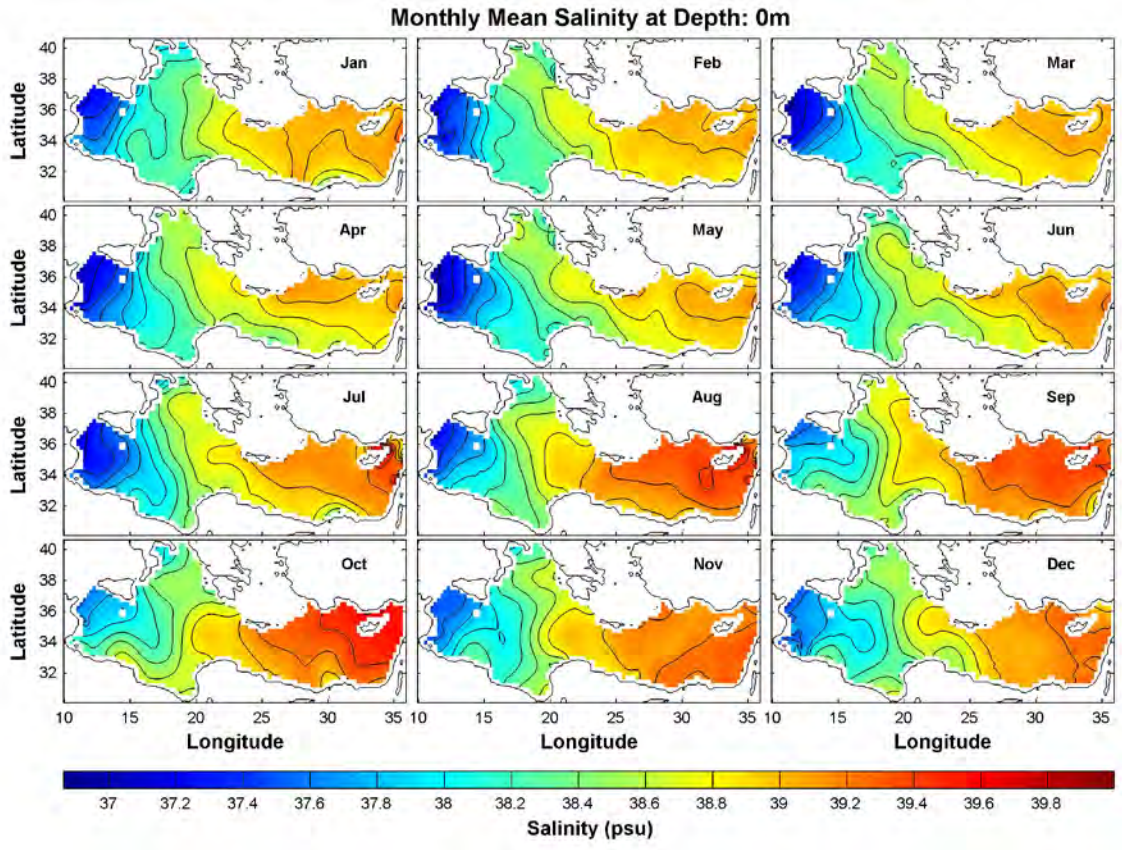

Figure 34 shows the climatological monthly mean salinity at 150m depth. The winter and spring seasons show a similar salinity distribution pattern. Winter and spring seasons are much saline with a salinity value of almost 39.2 psu at the 150m depth comparing to the winter and spring seasons at the surface with a salinity value of nearly 38.7 psu. Salinity variation shows almost a stable pattern through the all months except the Strait of Gibraltar and western coasts of Africa for March and April.

Figure 34. Climatological Monthly Mean Salinity (psu) at 150m Depth

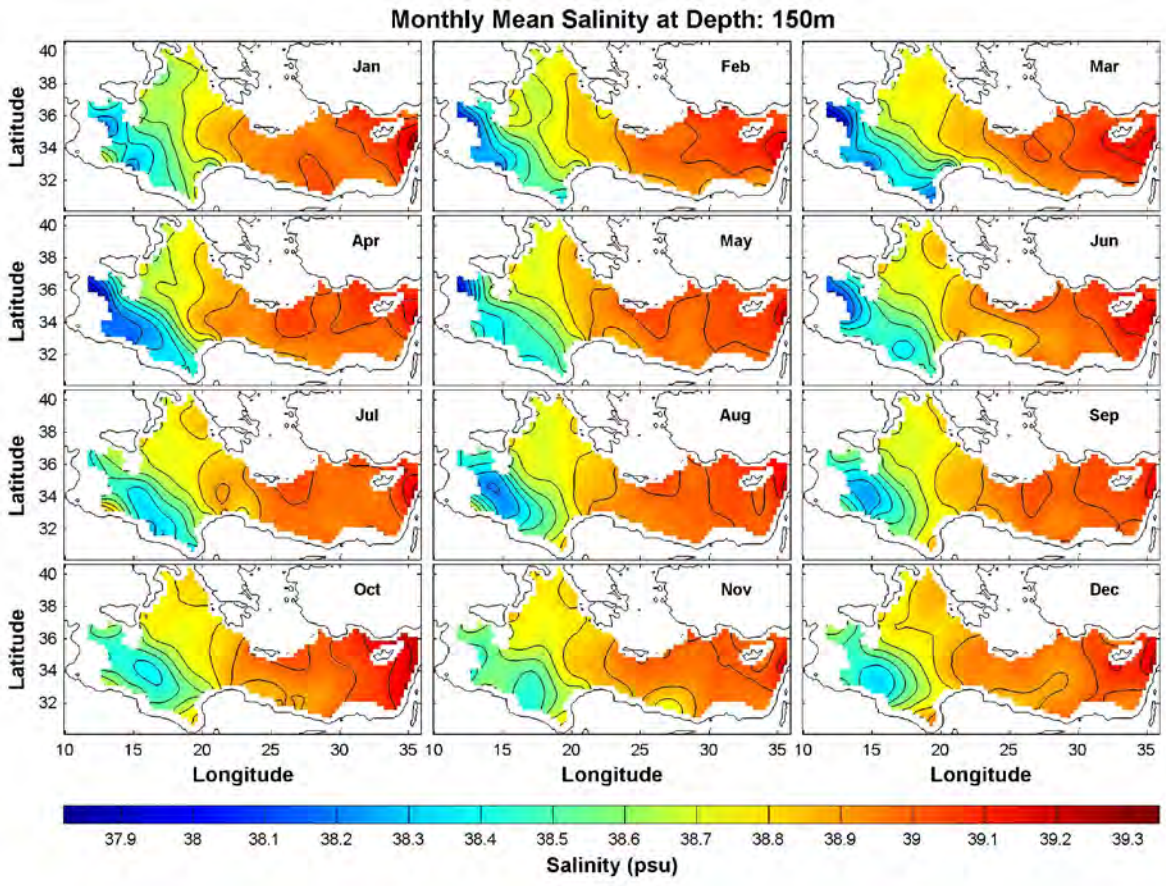

Figure 35 shows the climatological monthly mean salinity at 600m depth with no seasonal variability through the basin.

Figure 35. Climatological Monthly Mean Salinity (psu) at 600m Depth

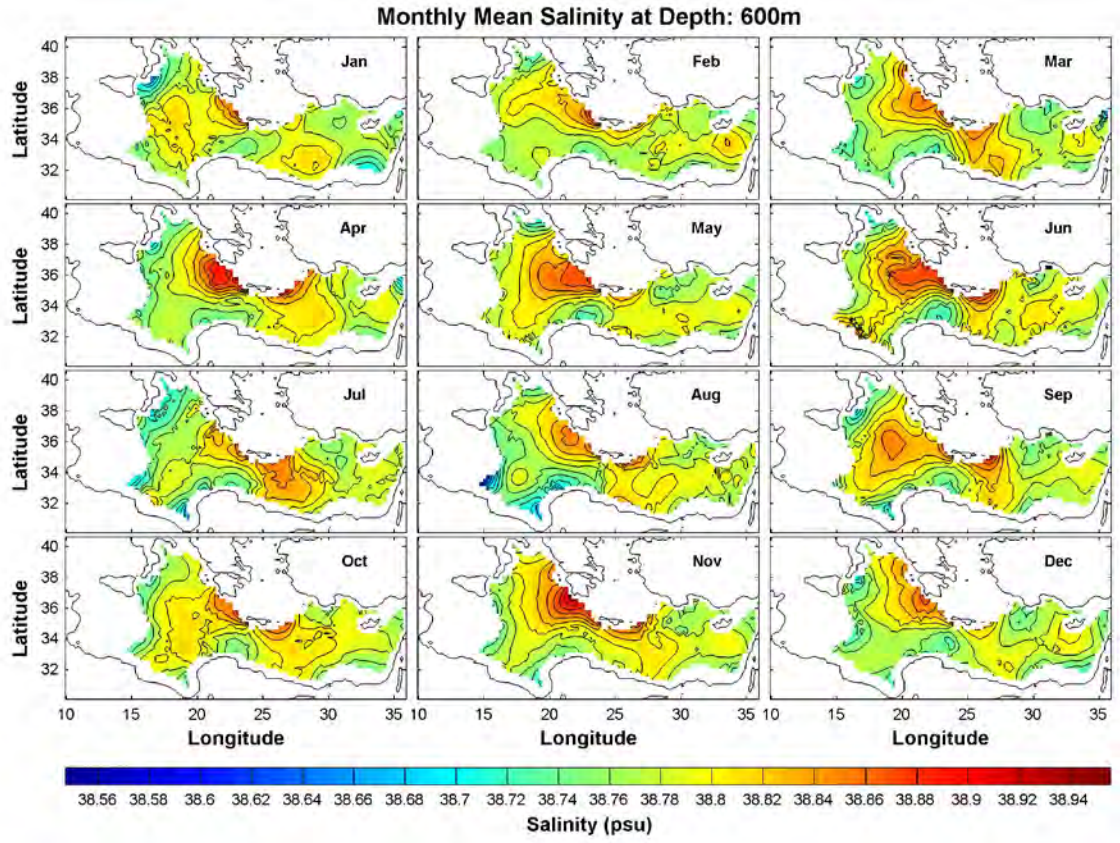

C. ABSOLUTE GEOSTROPHIC VELOCITY FIELD

Many studies related to the circulation patterns of the Eastern Mediterranean Sea have been explained since beginning of the 1900s. Although there are many studies towards the Eastern Mediterranean Sea circulation, there are still some debates about the actual circulation patterns of the area (Alhammoud et al., 2005). The structure of the actual circulation pattern of the Levantine Basin in the Eastern Mediterranean is way complex and it is needed to study further to be able to understand the actual circulation patterns. The main structures are basin-scale, sub-basin scale and mesoscale structures.

Moreover, there are permanent, recurrent and transient cyclonic and anticyclonic gyres and eddies in the interest area (Alhammoud et al., 2005). One of the first historical studies was carried out by Nielsen (1912). Until 1960s, the knowledge of the circulation pattern of the Eastern Mediterranean Sea was limited. Nielsen explained that the circulation was a basin-wide cyclonic gyre and the strongest current was close to the coast. He described that the Coriolis force affected the currents along the basin coast (Alhammoud et al., 2005). A new general circulation schematic was provided by Ovchinnikov (1966). Some cyclonic and anticyclonic sub-basin scales were detected by Ovchinnikov (1966), and Lacombe and Tchernia (1972) in the 1960s and 1970s (Alhammoud et al., 2005).

> In the Levantine basin (LB), they found an anticyclonic gyre at the southeastern corner of the basin and a cyclonic gyre between Rhodes and Cyprus, which might be related to the Shikmona anticyclone (SMA) and the Rhodes gyre (RG), respectively. Ovchinnikov (1966) also showed that the AW flows further eastward through the southern part of the Cretan passage and appears to reach as far as the eastern coast of the LB. Then this AW bifurcates near the Egyptian continental shelf. One branch continues eastward to reach the eastern edge of the LB. Then it turns northward to cross the Lattakia Basin up to the northeast of Cyprus and there it flows westward along the Asia Minor coast and between the Greek islands to exit via the northern part of the Cretan passage. The second branch flows offshore to join its twin northwest of Cyprus and there it merges with the first branch described above. (Alhammoud et al., 2005)

After the Ovchinnikov's schematic of the Mediterranean Sea circulation, POEM group made surveys in the Mediterranean Sea and explained a different pattern from the historical circulation schematics of the Mediterranean Sea.

> According to The POEM group (1992), among these changes was the presence of high energy and variable mesoscale structures consisting of eddies linked by meanders and jets. The POEM group (1992) provided a scheme of the circulation in the LB characterized by two systems of sub-basin gyres, an anticyclonic system in the south (Mersa-Matruh and Shikmona anticyclones; MMA and SMA, respectively) and a cyclonic one in the north (RG). The two systems are separated by a strong jet called the Central Levantine Basin Current (CLBC) by Ozsoy et al. (1989) or the Mid-Mediterranean Jet (MMJ) by Robinson et al. (1991). This jet, which is associated with the AW (characterized by its salinity minimum values), enters the LB via the Cretan passage and meanders eastward between the

> RG and the MMA. Then it bifurcates south of Cyprus into two branches, one merging with the SMA and the other turning northward then westward to feed the Asia Minor Current (AMC). The AMC flows westward into the Aegean Sea carrying with it the LSW marked by its high salinity and temperature. (Alhammoud et al., 2005)

After the studies of the POEM group, Mediterranean Forecast System (MFS) program was run and carried observations between 1998 and 2000. The result of this program also confirmed that sub-basin anticyclonic gyres in the southern part of the basin were persistent (Alhammoud et al., 2005). Figure 36 shows the historical studies about the circulation patterns of the Mediterranean Sea. Figure 36 (a) is from historical data by Nielsen, Figure 36 (b) is from surface geostrophic current by Ovchinnikov, Figure 36 (c) is from observations between 1985 and 1995 by POEM group, and Figure 36 (d) is from XBT observations between 1998 and 2000 by the MFS project. Figure 37 shows the circulation features schematic of the Mediterranean Sea for winter and summer seasons. Figure 38 shows the circulation features of the Eastern Mediterranean Sea.

Figure 36. Historical Studies of the Mediterranean Sea Surface Circulation Pattern

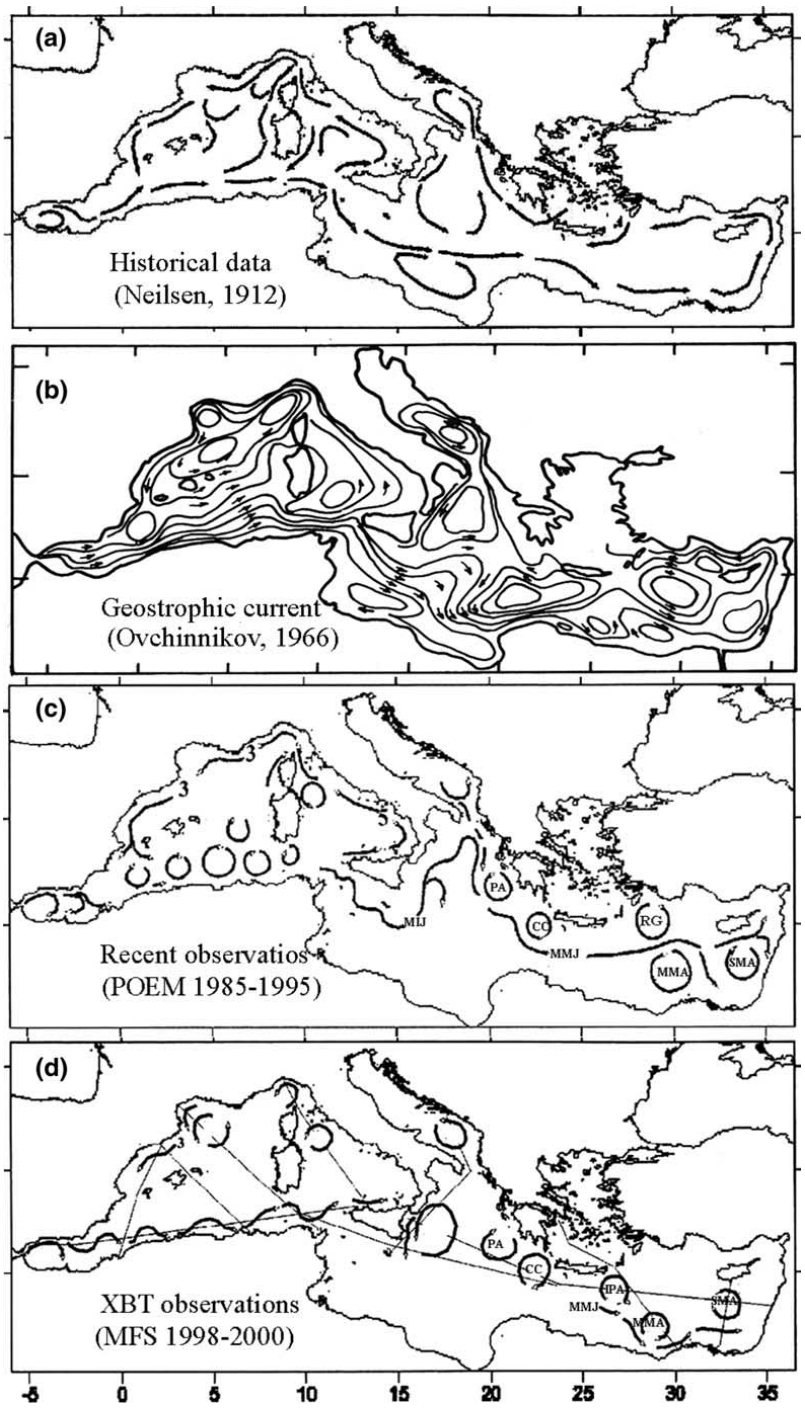

Source: Alhammoud, B., K. Béranger, L. Mortier, M. Crépon, and I. Dekeyser, 2005: Surface circulation of the Levantine Basin: comparison of model results with observations. *Prog.Oceanogr.*, **66**, 299–320.

Figure 37. Circulation Features of the Mediterranean Sea

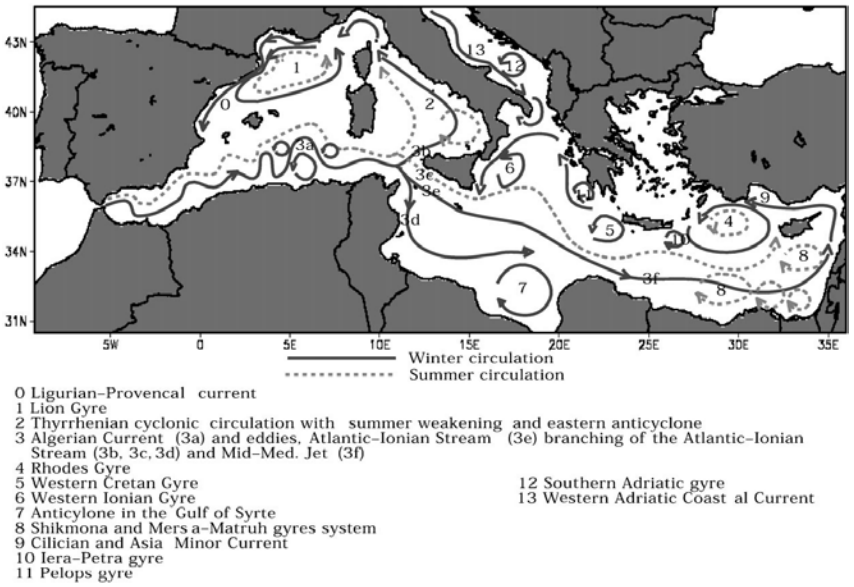

Source: Pinardi, N., E. Masetti, 2000: Variability of the large scale general circulation of the Mediterranean Sea from observations and modelling: a review. *Palaeogeogr., Palaeoclimatol., Palaeoecol.,* **158**, 153–173.

Figure 38. Circulation Features of the Eastern Mediterranean Sea

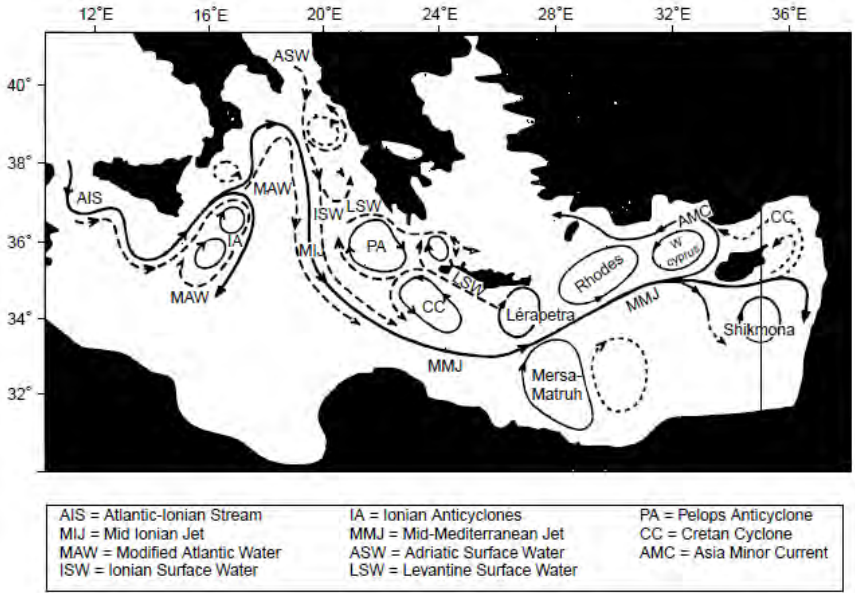

Source: Robinson, A. R., W. G. Leslie, A. Theocharis, and A. Lascaratos, 2001: Mediterranean sea circulation. *Ocean Currents: A Derivative of the Encyclopedia of Ocean Sciences,* 1689–1705, doi:10.1006/rwos.2001.0376.

Figure 39 shows the upper thermocline circulation features of the Eastern Mediterranean Sea. It explains the various observation cruises that were conducted about the Eastern Mediterranean Sea circulation patterns and their results. Circulation features have some characteristics as permanent, transient, and recurrent. Type P represents the permanent features, type R represents the recurrent features and type T represents the transient features. Cyclonic features are represented as C and, anticyclonic features are represented as AC.

Figure 39. Upper Thermocline Circulation Features of the Eastern Mediterranean

Feature	*Type*	*ON85*	*MA86*	*MA87*	*AS87*	*SO91*	*JA95*	*S97*	*ON98*
AIS	*P*	—	—	Y	Y	Y	Y	Y	N
MMC	P	Y	Y	—	Y	Y	Y	—	Y
AMC	P	Y	Y	—	Y	Y	Y	—	Y
CC	R	Y	N	Y	N	—	—	—	—
Se Lev. Jets	T	Y	Y	—	Y	—	—	—	—
Rhodes C	P	Y	Y	—	Y	Y	Y	—	Y
West Cyprus C	P	Y	Y	—	Y	Y	Y	—	—
MMA	P	Y	Y	—	Y	Y	Y	—	Y
Cretan C	P	Y	?	—	Y	Y	—	Y	Y
Shikmona AC	R	Y	Y	—	Y	Y	—	—	—
Latakia C	R	Y	N	N	Y	—	—	—	—
Antalya AC	R	?	Y	—	N	—	—	—	—
Pelops AC	P	—	Y	Y	Y	Y	—	Y	Y
Ionian eddies AC	T	—	—	—	Y	Y	—	Y	N
Cretan Sea eddies	T	Y	Y	—	Y	—	Y	—	Y
Ierapetra	R	Y	N	Y	Y	Y	Y	—	Y

Source: Source: Robinson, A. R., W. G. Leslie, A. Theocharis, and A. Lascaratos, 2001: Mediterranean sea circulation. *Ocean Currents: A Derivative of the Encyclopedia of Ocean Sciences,* 1689–1705, doi:10.1006/rwos.2001.0376.

The results of total mean absolute geostrophic velocity and climatological monthly mean absolute geostrophic velocities at different depths from 1960 to 2013 are seen in Figures 40, 41, 42, and 43, respectively.

Figure 40. Total Mean Absolute Geostrophic Velocity (cm/s) at Various Depths Calculated from the (T, S) Data Using the P-Vector Method

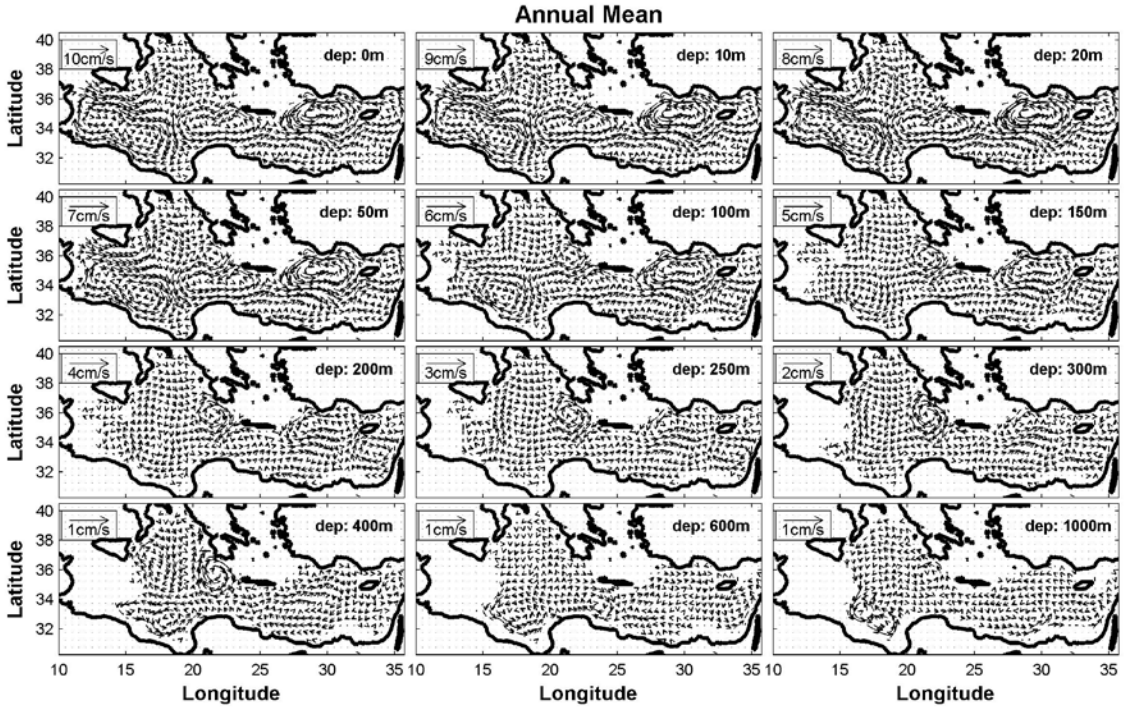

Figure 41. Climatological Monthly Mean Absolute Geostrophic Velocity (cm/s) at the Surface Calculated from the (T, S) Data Using the P-Vector Method

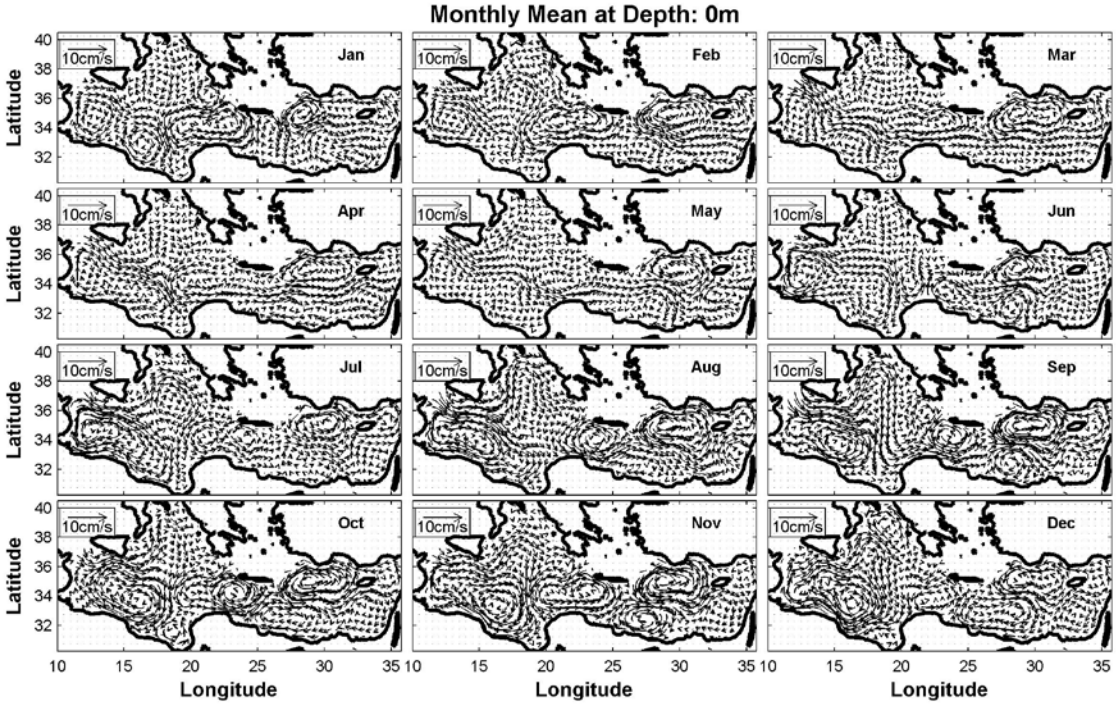

Figure 42. Climatological Monthly Mean Absolute Geostrophic Velocity (cm/s) at 150m Depth Calculated from the (T, S) Data Using the P-Vector Method

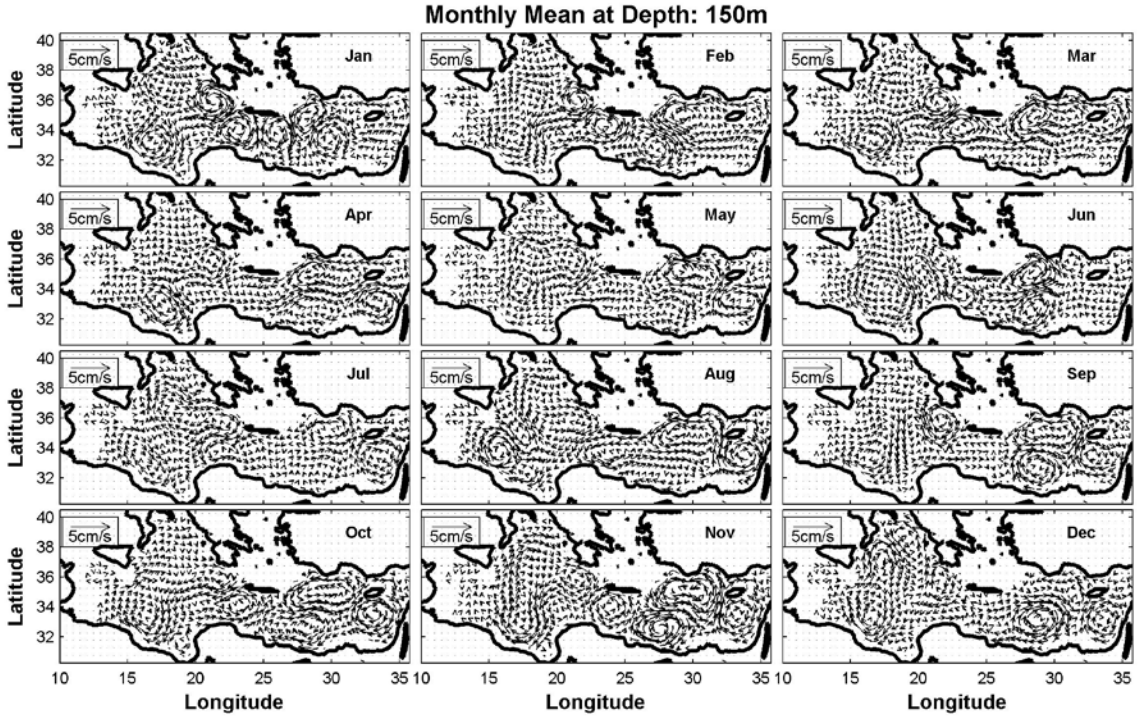

Figure 43. Climatological Monthly Mean Absolute Geostrophic Velocity (cm/s) at 600m Depth Calculated from the (T, S) Data Using the P-Vector Method

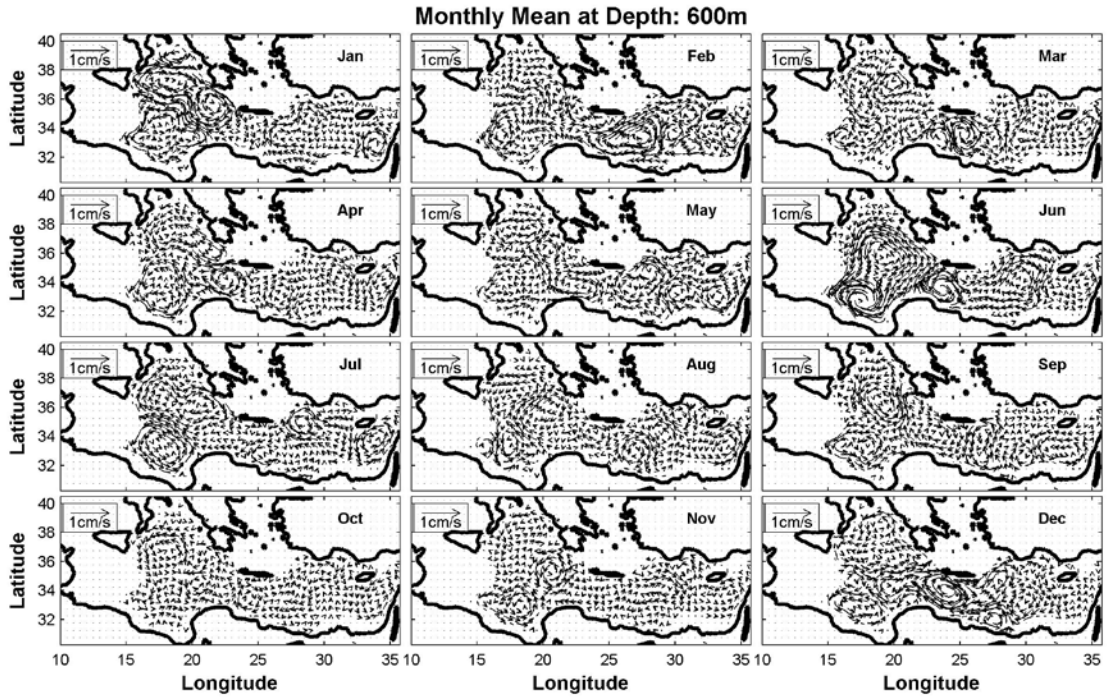

The results of the identified circulation features from the absolute geostrophic velocities of the Eastern Mediterranean Sea are listed in Table 7 for 0–150m depth, in Table 8 for 150–600m depth, and in Table 9 for depths below 600m.

Table 7. Monthly Mean Circulation Features in the Eastern Mediterranean Sea at 0–150m Depth

Feature / Month	Type	Jan	Feb	Mar	Apr	May	Jun	Jul	Aug	Sep	Oct	Nov	Dec
Atlantic Ionian Stream	P	Y	Y	Y	Y	Y	N	Y	Y	Y	Y	Y	Y
MM Jet/Current	P	Y	Y	Y	Y	Y	N	Y	Y	Y	Y	Y	Y
Asia Minor Current	P	Y	Y	Y	Y	Y	Y	Y	Y	Y	Y	Y	Y
Cilician Current	R	Y	Y	Y	Y	Y	Y	Y	Y	Y	Y	Y	Y
Rhodes C	P	Y	Y	Y	Y	Y	Y	Y	Y	Y	Y	Y	Y
West Cyprus C	P	Y	Y	Y	Y	Y	Y	Y	Y	Y	Y	Y	Y
Mersa-Matruh AC	P	Y	Y	N	Y	Y	Y	Y	Y	Y	Y	Y	Y
Cretan C	P	Y	Y	Y	Y	Y	Y	Y	Y	Y	Y	Y	Y
Shikmona AC	R	Y	N	N	Y	Y	Y	Y	Y	Y	Y	Y	Y
Latakia C	R	N	N	N	Y	Y	Y	Y	Y	Y	Y	Y	Y
Pelops AC	P	Y	Y	Y	Y	Y	Y	Y	Y	Y	Y	Y	Y
Ionian AC	T	Y	Y	Y	Y	Y	N	Y	N	N	N	Y	Y
Ierapetra AC	R	Y	Y	N	N	N	N	N	N	N	N	N	N
Cretan Sea Eddies	T	Y	Y	Y	N	Y	N	Y	Y	Y	Y	Y	Y

Table 8. Monthly Mean Circulation Features in the Eastern Mediterranean Sea at 150–600m Depth

Feature / Month	Type	Jan	Feb	Mar	Apr	May	Jun	Jul	Aug	Sep	Oct	Nov	Dec
Atlantic Ionian Stream	P	Y	Y	Y	N	N	N	N	N	N	N	N	N
MM Jet/Current	P	N	Y	Y	Y	N	N	N	N	N	N	N	N
Asia Minor Current	P	Y	Y	Y	Y	Y	N	N	N	N	N	N	N
Cilician Current	R	Y	Y	Y	Y	Y	N	N	N	N	N	N	N
Rhodes C	P	Y	Y	Y	Y	Y	Y	Y	Y	Y	Y	Y	N
West Cyprus C	P	Y	Y	Y	Y	Y	Y	Y	Y	Y	Y	Y	N
Mersa-Matruh AC	P	Y	Y	N	N	Y	Y	N	Y	Y	Y	Y	Y
Cretan C	P	Y	Y	Y	Y	Y	Y	Y	Y	N	Y	Y	Y
Shikmona AC	R	Y	N	N	Y	Y	Y	Y	Y	Y	Y	Y	Y
Latakia C	R	Y	Y	Y	Y	Y	Y	Y	N	N	N	N	N
Pelops AC	P	Y	Y	Y	Y	Y	Y	Y	Y	Y	Y	Y	Y
Ionian AC	T	Y	Y	Y	Y	Y	N	Y	N	N	N	Y	Y
Ierapetra AC	R	Y	Y	N	N	N	N	N	N	N	N	N	N
Cretan Sea Eddies	T	Y	Y	Y	Y	Y	N	Y	Y	N	Y	Y	Y

Table 9. Monthly Mean Circulation Features in the Eastern Mediterranean Sea at Depths below 600m

Feature / Month	Type	Jan	Feb	Mar	Apr	May	Jun	Jul	Aug	Sep	Oct	Nov	Dec
Atlantic Ionian Stream	P	N	N	N	N	N	N	N	N	N	N	N	N
MM Jet/Current	P	N	N	N	N	N	N	N	N	N	N	N	N
Asia Minor Current	P	N	N	N	N	N	N	N	N	N	N	N	N
Cilician Current	R	N	N	N	N	N	N	N	N	N	N	N	N
Rhodes C	P	N	N	N	N	N	N	N	N	N	N	N	N
West Cyprus C	P	N	N	N	N	N	N	N	N	N	N	N	N
Mersa-Matruh AC	P	N	N	N	N	N	N	N	N	N	N	N	N
Cretan C	P	N	N	N	N	N	N	N	N	N	N	N	N
Shikmona AC	R	N	N	N	N	N	N	N	N	N	N	N	N
Latakia C	R	N	N	N	N	N	N	N	N	N	N	N	N
Pelops AC	P	N	N	N	N	N	N	N	N	N	N	N	N
Ionian AC	T	N	N	N	Y	N	N	N	Y	N	N	N	N
Ierapetra AC	R	N	N	N	N	N	N	N	N	N	N	N	N
Cretan Sea Eddies	T	Y	N	Y	Y	Y	Y	Y	N	N	Y	Y	Y

It is observed that the circulation features weakens as depth goes down. Some of the features are still existent in some months at the 150–600m depth, whereas the majority of the features are not existent at the depths below 600m. However, there might be some other features induced by changing atmospheric factors and thermohaline forcing.

D. HEAT CONTENT

1. Surface Layer (0 – 150m)

Figure 44 shows the monthly variability of heat content at the surface layer. The heat content variability is nearly zero with exception of Gulf of Gabes in December. From December to April, variability is negative with values of between $-0.4 \times 10^9 J/m^2$ and $-1.4 \times 10^9 J/m^2$. June shows transition characteristics between negative and positive heat content variabilities, while May shows slightly negative heat content variability. From beginning of June to September, heat content variability shows a positive pattern. Heat content variability increases from $0.2 \times 10^9 J/m^2$ to $1.6 \times 10^9 J/m^2$ between June and September. Heat content at the surface layer explicitly shows seasonal variability.

Figure 44. Monthly Variability of Heat Content (J/m^2) at the Surface Layer

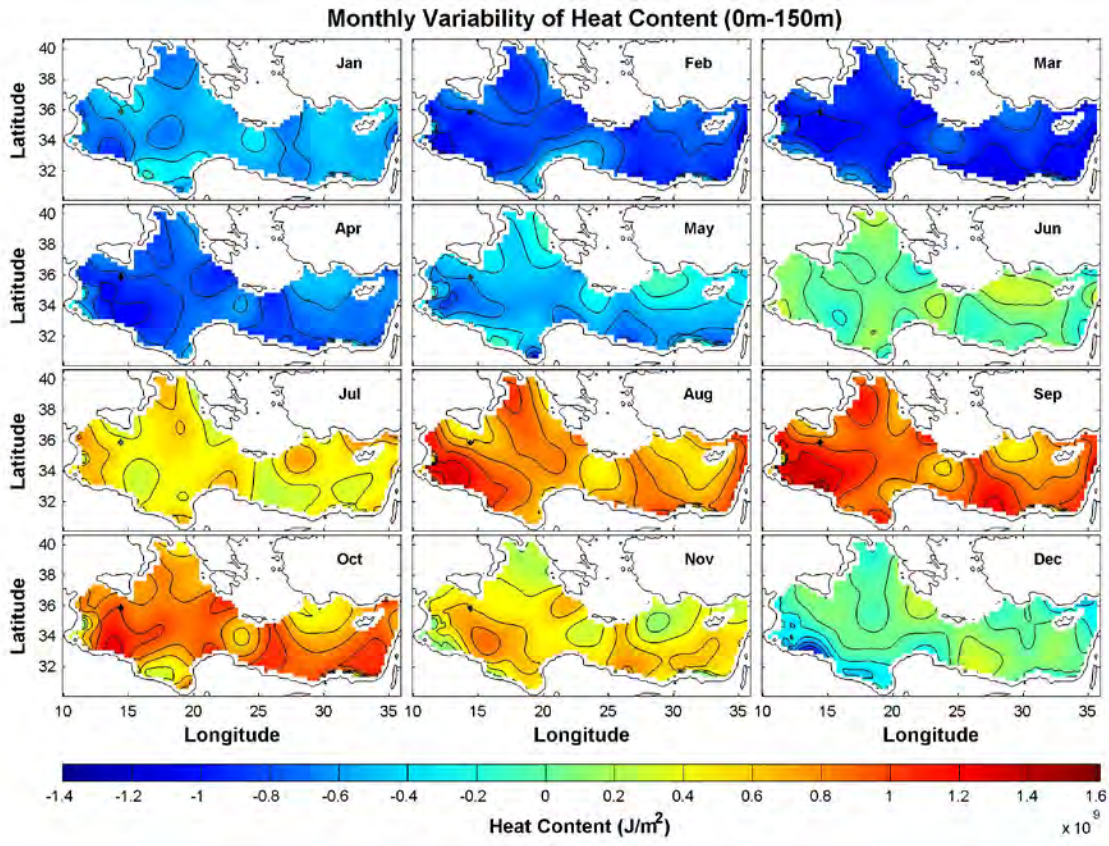

2. Intermediate Layer (150 – 600m)

Figure 45 shows the monthly variability of heat content at the intermediate layer. At a quick glance to heat content variability for all months, it is observed that heat content variability is slightly up or down on the zero contour line, which means that the heat content difference is almost zero with exceptions in some specific areas such as at the corner between Turkey and Syria, and at around the Gulf of Sidra in Libya. There is no observed significant heat content variability at the intermediate layer.

Figure 45. Monthly Variability of Heat Content (J/m^2) at the Intermediate Layer

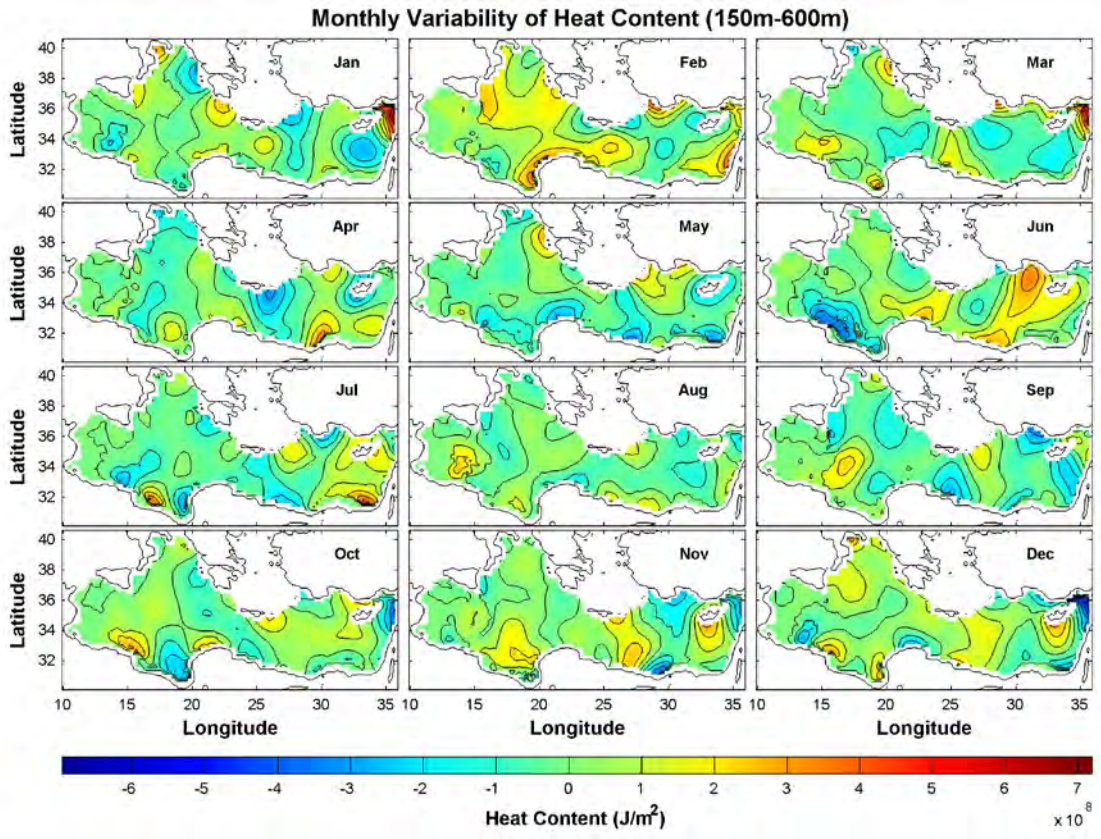

3. Deep Layer (600m - Bottom)

Figure 46 shows the monthly variability of heat content at the deep layer. The entire basin almost shows a negative heat content variability pattern with some fluctuations in February, June and July.

When the three different layers are compared at once, it is seen that the surface layer is the most sensitive one to the heat content variability that is affected by the external mechanisms such as winds, solar heating, and winter cooling. As the depth increases through the intermediate and deep layers, monthly heat content and annual heat content nearly balances each other. Thus, very slight variation in the heat content is observed at the both intermediate and deep layers. It is observed that there is almost no seasonal heat content variability at the deep layer.

Figure 46. Monthly Variability of Heat Content (J/m^2) at the Deep Layer

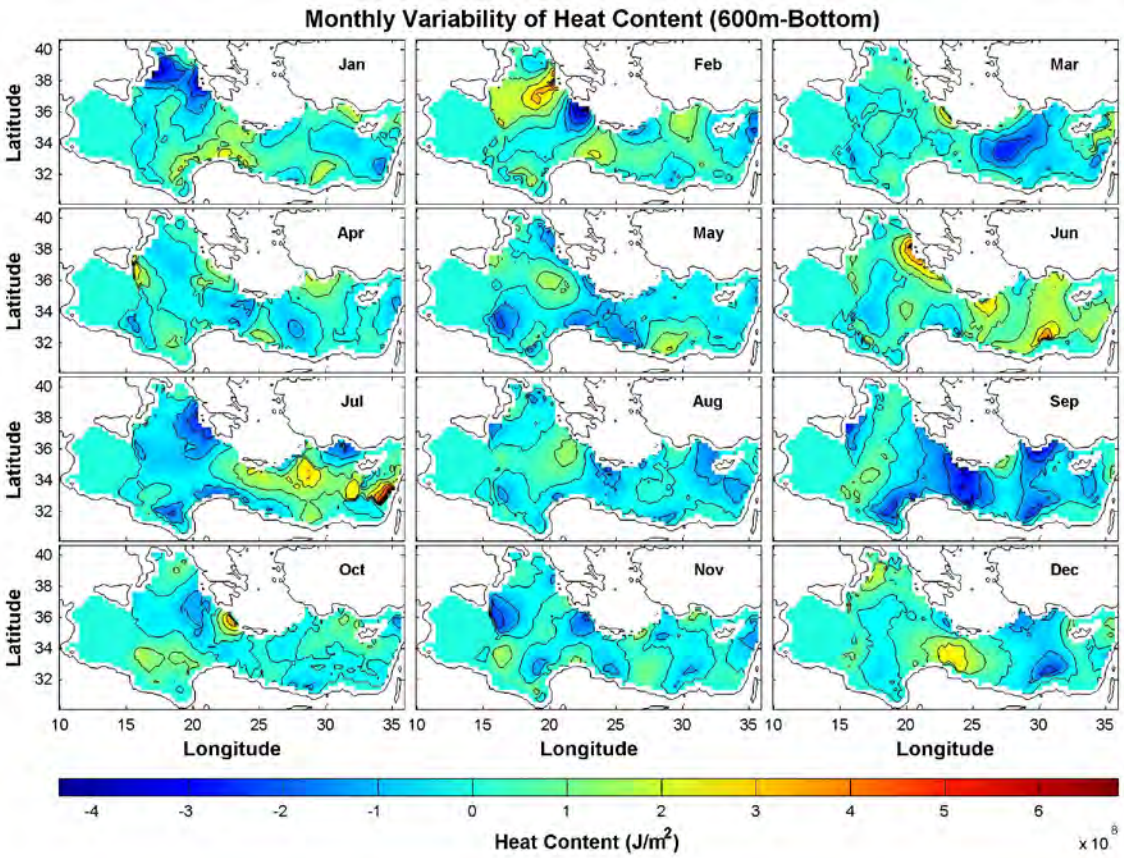

E. FRESHWATER CONTENT

1. Surface Layer (0 – 150m)

Freshwater content is obtained by taking the difference of the present and reference salinities and divided by the reference salinity, which is 40 psu. Then, it is integrated through the layer depth. After the integration, freshwater content is obtained in meter unit. Figure 47 shows the monthly variability of freshwater content at the surface layer.

Figure 47. Monthly Variability of Freshwater Content (m) at the Surface Layer

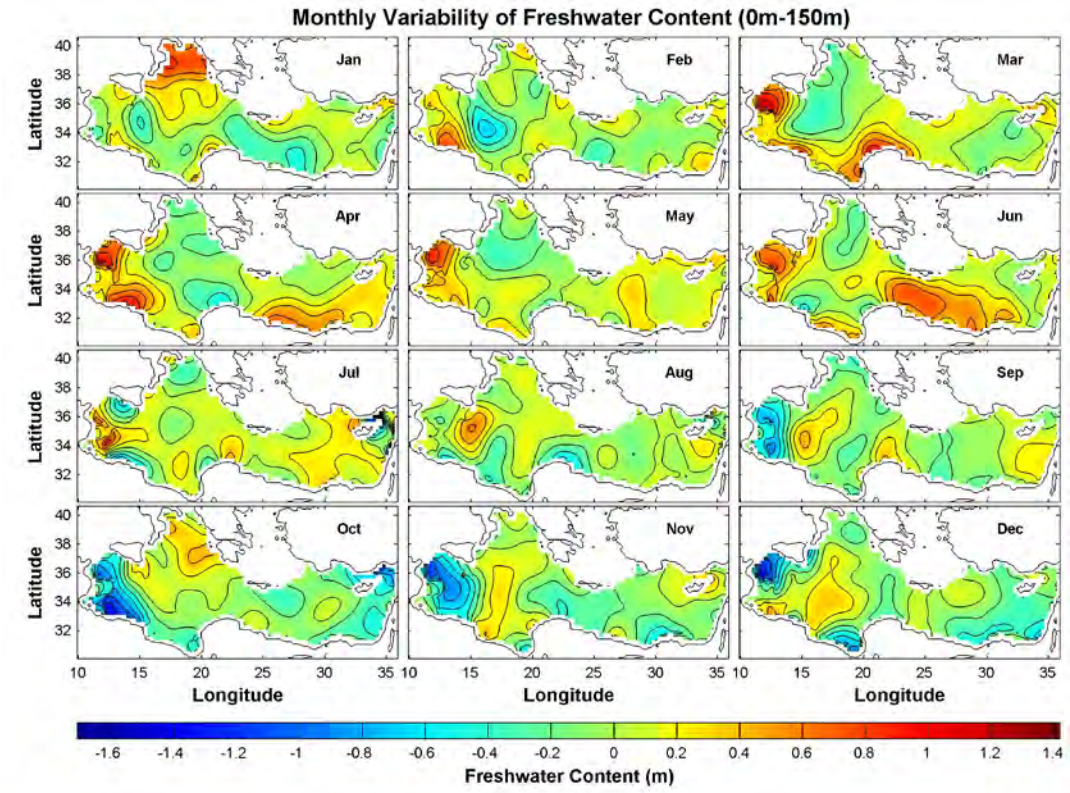

From January to June, the variability of freshwater content is in slightly positive values almost through the basin and in much positive values in the entrance of Adriatic Sea, and at the Strait of Sicily. From July to December, it seems that the variability of freshwater content shifted reversely from positive to negative values roughly for the same locations.

The maximum freshwater content variability is observed in March and April at the Strait of Sicily, whereas the minimum freshwater content variability is observed in October at the Gulf of Gabes, which is located at the coast of Tunisia and in December at the Strait of Sicily.

2. Intermediate Layer (150 – 600m)

Figure 48 shows the monthly variability of freshwater content at the intermediate layer. It is observed that nearly entire basin shows a negative freshwater content variability for all months except August with a very minor location around the Tripoli. The general pattern expresses that the monthly mean freshwater content falls behind the annual mean freshwater content.

Figure 48. Monthly Variability of Freshwater Content (m) at the Intermediate Layer

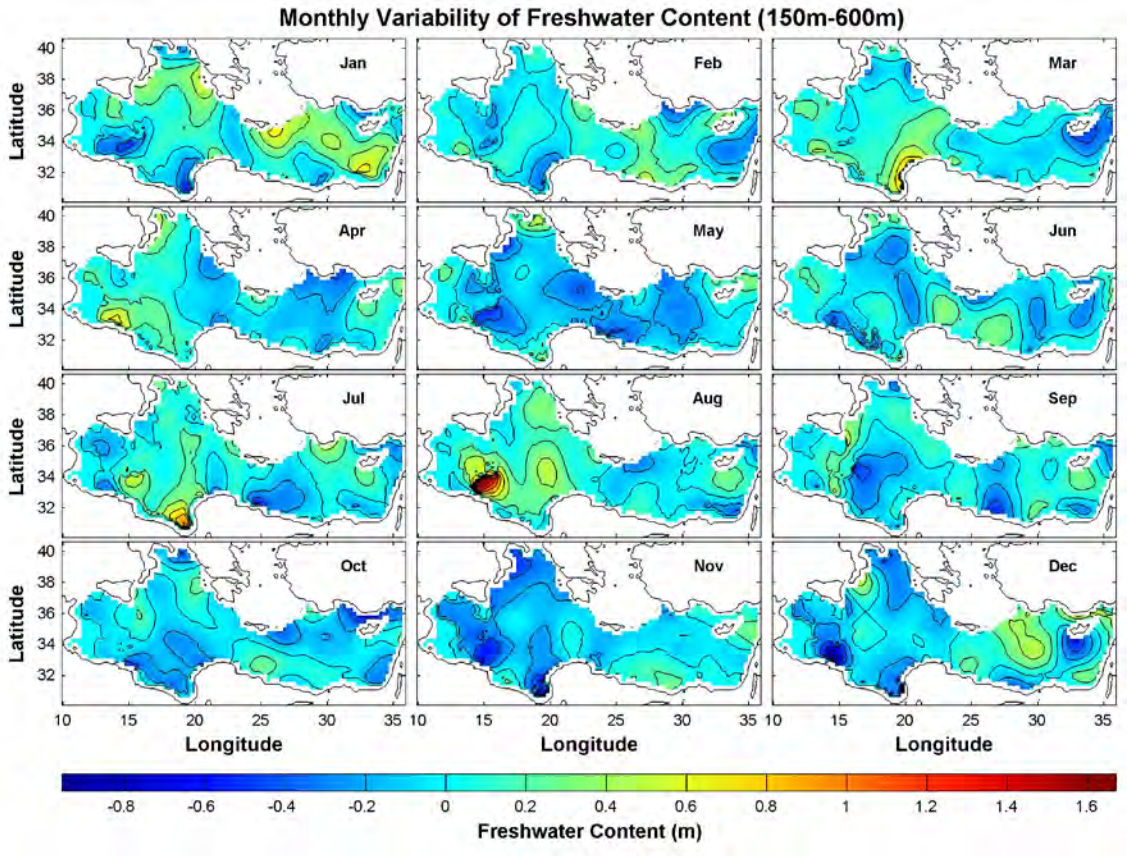

3. Deep Layer (600m – Bottom)

Figure 49 shows the monthly variability of freshwater content at the deep layer. It is observed that there is not a stable pattern of freshwater content monthly variability through the entire basin. July draws attention about high positive freshwater content

variability in the Ionian Sea, whereas May and June shows a high negative freshwater content variability in the same area.

Figure 49. Monthly Variability of Freshwater Content (m) at the Deep Layer

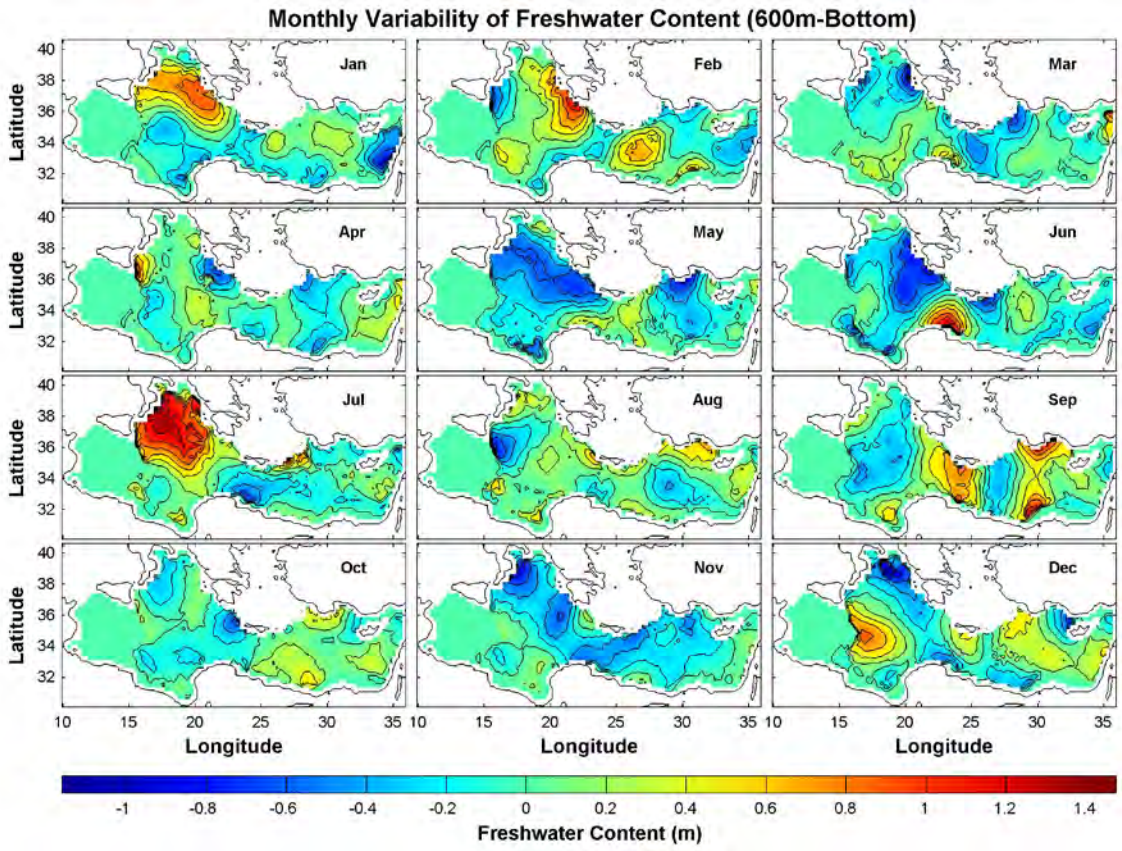

VI. INTERANNUAL VARIABILITY

Empirical Orthogonal Function (EOF) method is used in this chapter to be able to analyze the inter-annual variability of heat content and freshwater content in three layers. Each mode represents a percentage of variance. In this study, we focus on the first three modes, which totally cover almost 45% of the variances. Inter-annual variability focuses on anomalies that occur from one year to another. So, it provides information about yearly changes for a long time-series. In this study, inter-annual variability is searched for 54 years, from 1960 to 2013.

A. FIRST THREE EOF MODES OF HEAT CONTENT ANOMALIES FOR THREE LAYERS

EOF mode-1 covers nearly 28% of the time changes of variance for the Eastern Mediterranean Sea. Figure 50 shows the EOF mode-1 and associated Principal Component-1 (PC-1) for three layers. EOF mode-1 represents the spatial variation, while the PC-1 represents the temporal variation and related amplitudes. According to the temporal amplitude, it can be interpreted that in which area's heat content strengthens, while the other area's heat content weakens. At the surface layer, the maximum anomaly of heat content is observed around the Crete. The PC amplitude maximum is observed nearly in 1993 with a negative sign, whereas the PC amplitude maximum is seen nearly in 2012 with a positive sign. Heat content anomaly in a point is determined by multiplying the EOF values and PC amplitudes. For instance, heat content around the Crete in 1993 decreases with a value of (0.03) X (-20 x $10^9 J/m^2$) = -0.6 x $10^9 J/m^2$. However, same spot's heat content in 2012 increases with a value of (0.03) X (+20 x $10^9 J/m^2$) = +0.6 x $10^9 J/m^2$. The red contour line shows the zero magnitude, where there is almost no heat content anomaly for the areas around that line. For temporal pattern, heat content anomaly is positive from 1960 to 1983 with some exceptions such as 1966, 1968, and 1977. Positive heat content anomaly means that heat content increases within that period. From 1980 to 2000, heat content anomaly is negative, which means that heat content decreases. From 2000 to 2013, heat content anomaly is positive again, which means that heat content increases.

At the intermediate layer, the peak heat content anomaly occurs around the Crete with extended coverage. The area, where peak heat content anomaly occurs, runs from south-west coast of Greece to east of Crete. In this area, the darkest red contour expresses that the magnitude of the heat content anomaly is larger than the same area at the surface layer. At the deep layer, it is observed that there is almost no heat content anomaly through the years.

Figure 50. EOF Mode-1 and PC-1 of Surface Layer (0-150m), Intermediate Layer (150-600m) and Deep Layer (600-bottom) Heat Content (J/m^2)

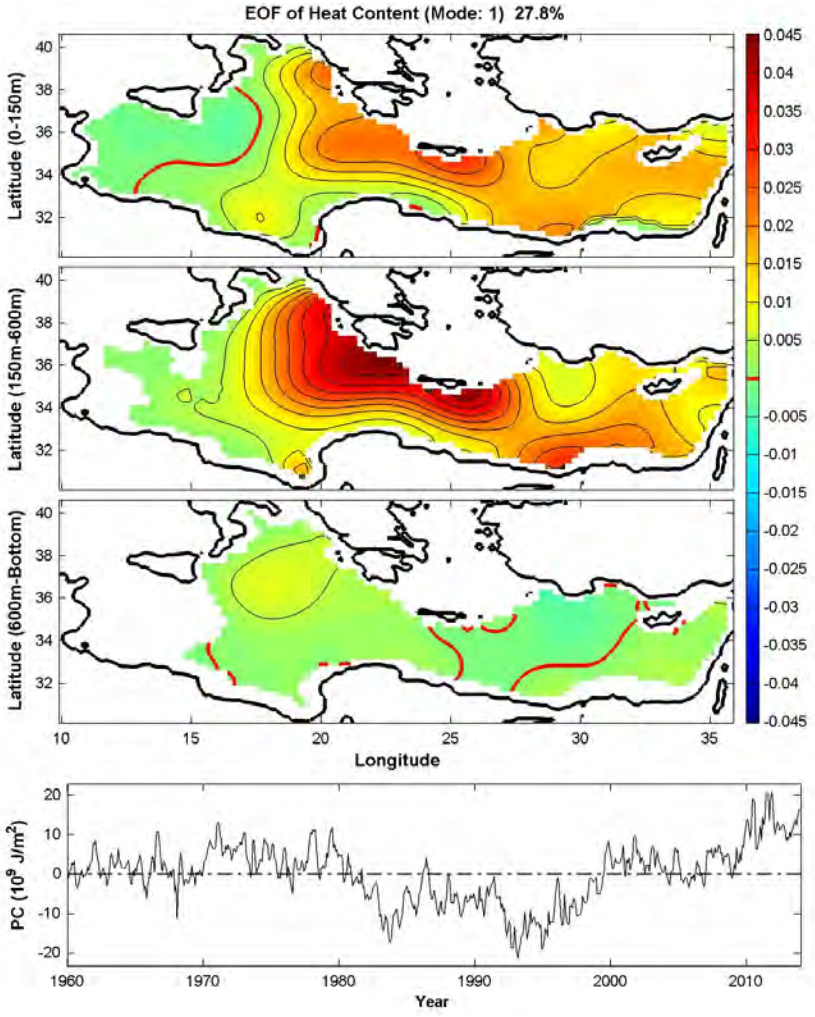

Figure 51 and Figure 52 show the EOF mode-2 and EOF mode-3, respectively. The idea about defining the heat content anomaly behind these modes is same with the EOF mode-1. These modes represent the less coverage of the time change of variances. The surface layer in the EOF mode-2 shows almost an opposite characteristic with the surface layer in the EOF mode-1. The EOF mode-2 heat content anomaly at the surface layer shows negative trend, whereas the EOF mode-1 heat content anomaly at the surface layer shows positive trend.

Figure 51. EOF Mode-2 and PC-2 of Surface Layer (0-150m), Intermediate Layer (150-600m) and Deep Layer (600-bottom) Heat Content (J/m^2)

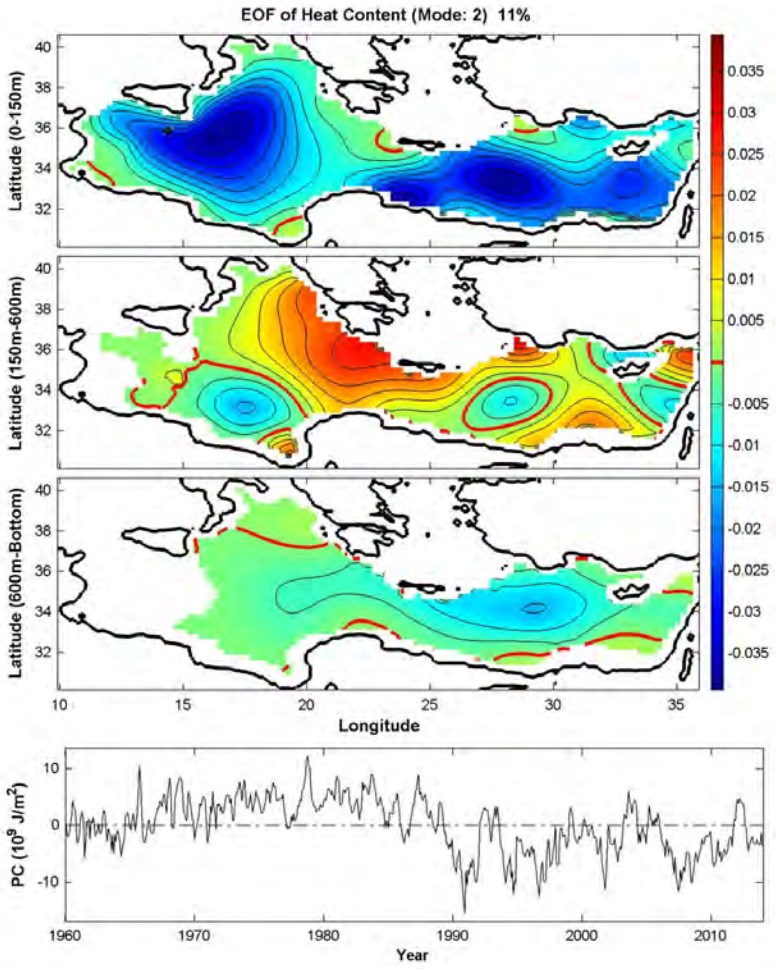

Figure 52. EOF Mode-3 and PC-3 of Surface Layer (0-150m), Intermediate Layer (150-600m) and Deep Layer (600-bottom) Heat Content (J/m^2)

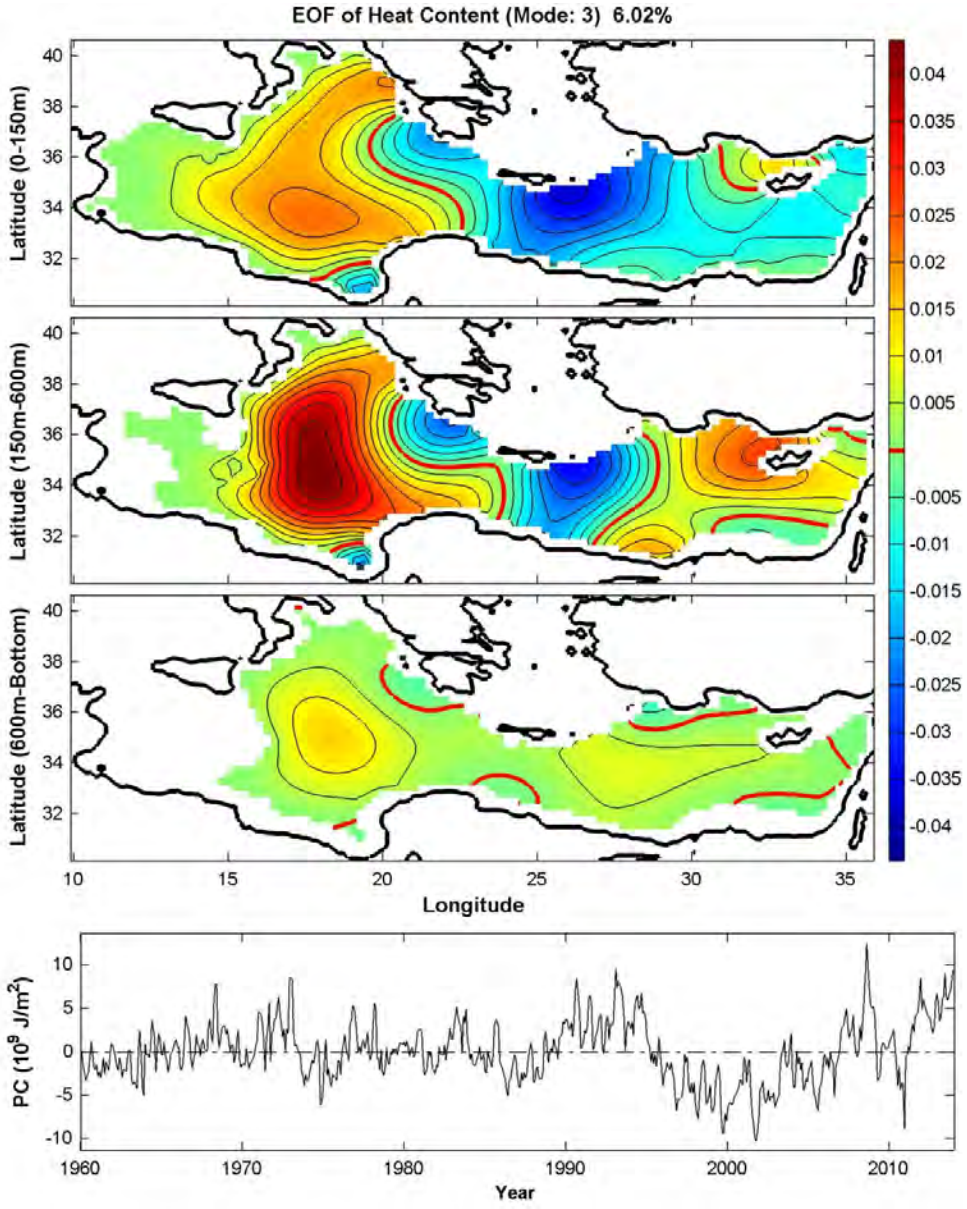

B. FIRST THREE EOF MODES OF FRESHWATER CONTENT ANOMALIES FOR THREE LAYERS

EOF mode-1 covers nearly 25% of the time changes of variance for the Eastern Mediterranean Sea. Figure 53 shows the EOF mode-1 and Principal Component-1 (PC-1) for three layers. EOF mode-1 represents the spatial variation, while the PC-1 represents the temporal variation and related amplitudes.

At the surface layer, the maximum anomaly of freshwater content is observed in the Ionian Sea, between south-west coast of Greece and Malta. At a quick glance, the temporal amplitude is observed as maximum nearly in 2013 with a negative sign, whereas the temporal amplitude is observed as maximum nearly in 1972 with a positive sign. Freshwater content anomaly in a point is determined by multiplying the EOF values and PC amplitudes. For instance, freshwater content around the Sparta in 2013 decreases with a value of (0.015) X (-30 m) = -0.45m. However, same spot's freshwater content in 1972 increases with a value of (0.015) X (+60m) = +0.9m. The red contour line shows the zero magnitude, where there is almost no freshwater content anomaly for the areas around that line. For temporal pattern until 2005, freshwater content fluctuates between positive and negative values with some positive exceptions such as 1972, 1974, and 1992. Positive freshwater content anomaly means that freshwater content increases within that period. From 2005 to 2013, freshwater content anomaly is negative, which means that freshwater content decreases within that period. At the intermediate layer, the peak freshwater content anomaly develops in the middle of the Ionian Sea. West of the Cyprus is another significant spot that freshwater content anomaly is important. In this area, the darkest red contour expresses that the magnitude of the freshwater content is larger than the same area for the surface layer. At the deep layer, it is observed that magnitude of the freshwater content increases in the core of Ionian Sea and in the center of the West Cyprus' contour. Freshwater content anomaly at deep layer is larger than both surface layer and intermediate layers. Figure 54 and Figure 55 show the EOF mode-2 and EOF mode-3, respectively. The idea about defining the freshwater content anomaly behind these modes is same with the EOF mode-1. These modes represent the less coverage of the time change of variances.

In the Levantine basin, freshwater content anomaly at the deep layer is much positive than both at the intermediate and at the surface layers' freshwater content anomalies for EOF mode-1, whereas the structure is reverse for EOF mode-2.

Figure 53. EOF Mode-1 and PC-1 of Surface Layer (0-150m), Intermediate Layer (150-600m) and Deep Layer (600-bottom) Freshwater Content (m)

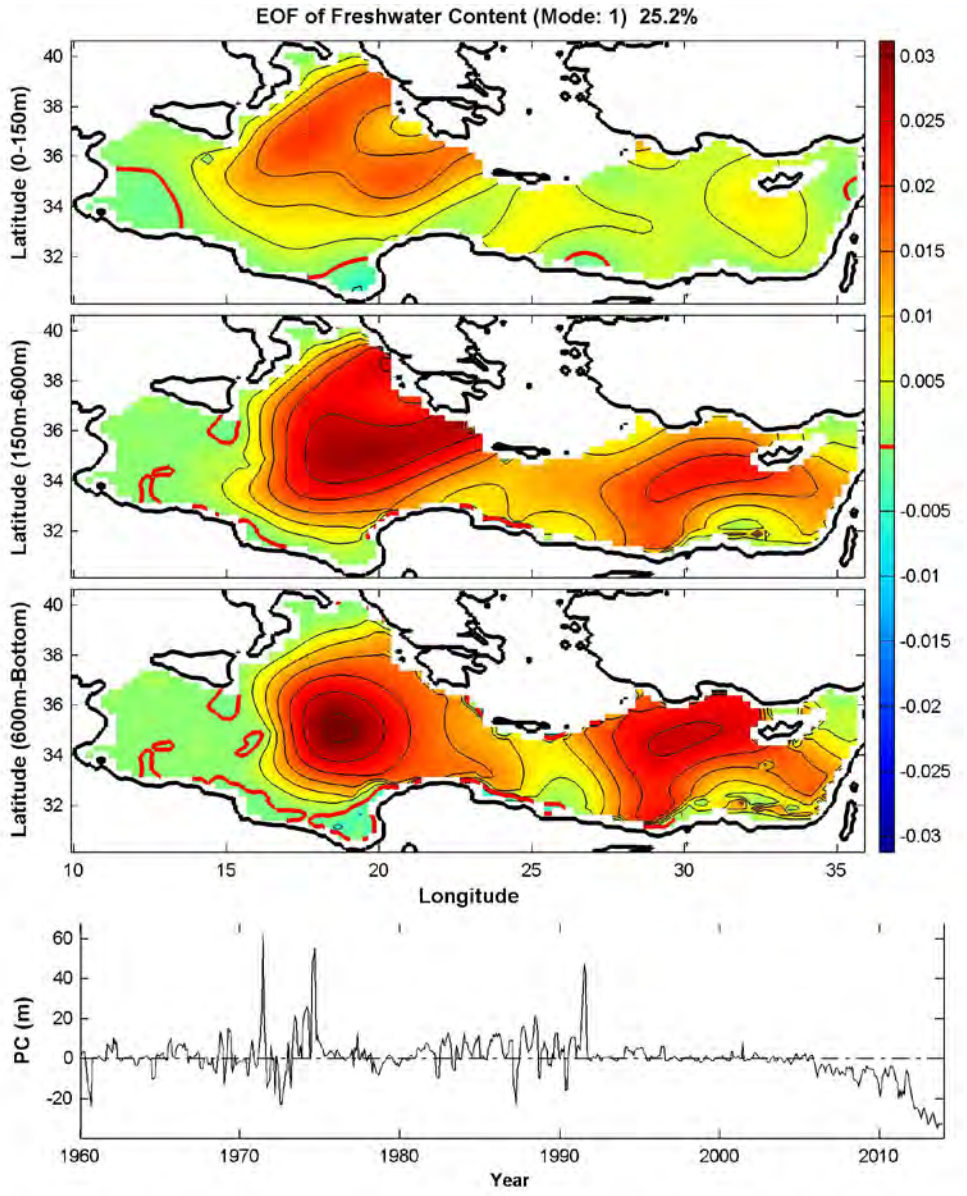

Figure 54. EOF Mode-2 and PC-2 of Surface Layer (0-150m), Intermediate Layer (150-600m) and Deep Layer (600-bottom) Freshwater Content (m)

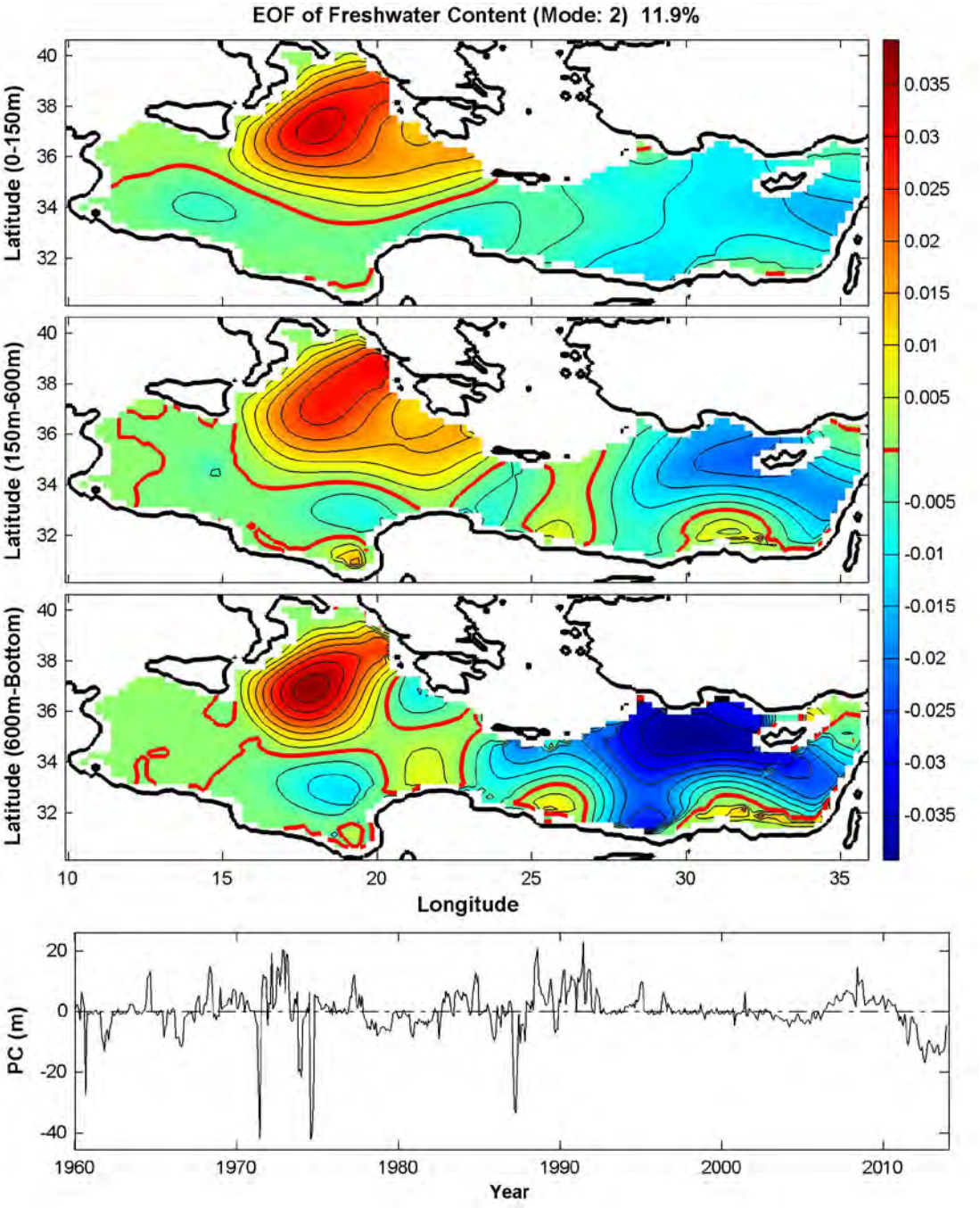

Figure 55. EOF Mode-3 and PC-3 of Surface Layer (0-150m), Intermediate Layer (150-600m) and Deep Layer (600-bottom) Freshwater Content (m)

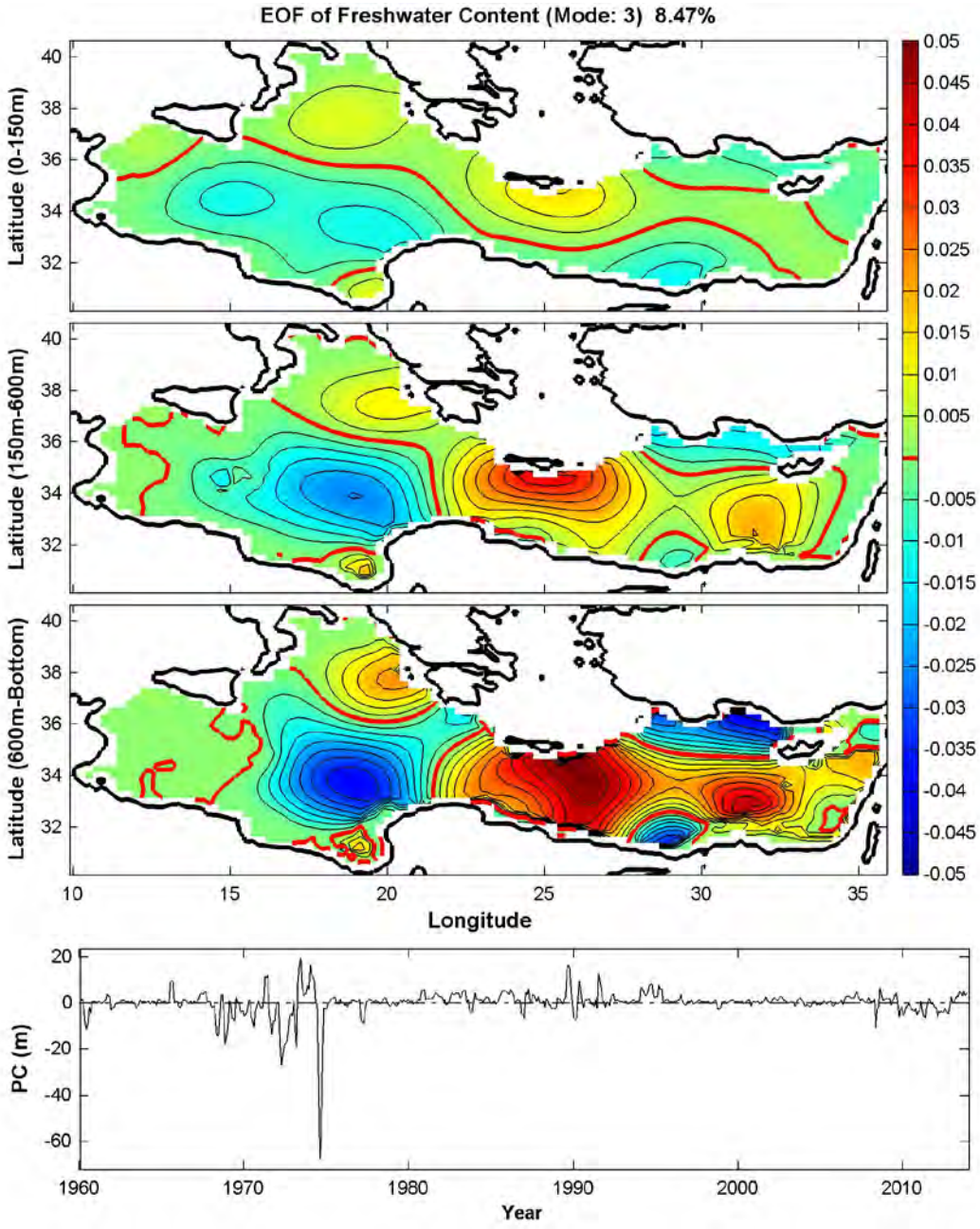

VII. CONCLUSIONS AND FUTURE RECOMMENDATIONS

A. CONCLUSIONS

The data, which were used in this thesis, were obtained from World Ocean Database 2013 (WOD13). The optimal spectral decomposition (OSD) method was used to establish the synoptic monthly varying three-dimensional gridded temperature and salinity data with 0.25°x0.25° horizontal resolution and 57 vertical depth levels. The analysis included 164,906 temperature profiles and 53,606 salinity profiles. After the establishment of gridded data, the seasonal and inter-annual variability of thermohaline structure and circulation of the Eastern Mediterranean Sea were investigated from January 1960 to December 2013.

Sea surface temperature increases from west to east and decreases from south to north. Sea surface shows high seasonal temperature variability, whereas the depths below surface show slight seasonal variation, relatively. Sea surface salinity increases from west to east. There is almost no seasonal salinity variability in winter and spring seasons, while the summer and fall seasons show slight seasonal variation at the surface. Below surface, there is no seasonal variation. Sea surface absolute geostrophic velocity shows high seasonal variability in circulation features. Below the surface, absolute geostrophic velocity weakens and features change their structures along with their magnitudes.

EOF analyses were studied for inter-annual variability of heat content and freshwater content anomalies. For heat content, the intermediate layer heat content anomaly is larger than the surface layer. However, inter-annual variability of heat content anomaly at the deep layer is very weak. For freshwater content, the deep layer and intermediate layer show similar freshwater content anomalies and both of them are larger than the surface layer. It is observed that heat content anomalies are much evident and noteworthy than freshwater content anomalies.

B. FUTURE RECOMMENDATIONS

The Western Mediterranean Sea is the counter-part of the Eastern Mediterranean Sea. Atlantic Water (AW) provides freshwater flux and heat flux to the Eastern Mediterranean Sea through the Strait of Gibraltar. The circulation patterns, salinity, and temperature variations in the Eastern Mediterranean Sea are widely affected by the Western Mediterranean Sea. Thus, the Western Mediterranean Sea should be studied at the same time with the Eastern Mediterranean Sea to be able to infer much clear and detailed result.

In this thesis, observational data was used. The research of ocean variability depends on both studies with observational data and modeling studies. Sometimes, the observational datasets may be insufficient or separated temporally and spatially. Thus, it may not allow us to make detailed research about the mechanisms that drive the variability of the Eastern Mediterranean Sea. So, a modeling study along with the observational data studies may be useful in order to have a better understanding.

The Adriatic Sea and Aegean Sea are the other components of the Eastern Mediterranean Sea. For better results, those seas should be included in the future researches.

Freshwater content anomaly shows a negative pattern, while the heat content anomaly shows a positive pattern since 2005. This might be due to the global warming and climate change. Thus, a further study may be useful to be able to interpret this relation.

APPENDIX A. MONTHLY MEAN TEMPERATURE AT DIFFERENT DEPTHS

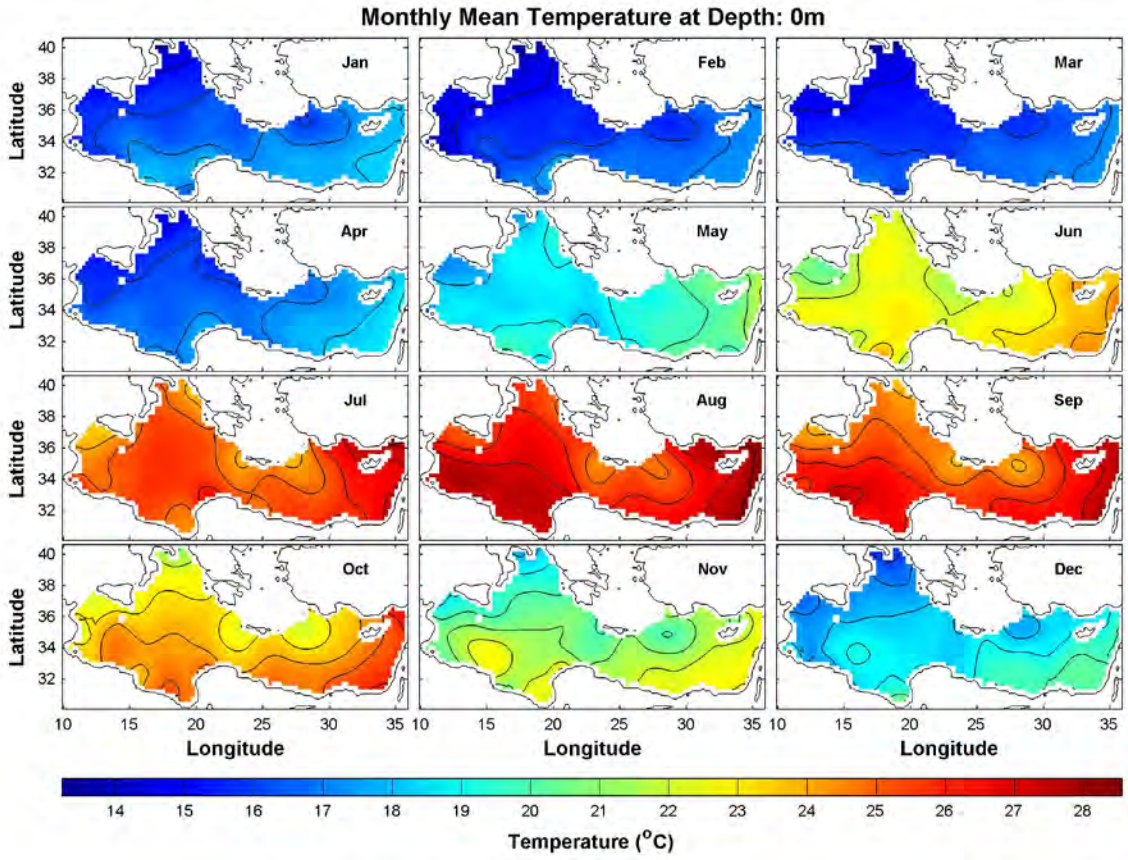

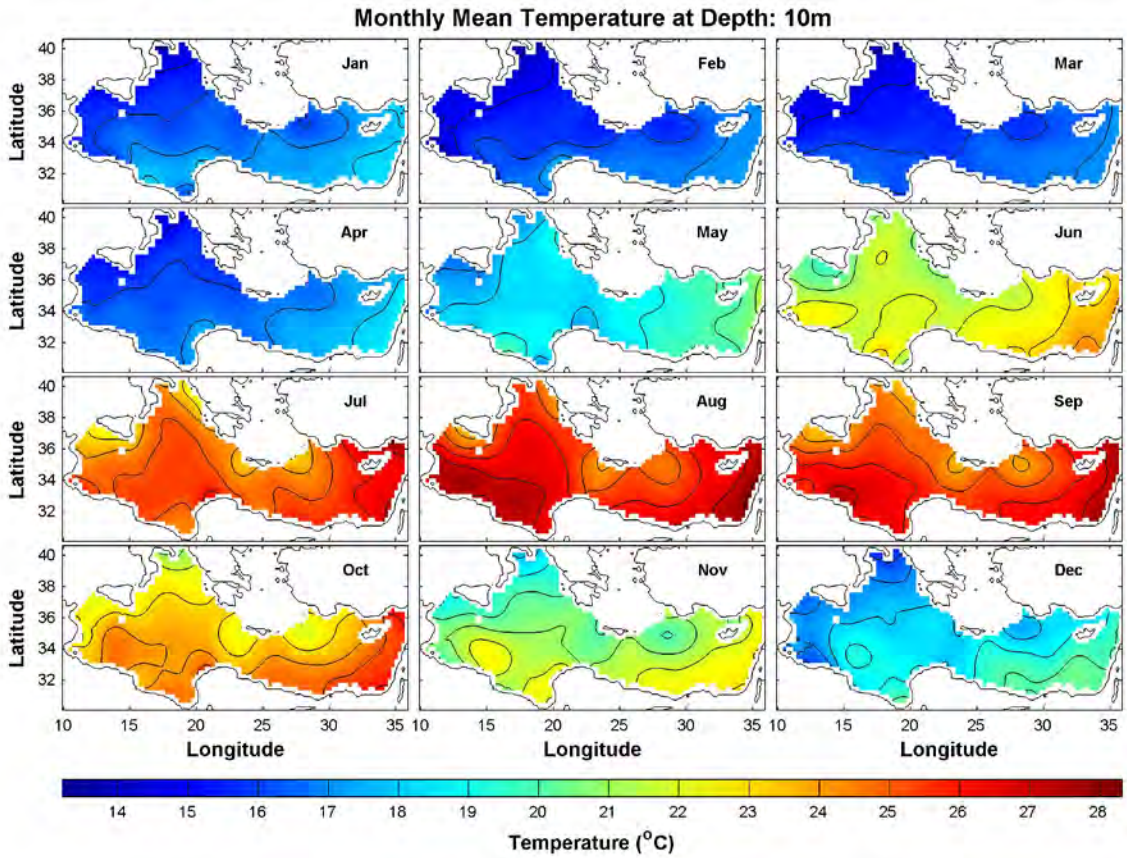
Monthly Mean Temperature at Depth: 10m
Jan
Feb
Mar
Apr
May
Jun
Jul
Aug
Sep
Oct
Nov
Dec
Latitude
Longitude
40
38
36
34
32
10
15
20
25
30
35
14
15
16
17
18
19
20
21
22
23
24
25
26
27
28
Temperature (°C)

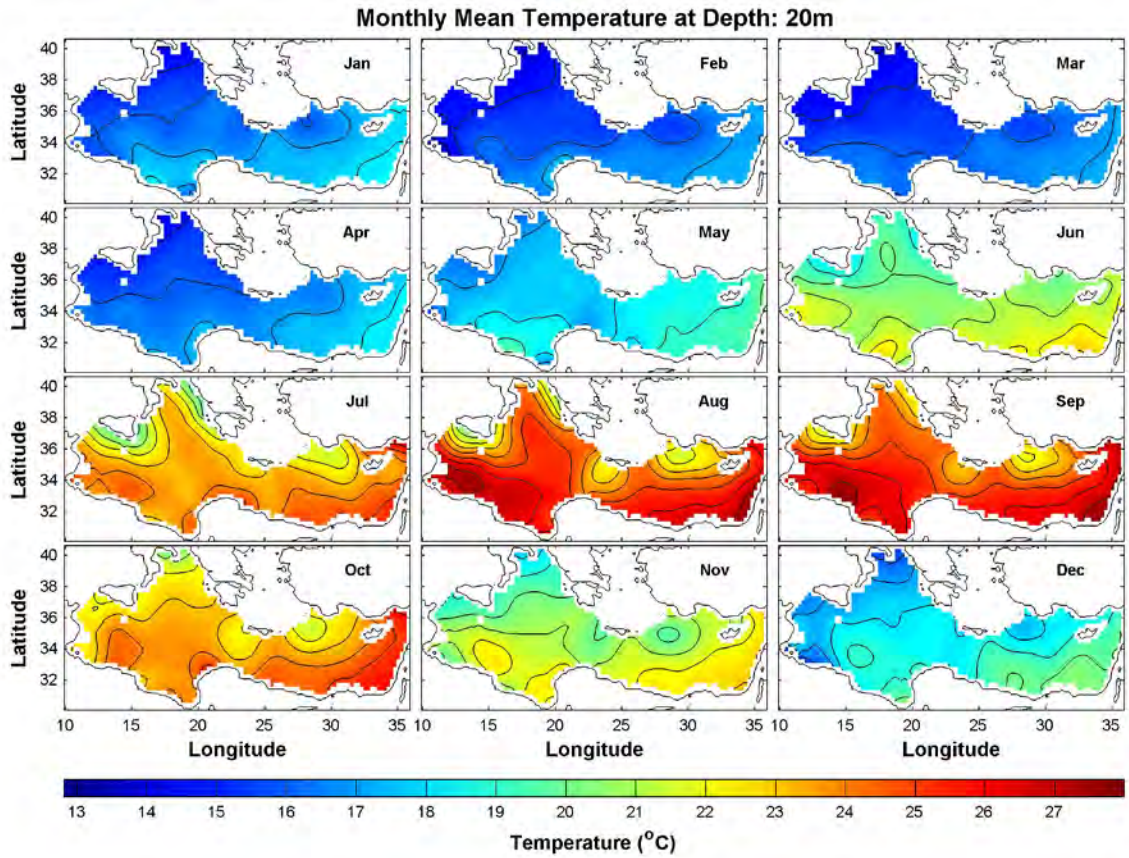
Monthly Mean Temperature at Depth: 20m
Jan
Feb
Mar
Apr
May
Jun
Jul
Aug
Sep
Oct
Nov
Dec
Latitude
Longitude
40
38
36
34
32
10
15
20
25
30
35
13
14
15
16
17
18
19
20
21
22
23
24
25
26
27
Temperature (°C)

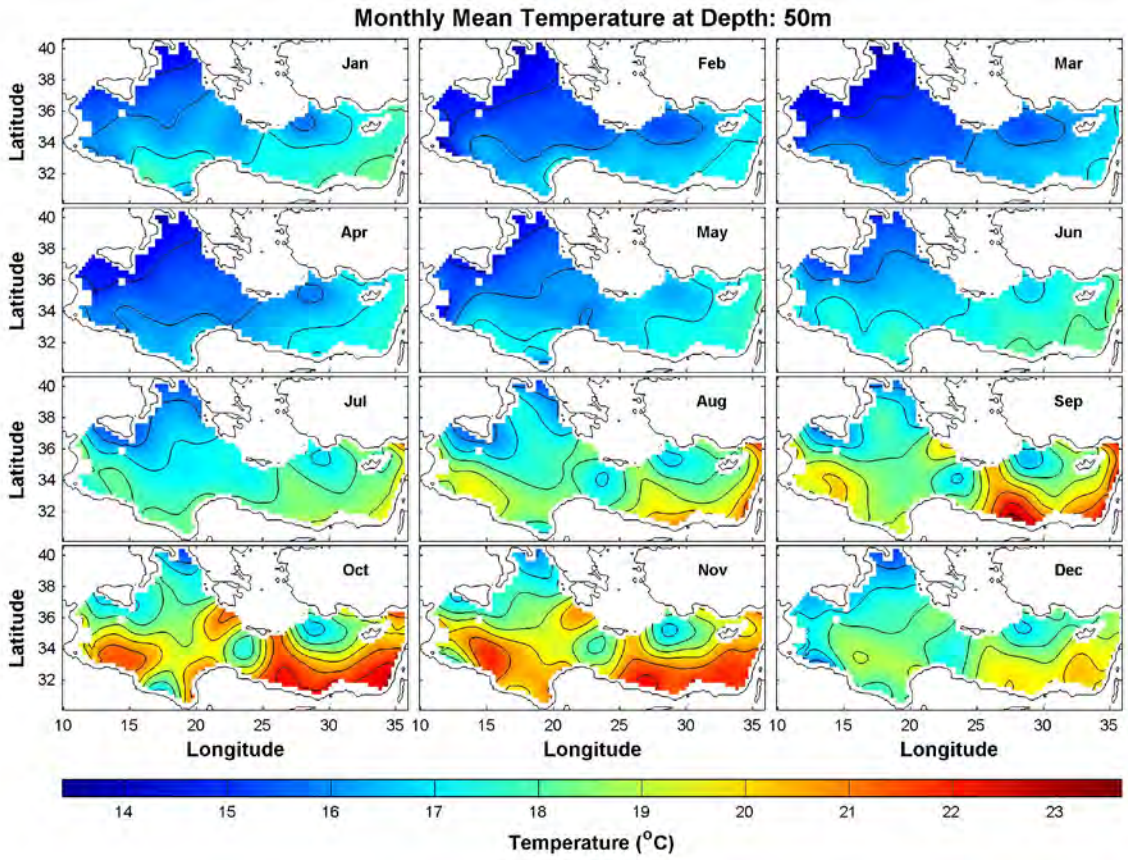
Monthly Mean Temperature at Depth: 50m
Jan
Feb
Mar
Apr
May
Jun
Jul
Aug
Sep
Oct
Nov
Dec
Latitude
Longitude
40
38
36
34
32
10
15
20
25
30
35
14
15
16
17
18
19
20
21
22
23
Temperature (°C)

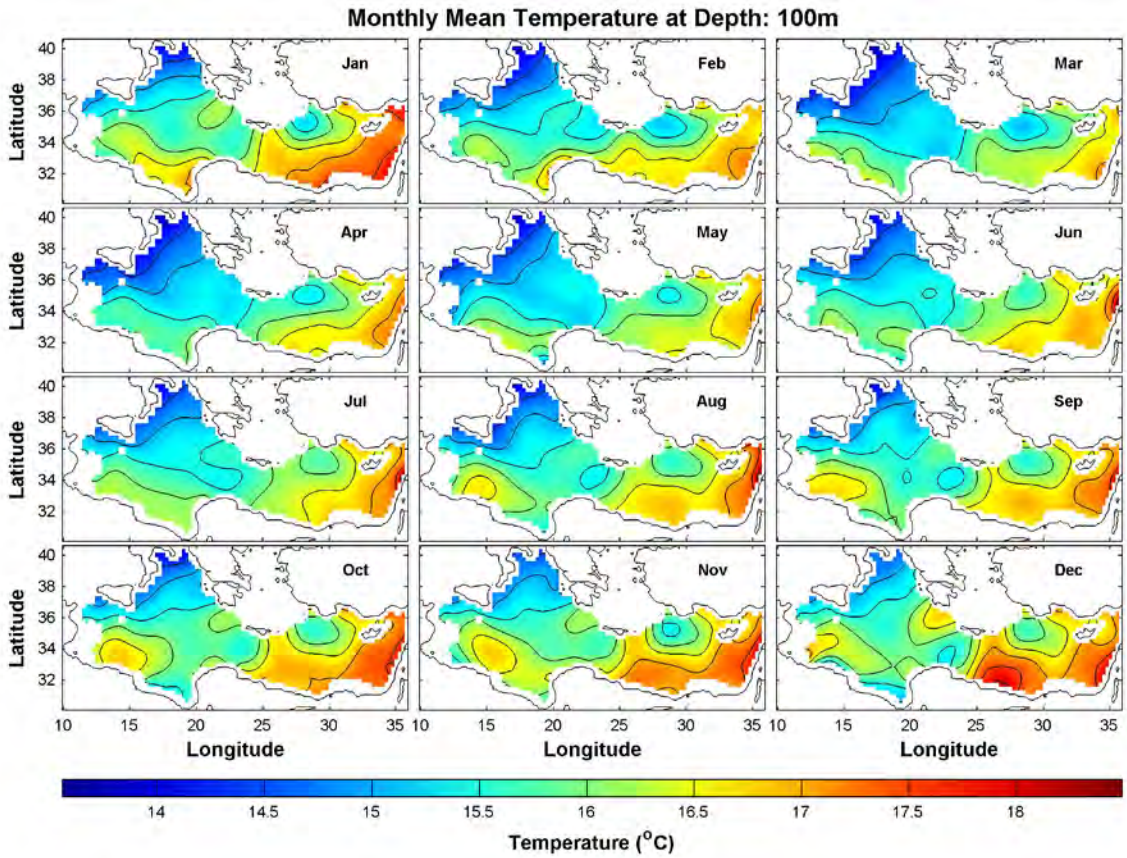
Monthly Mean Temperature at Depth: 100m
Jan
Feb
Mar
Apr
May
Jun
Jul
Aug
Sep
Oct
Nov
Dec
Latitude
Longitude
40
38
36
34
32
10
15
20
25
30
35
14
14.5
15
15.5
16
16.5
17
17.5
18
Temperature (°C)

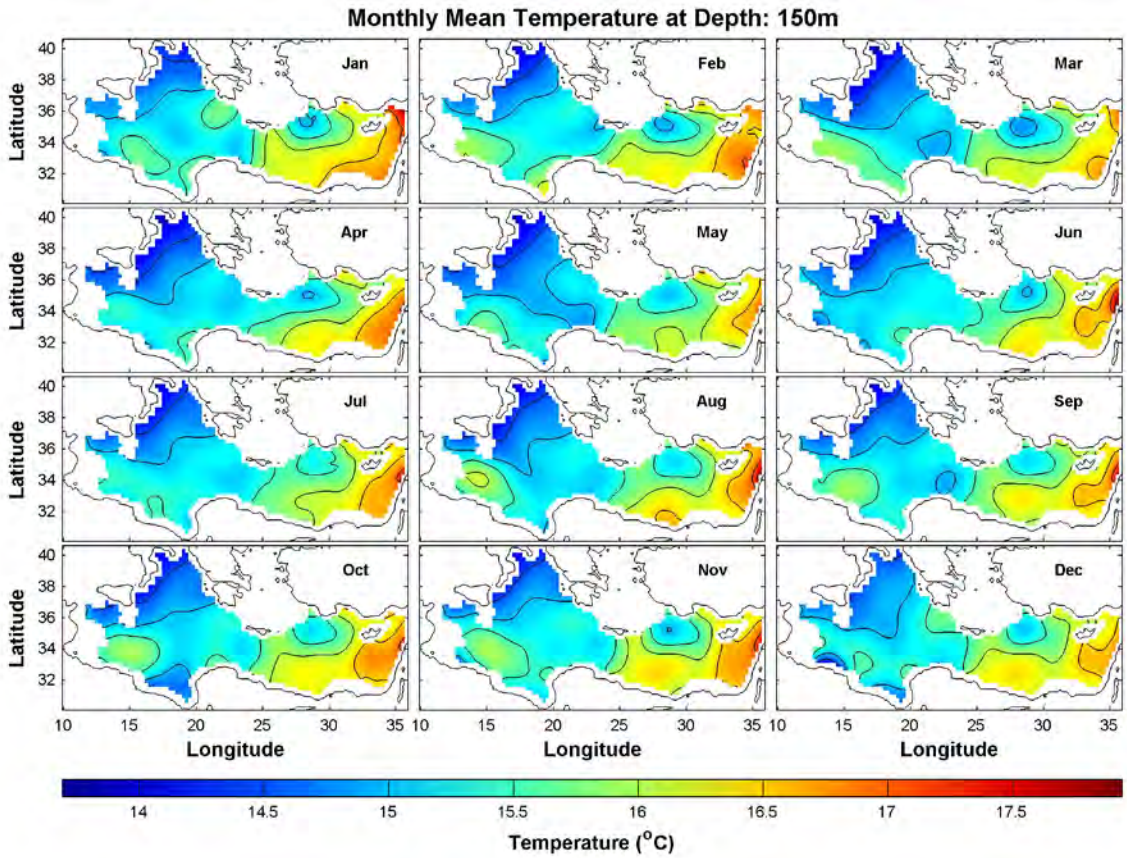
Monthly Mean Temperature at Depth: 150m
Jan
Feb
Mar
Apr
May
Jun
Jul
Aug
Sep
Oct
Nov
Dec
Latitude
Longitude
40
38
36
34
32
10
15
20
25
30
35
14
14.5
15
15.5
16
16.5
17
17.5
Temperature (°C)

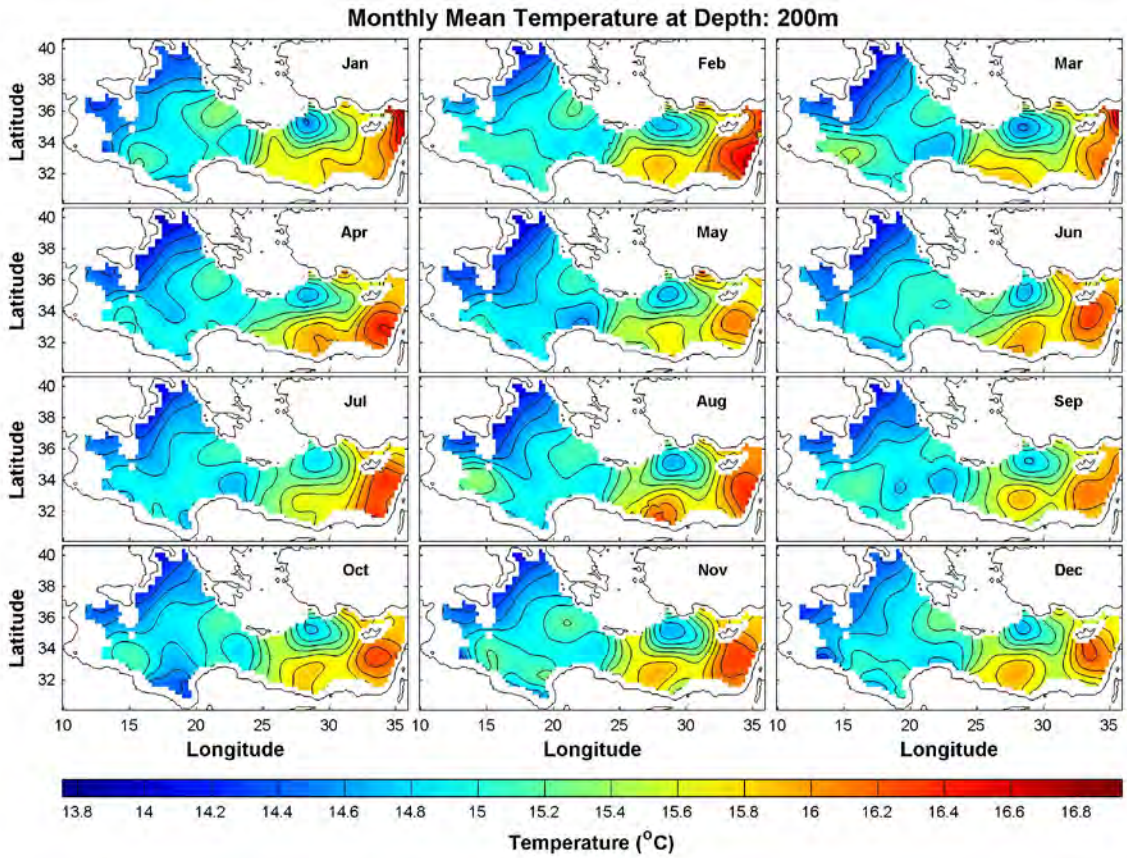
Monthly Mean Temperature at Depth: 200m
Jan
Feb
Mar
Apr
May
Jun
Jul
Aug
Sep
Oct
Nov
Dec
Latitude
Longitude
40
38
36
34
32
10
15
20
25
30
35
13.8
14
14.2
14.4
14.6
14.8
15
15.2
15.4
15.6
15.8
16
16.2
16.4
16.6
16.8
Temperature (°C)

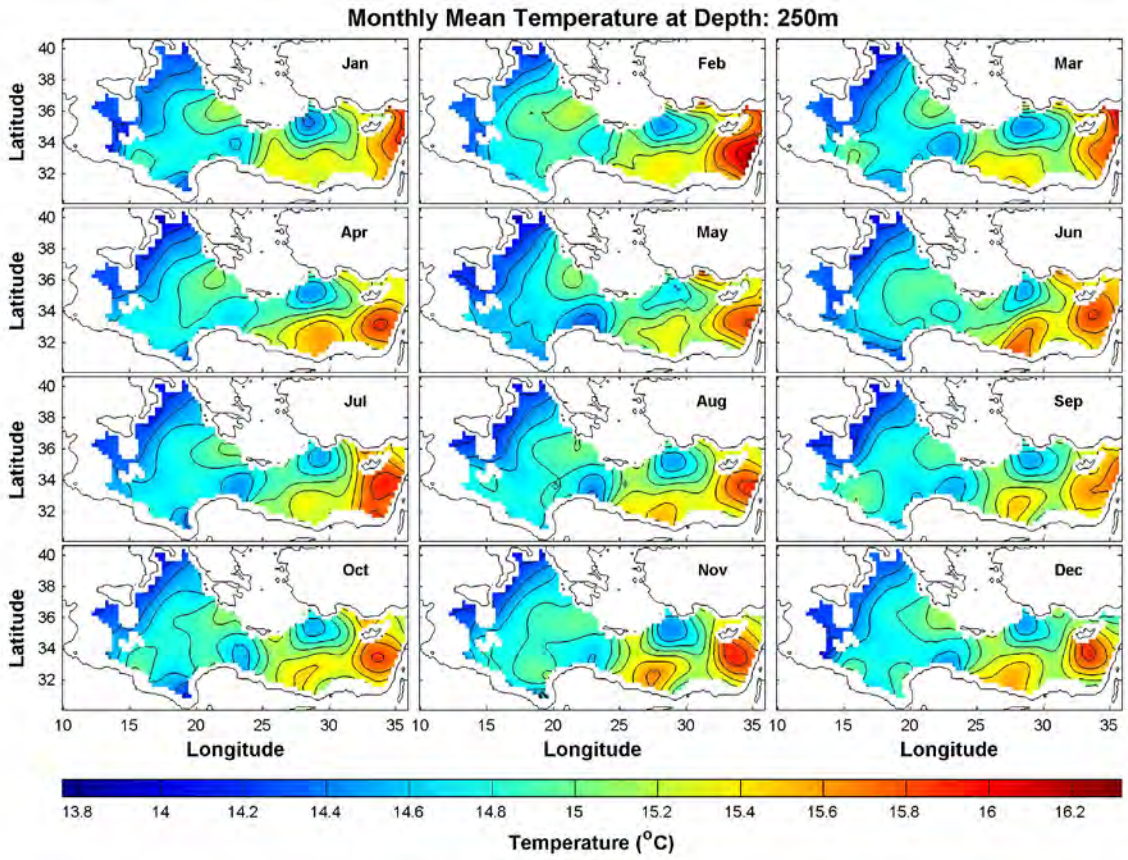
Monthly Mean Temperature at Depth: 250m
Jan
Feb
Mar
Apr
May
Jun
Jul
Aug
Sep
Oct
Nov
Dec
Latitude
Longitude
40
38
36
34
32
10
15
20
25
30
35
13.8
14
14.2
14.4
14.6
14.8
15
15.2
15.4
15.6
15.8
16
16.2
Temperature (°C)

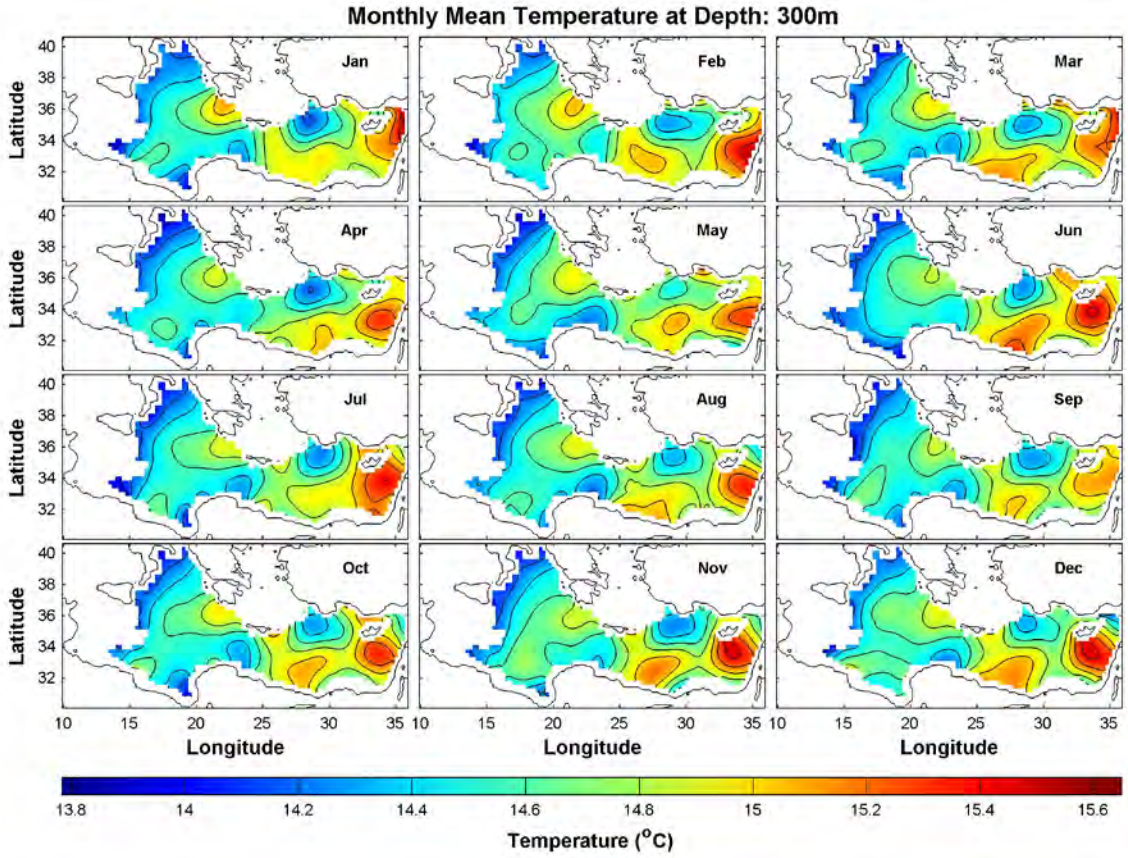
Monthly Mean Temperature at Depth: 300m
Jan
Feb
Mar
Apr
May
Jun
Jul
Aug
Sep
Oct
Nov
Dec
Latitude
Longitude
40
38
36
34
32
10
15
20
25
30
35
13.8
14
14.2
14.4
14.6
14.8
15
15.2
15.4
15.6
Temperature (°C)

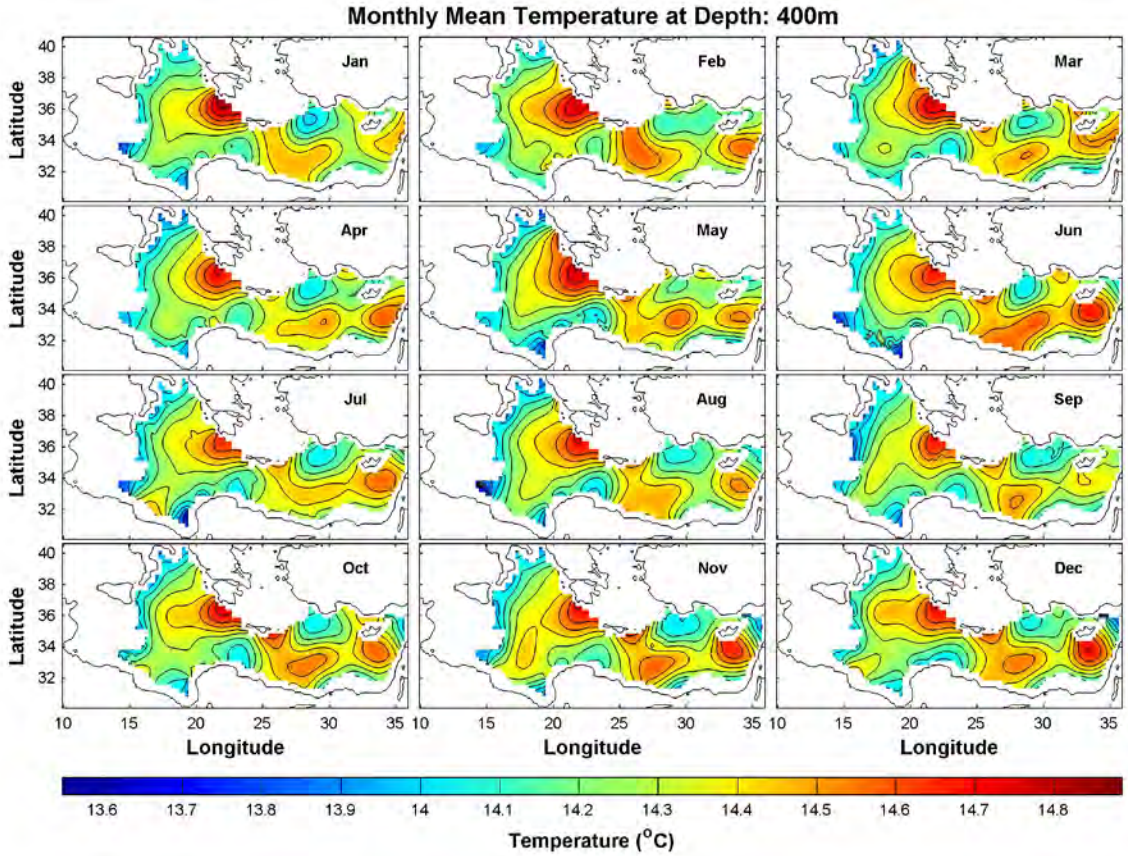
Monthly Mean Temperature at Depth: 400m
Jan
Feb
Mar
Apr
May
Jun
Jul
Aug
Sep
Oct
Nov
Dec
Latitude
Longitude
40
38
36
34
32
10
15
20
25
30
35
13.6
13.7
13.8
13.9
14
14.1
14.2
14.3
14.4
14.5
14.6
14.7
14.8
Temperature (°C)

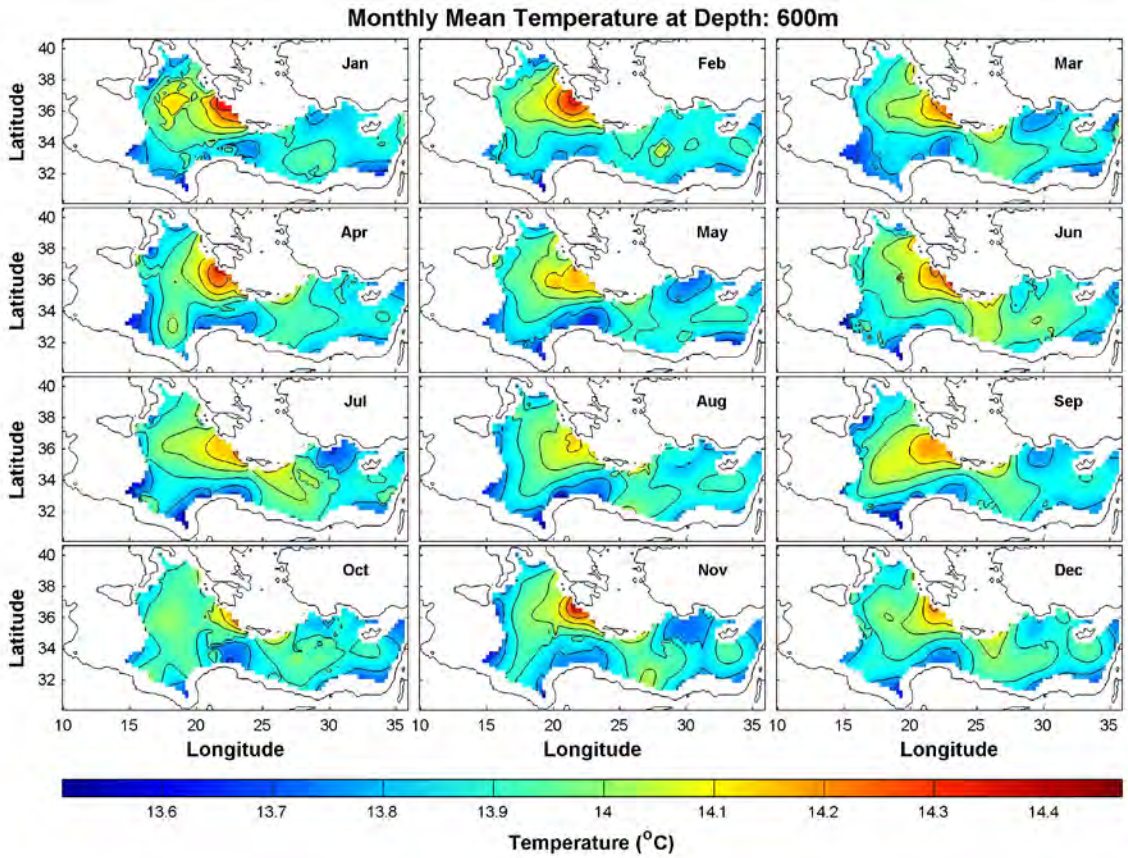
Monthly Mean Temperature at Depth: 600m
Jan
Feb
Mar
Apr
May
Jun
Jul
Aug
Sep
Oct
Nov
Dec
Latitude
Longitude
40
38
36
34
32
10
15
20
25
30
35
13.6
13.7
13.8
13.9
14
14.1
14.2
14.3
14.4
Temperature (°C)

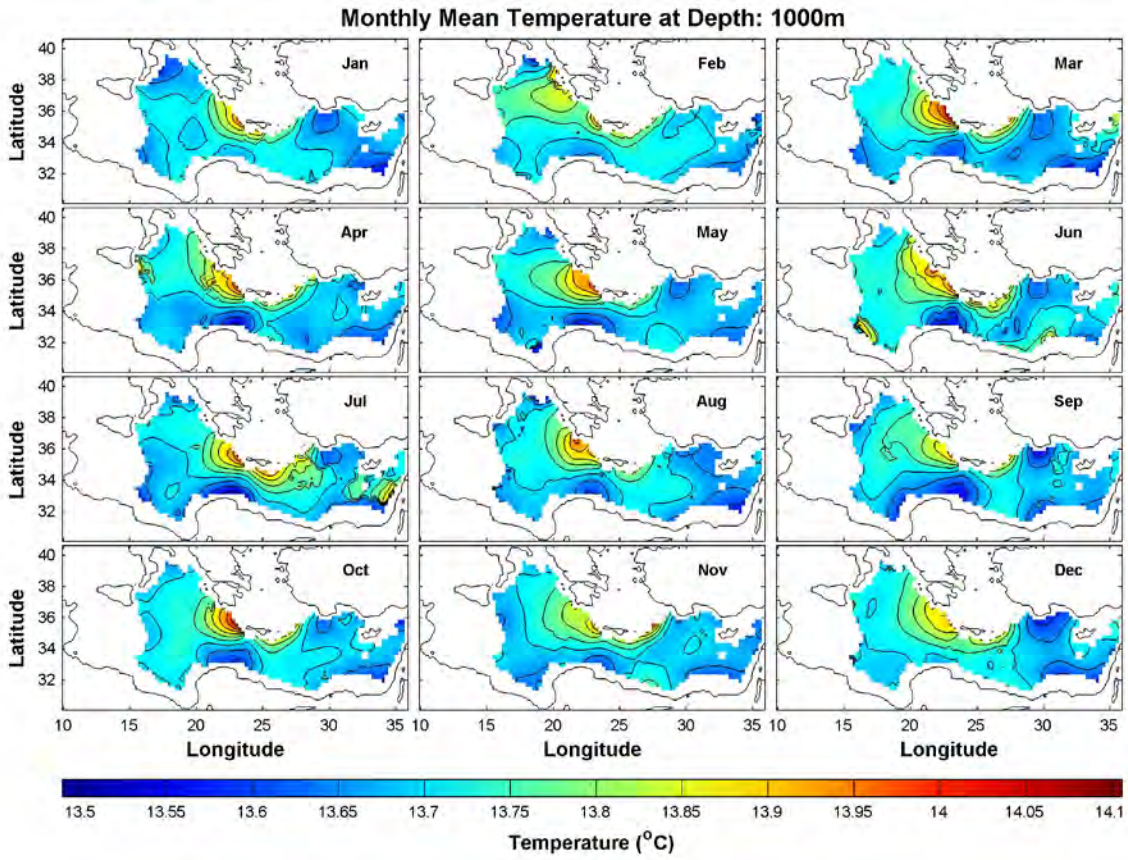
Monthly Mean Temperature at Depth: 1000m
Jan
Feb
Mar
Apr
May
Jun
Jul
Aug
Sep
Oct
Nov
Dec
Latitude
Longitude
40
38
36
34
32
10
15
20
25
30
35
13.5
13.55
13.6
13.65
13.7
13.75
13.8
13.85
13.9
13.95
14
14.05
14.1
Temperature (°C)

APPENDIX B. MONTHLY MEAN SALINITY AT DIFFERENT DEPTHS

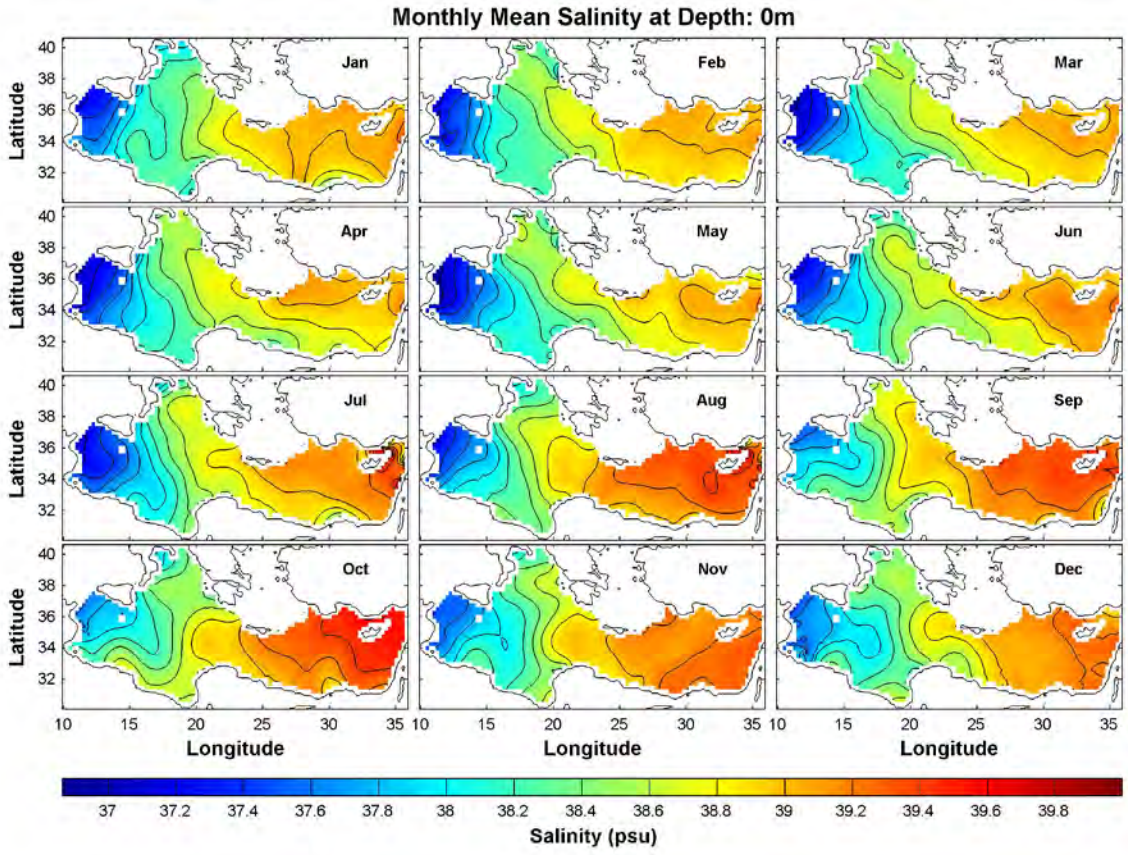

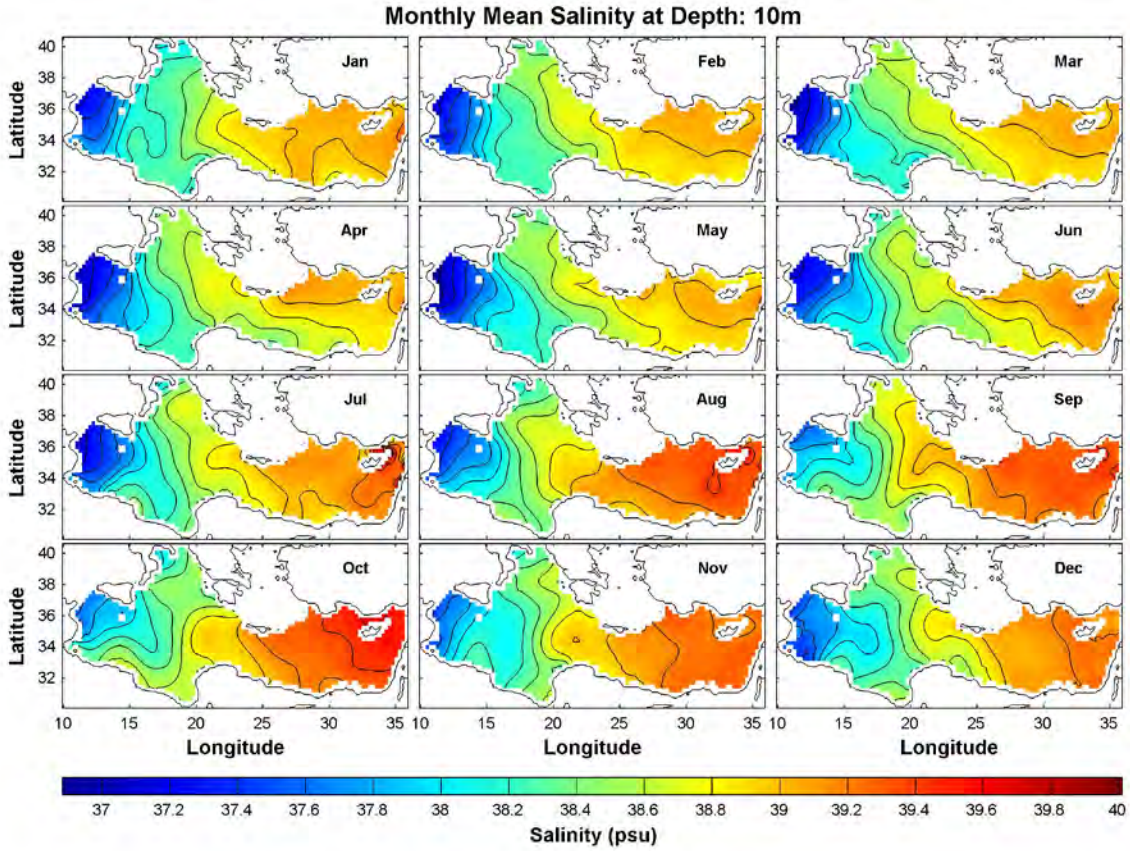
Monthly Mean Salinity at Depth: 10m
Jan
Feb
Mar
Apr
May
Jun
Jul
Aug
Sep
Oct
Nov
Dec
Latitude
Longitude
40
38
36
34
32
10
15
20
25
30
35
37
37.2
37.4
37.6
37.8
38
38.2
38.4
38.6
38.8
39
39.2
39.4
39.6
39.8
40
Salinity (psu)

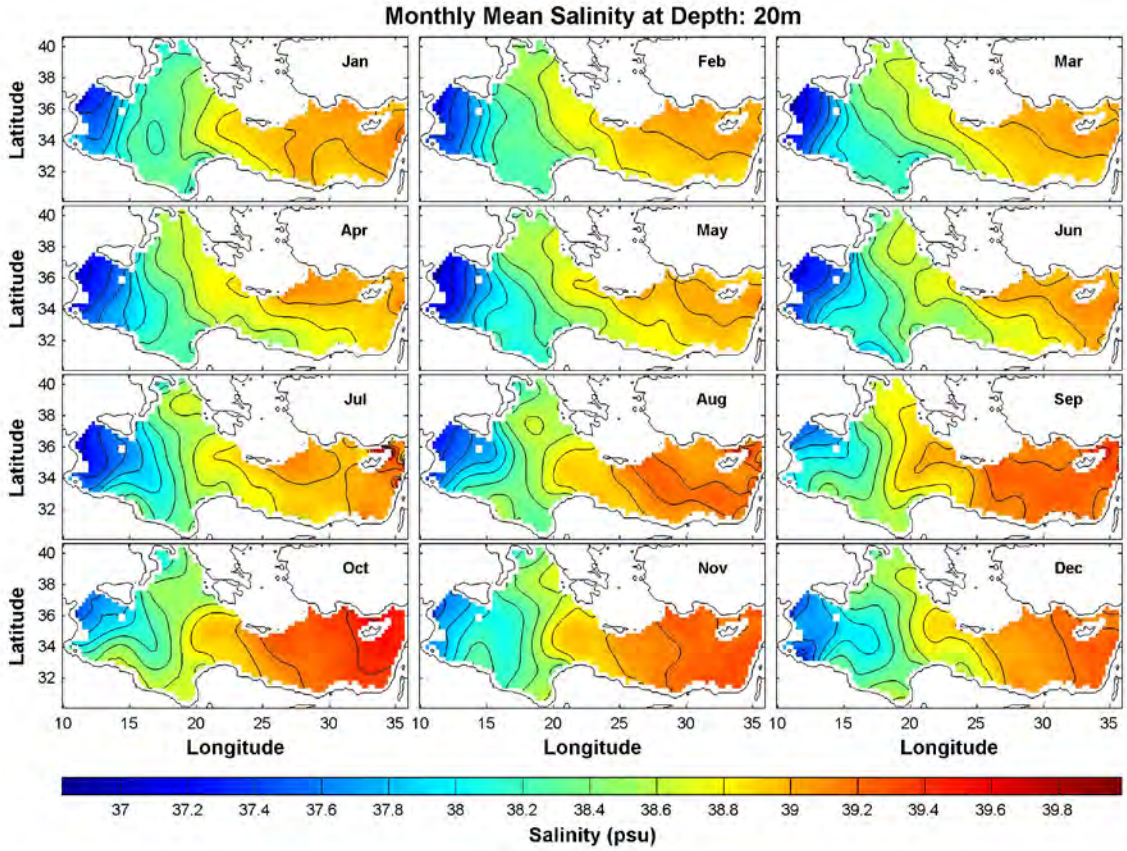
Monthly Mean Salinity at Depth: 20m
Jan
Feb
Mar
Apr
May
Jun
Jul
Aug
Sep
Oct
Nov
Dec
Latitude
Longitude
40
38
36
34
32
10
15
20
25
30
35
37
37.2
37.4
37.6
37.8
38
38.2
38.4
38.6
38.8
39
39.2
39.4
39.6
39.8
Salinity (psu)

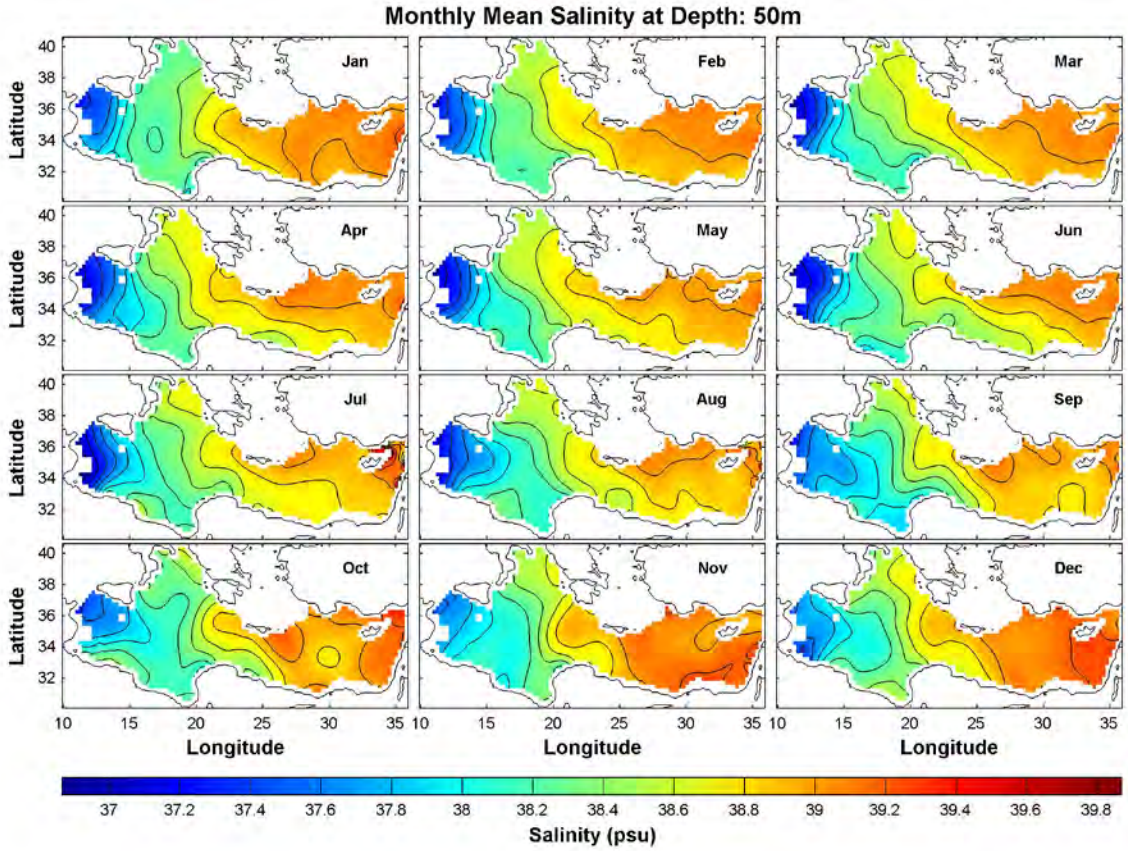
Monthly Mean Salinity at Depth: 50m
Jan
Feb
Mar
Apr
May
Jun
Jul
Aug
Sep
Oct
Nov
Dec
Latitude
Longitude
40
38
36
34
32
10
15
20
25
30
35
37
37.2
37.4
37.6
37.8
38
38.2
38.4
38.6
38.8
39
39.2
39.4
39.6
39.8
Salinity (psu)

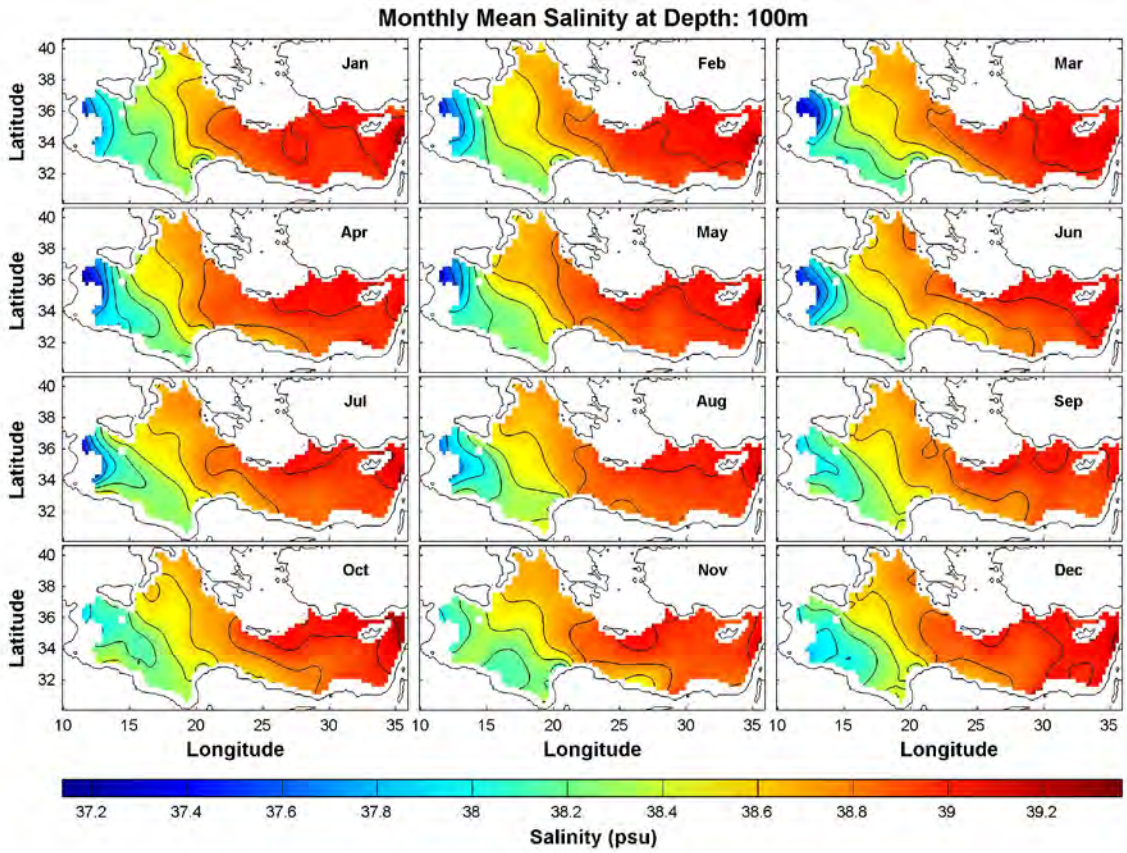
Monthly Mean Salinity at Depth: 100m
Jan
Feb
Mar
Apr
May
Jun
Jul
Aug
Sep
Oct
Nov
Dec
Latitude
Longitude
40
38
36
34
32
10
15
20
25
30
35
37.2
37.4
37.6
37.8
38
38.2
38.4
38.6
38.8
39
39.2
Salinity (psu)

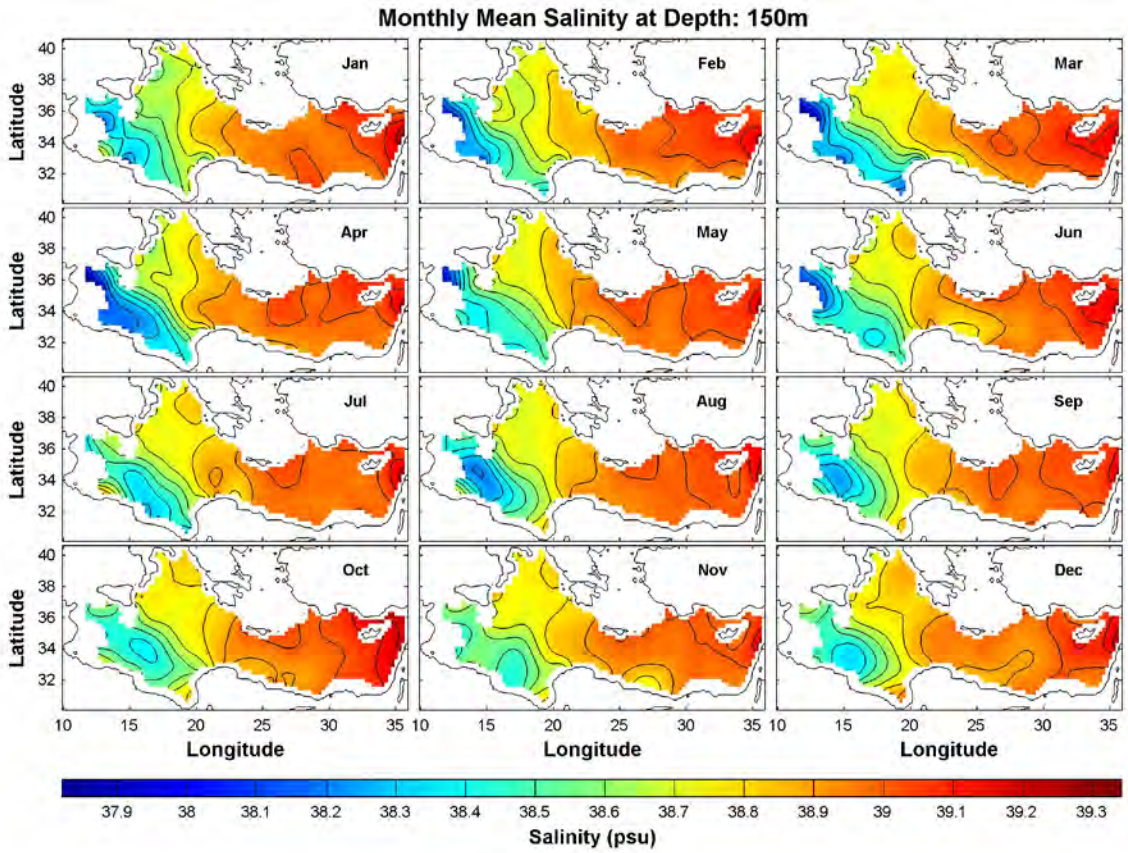
Monthly Mean Salinity at Depth: 150m
Jan
Feb
Mar
Apr
May
Jun
Jul
Aug
Sep
Oct
Nov
Dec
Latitude
Longitude
40
38
36
34
32
10
15
20
25
30
35
37.9
38
38.1
38.2
38.3
38.4
38.5
38.6
38.7
38.8
38.9
39
39.1
39.2
39.3
Salinity (psu)

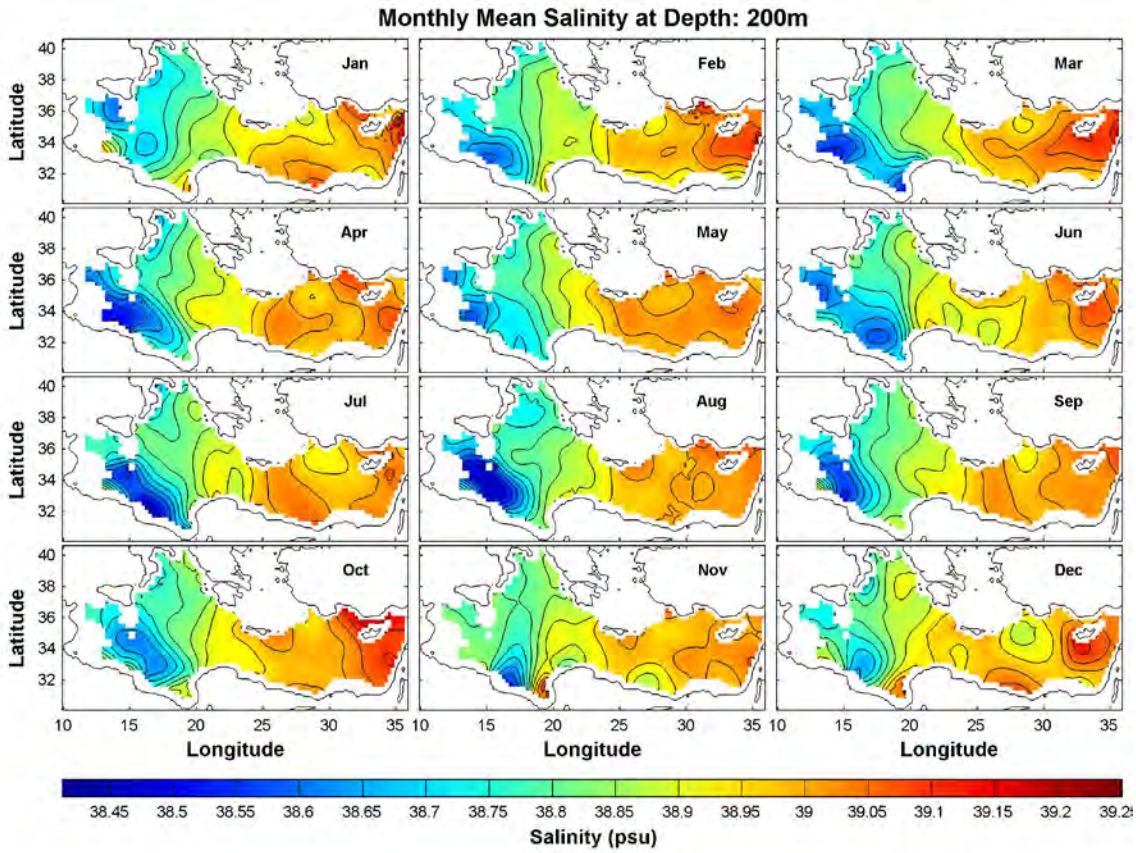
Monthly Mean Salinity at Depth: 200m
Jan
Feb
Mar
Apr
May
Jun
Jul
Aug
Sep
Oct
Nov
Dec
Latitude
Longitude
40
38
36
34
32
10
15
20
25
30
35
38.45
38.5
38.55
38.6
38.65
38.7
38.75
38.8
38.85
38.9
38.95
39
39.05
39.1
39.15
39.2
Salinity (psu)

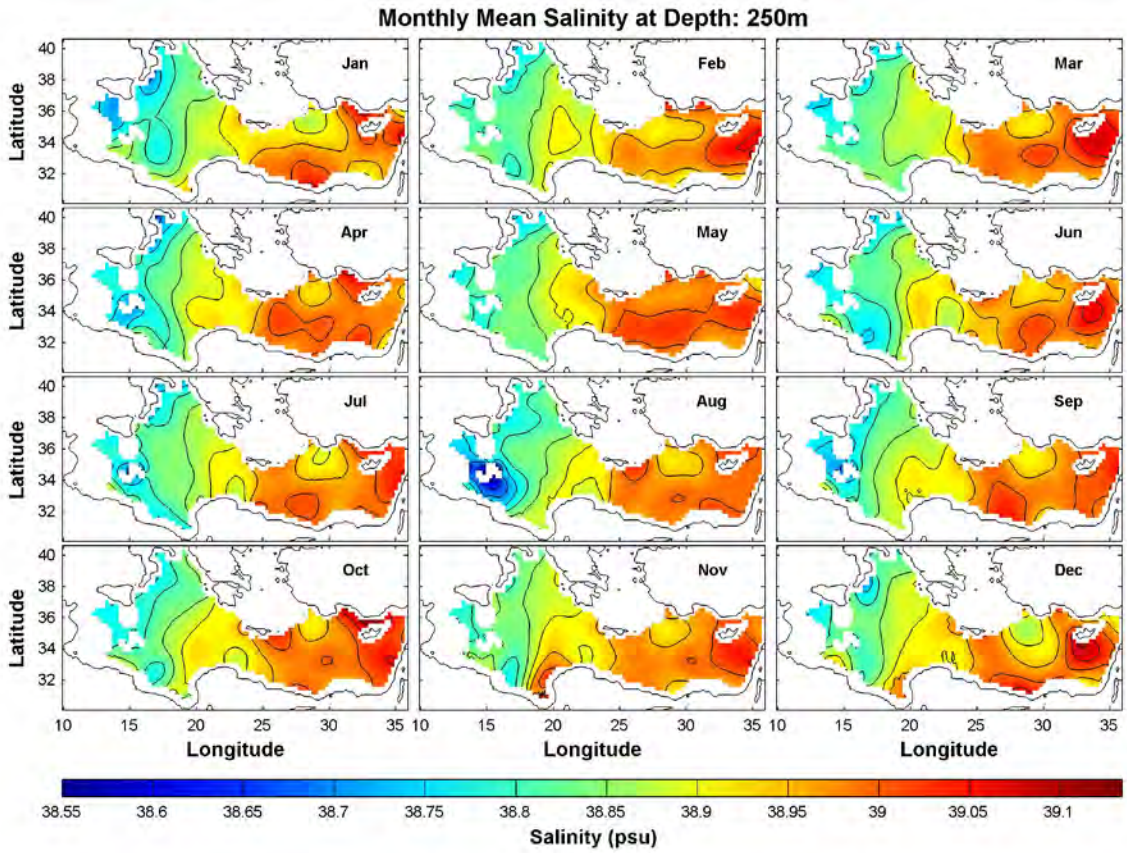
Monthly Mean Salinity at Depth: 250m
Jan
Feb
Mar
Apr
May
Jun
Jul
Aug
Sep
Oct
Nov
Dec
Latitude
Longitude
40
38
36
34
32
10
15
20
25
30
35
38.55
38.6
38.65
38.7
38.75
38.8
38.85
38.9
38.95
39
39.05
39.1
Salinity (psu)

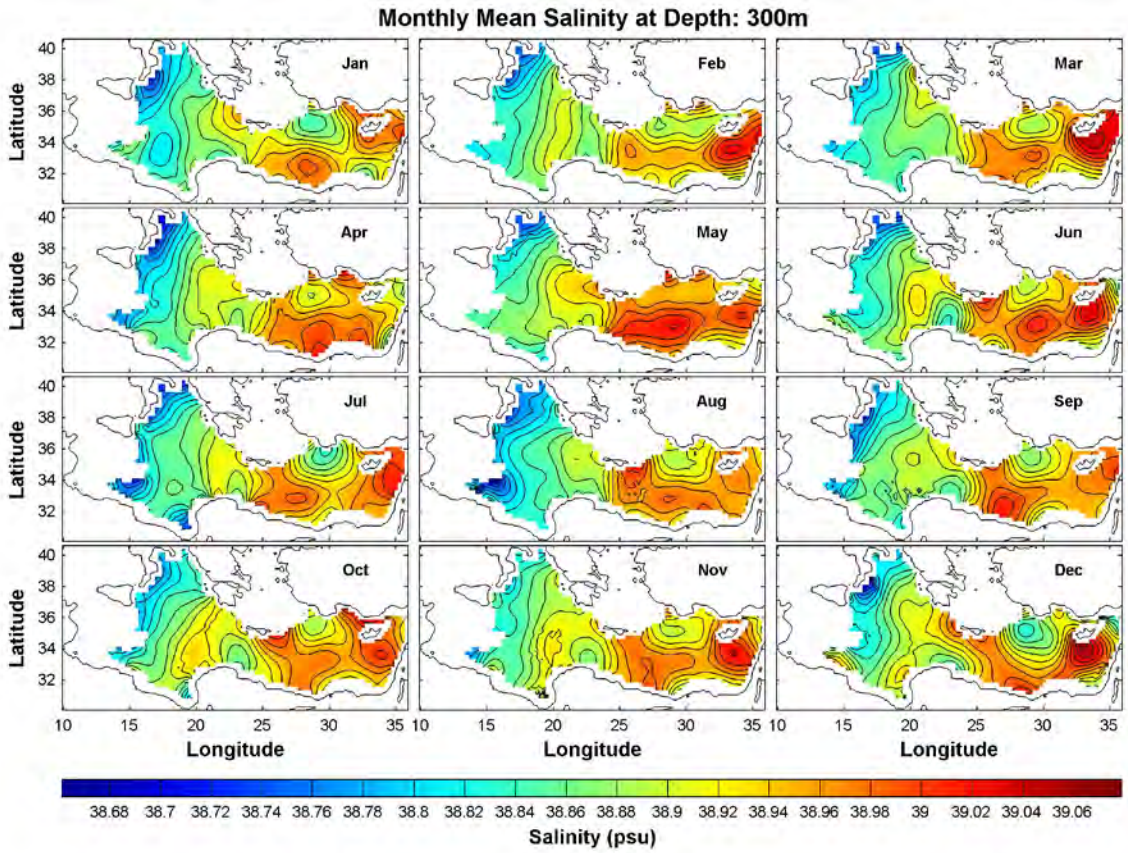
Monthly Mean Salinity at Depth: 300m
Jan
Feb
Mar
Apr
May
Jun
Jul
Aug
Sep
Oct
Nov
Dec
Latitude
Longitude
40
38
36
34
32
10
15
20
25
30
35
38.68 38.7 38.72 38.74 38.76 38.78 38.8 38.82 38.84 38.86 38.88 38.9 38.92 38.94 38.96 38.98 39 39.02 39.04 39.06
Salinity (psu)

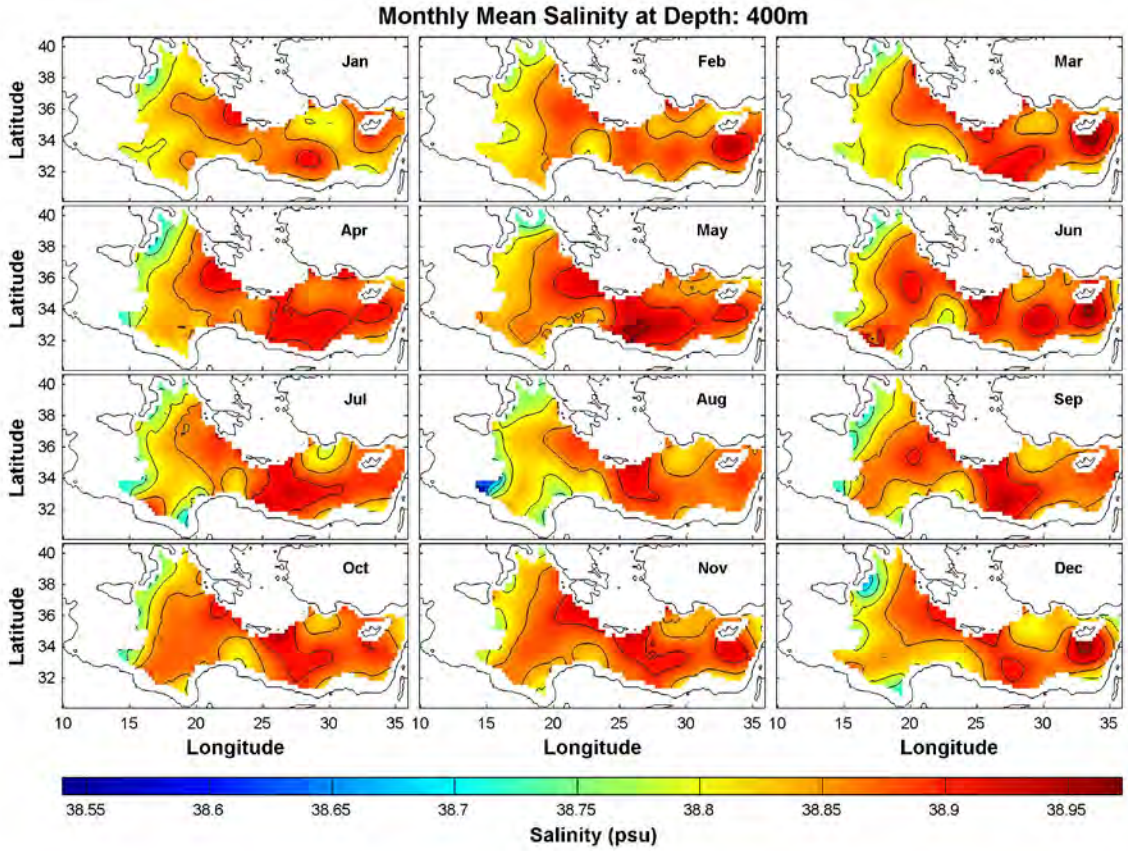
Monthly Mean Salinity at Depth: 400m
Jan
Feb
Mar
Apr
May
Jun
Jul
Aug
Sep
Oct
Nov
Dec
Latitude
Longitude
40
38
36
34
32
10
15
20
25
30
35
38.55
38.6
38.65
38.7
38.75
38.8
38.85
38.9
38.95
Salinity (psu)

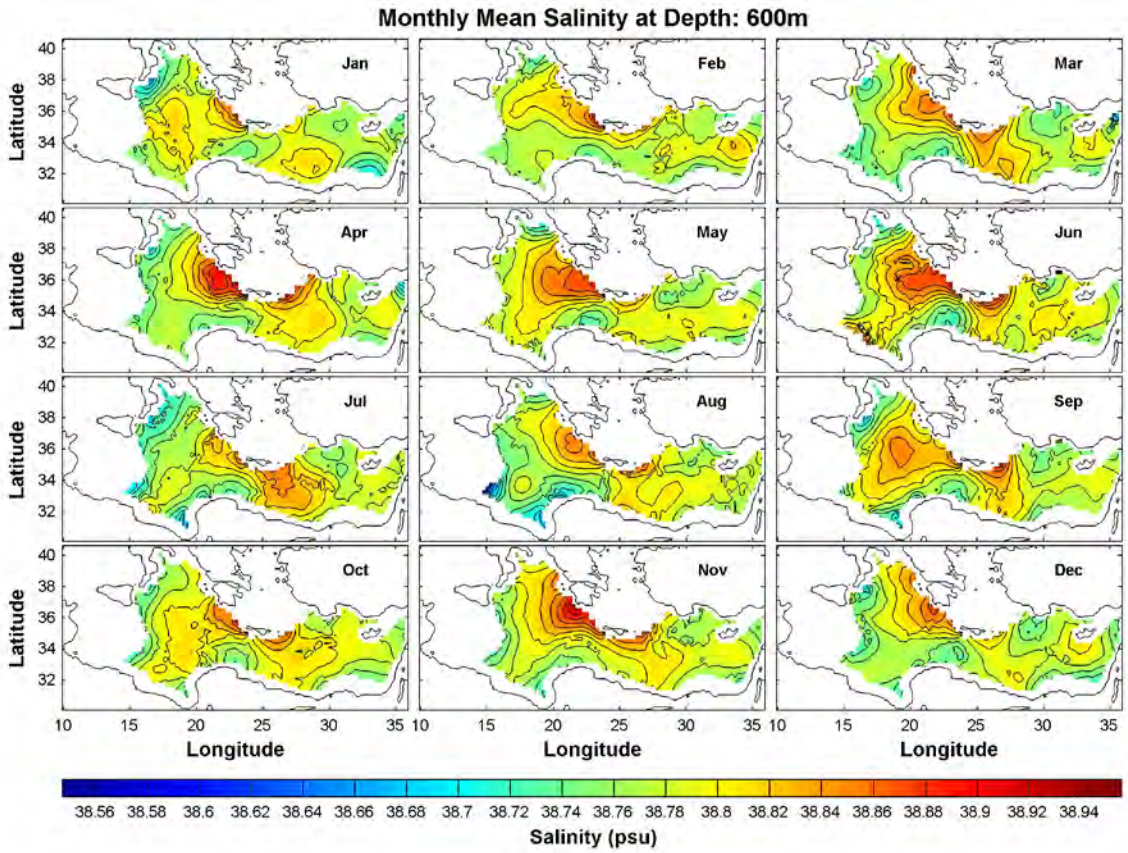
Monthly Mean Salinity at Depth: 600m
Jan
Feb
Mar
Apr
May
Jun
Jul
Aug
Sep
Oct
Nov
Dec
Latitude
Longitude
40
38
36
34
32
10
15
20
25
30
35
38.56 38.58 38.6 38.62 38.64 38.66 38.68 38.7 38.72 38.74 38.76 38.78 38.8 38.82 38.84 38.86 38.88 38.9 38.92 38.94
Salinity (psu)

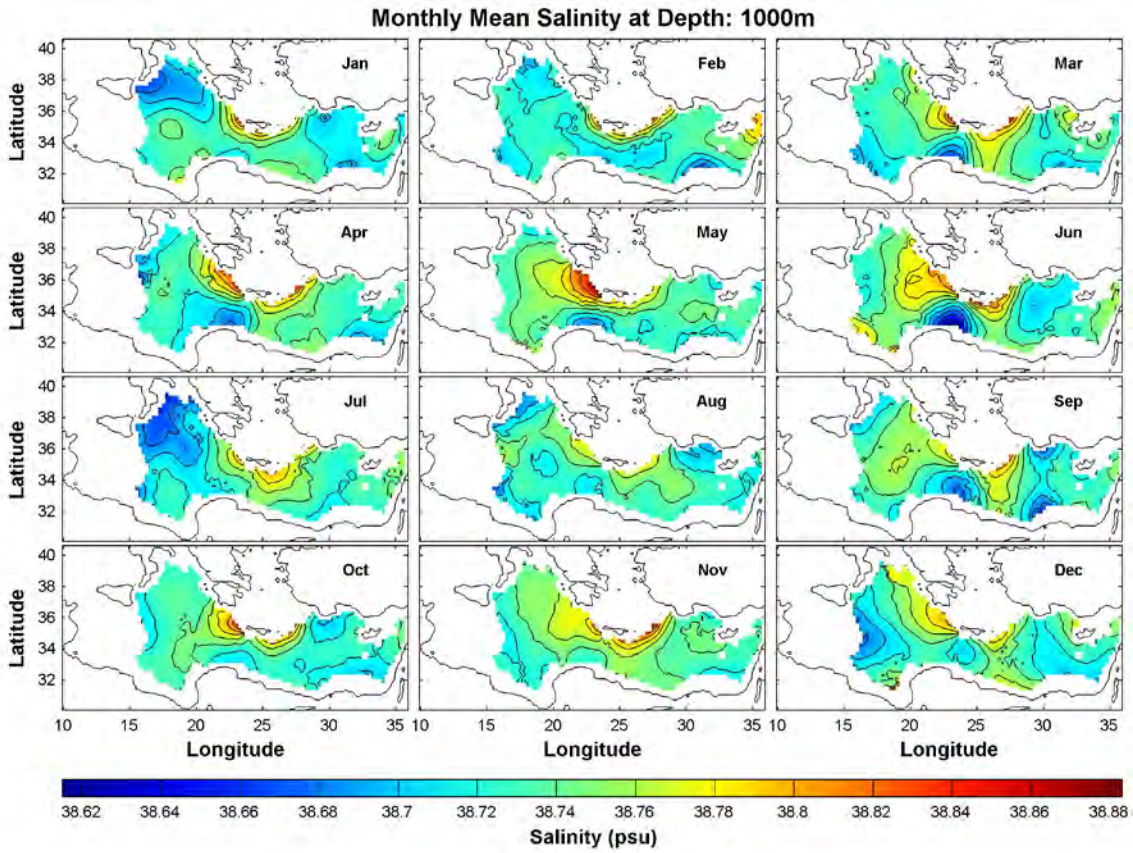
Monthly Mean Salinity at Depth: 1000m
Jan
Feb
Mar
Apr
May
Jun
Jul
Aug
Sep
Oct
Nov
Dec
Latitude
Longitude
40
38
36
34
32
10
15
20
25
30
35
38.62
38.64
38.66
38.68
38.7
38.72
38.74
38.76
38.78
38.8
38.82
38.84
38.86
38.88
Salinity (psu)

APPENDIX C. MONTHLY MEAN ABSOLUTE GEOSTROPHIC VELOCITY AT DIFFERENT DEPTHS

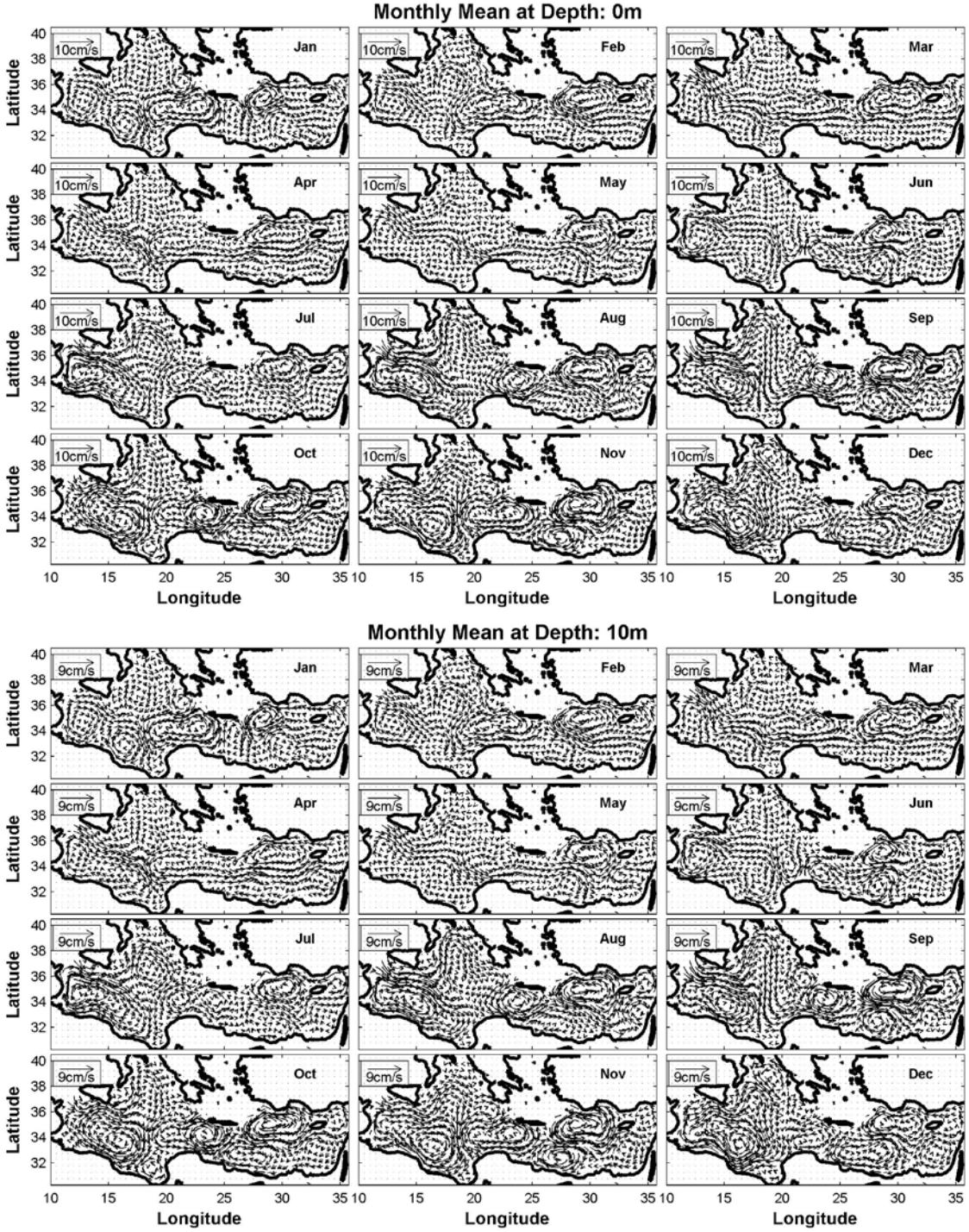

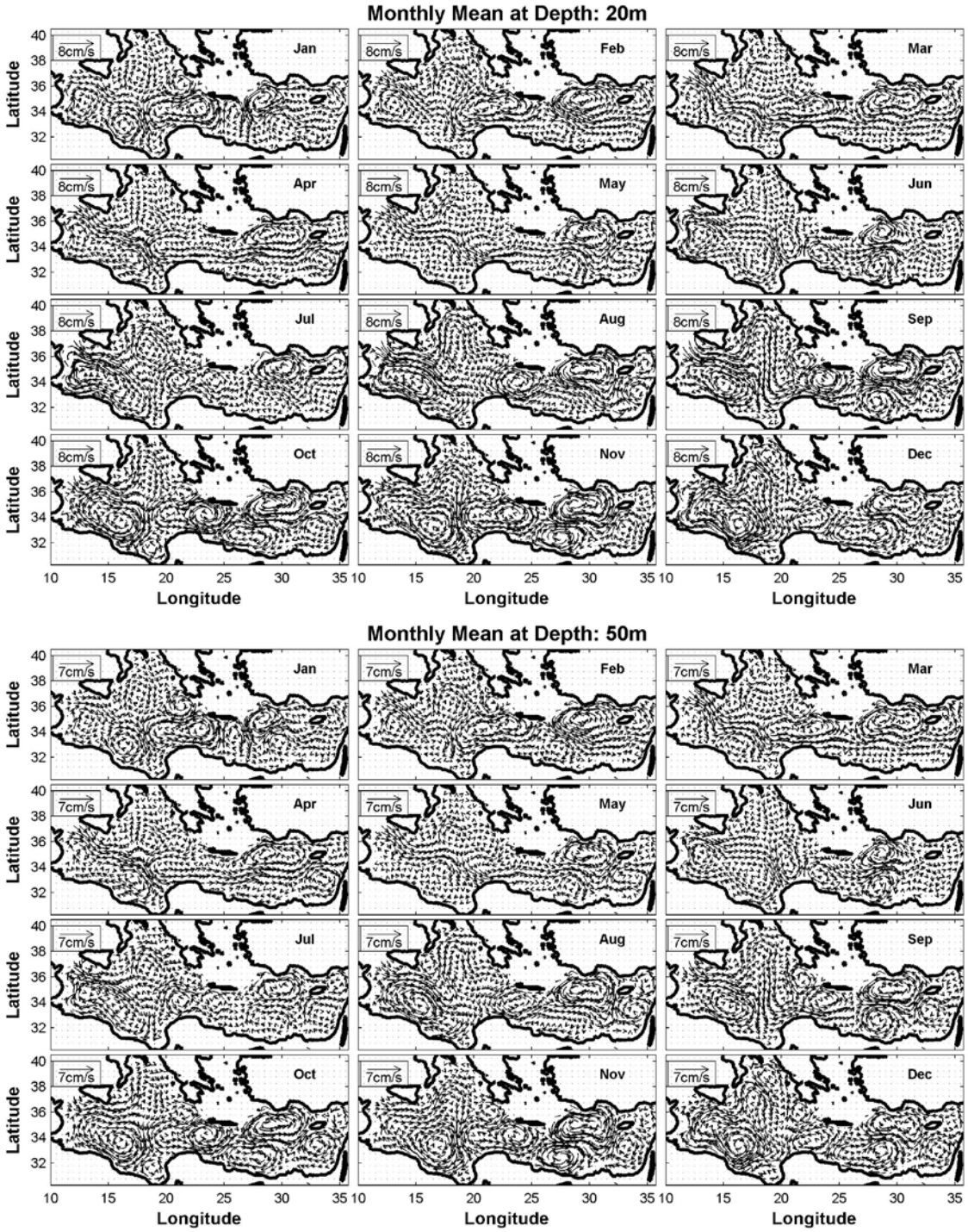
Monthly Mean at Depth: 20m
8cm/s
Jan
Feb
Mar
Apr
May
Jun
Jul
Aug
Sep
Oct
Nov
Dec
Latitude
Longitude
Monthly Mean at Depth: 50m
7cm/s
Jan
Feb
Mar
Apr
May
Jun
Jul
Aug
Sep
Oct
Nov
Dec
Latitude
Longitude

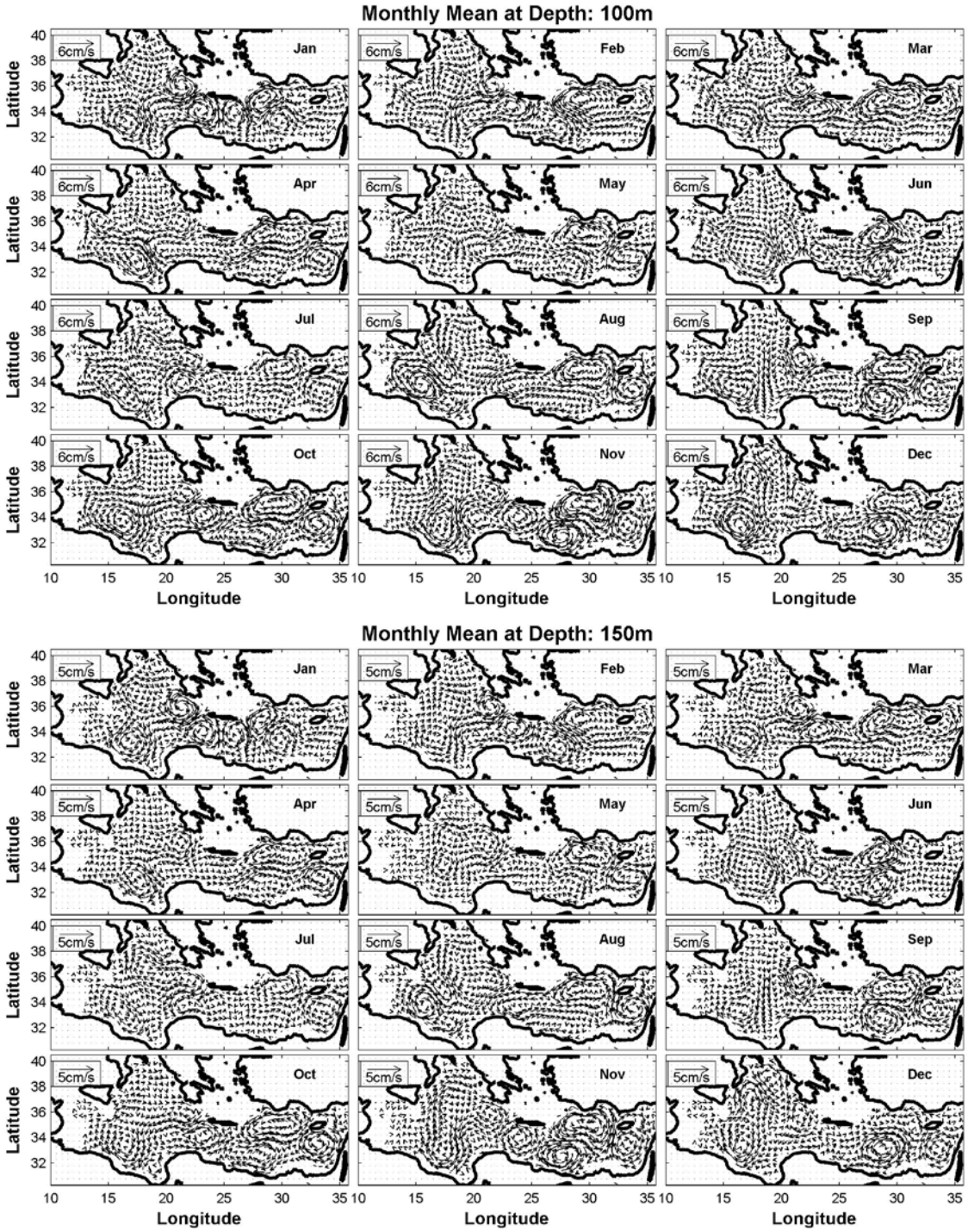
Monthly Mean at Depth: 100m
Jan
Feb
Mar
Apr
May
Jun
Jul
Aug
Sep
Oct
Nov
Dec
6cm/s
Latitude
Longitude
Monthly Mean at Depth: 150m
5cm/s

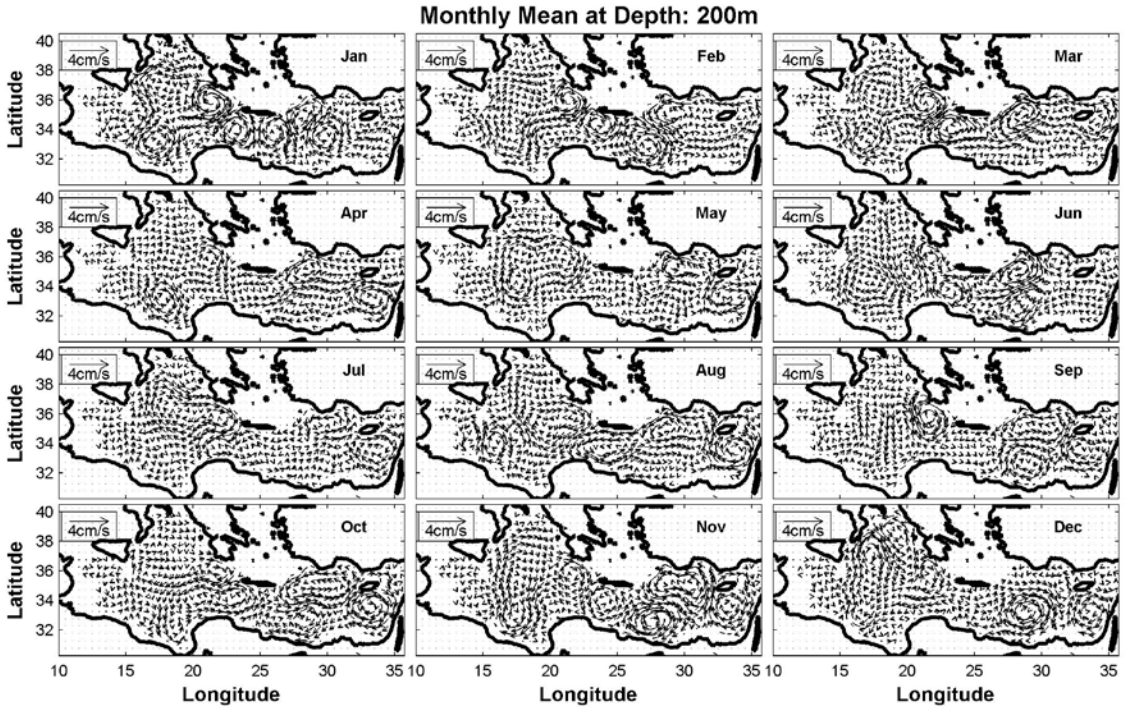
Monthly Mean at Depth: 200m
Jan
Feb
Mar
Apr
May
Jun
Jul
Aug
Sep
Oct
Nov
Dec
4cm/s
Latitude
Longitude

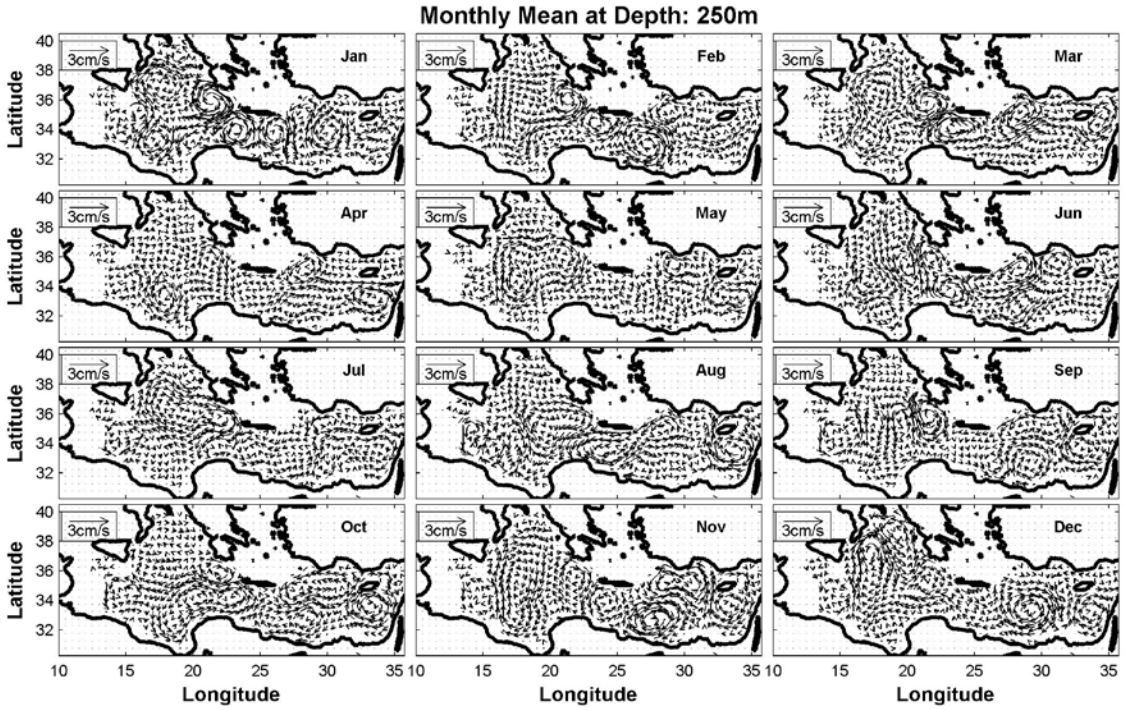
Monthly Mean at Depth: 250m
Jan
Feb
Mar
Apr
May
Jun
Jul
Aug
Sep
Oct
Nov
Dec
3cm/s
Latitude
Longitude

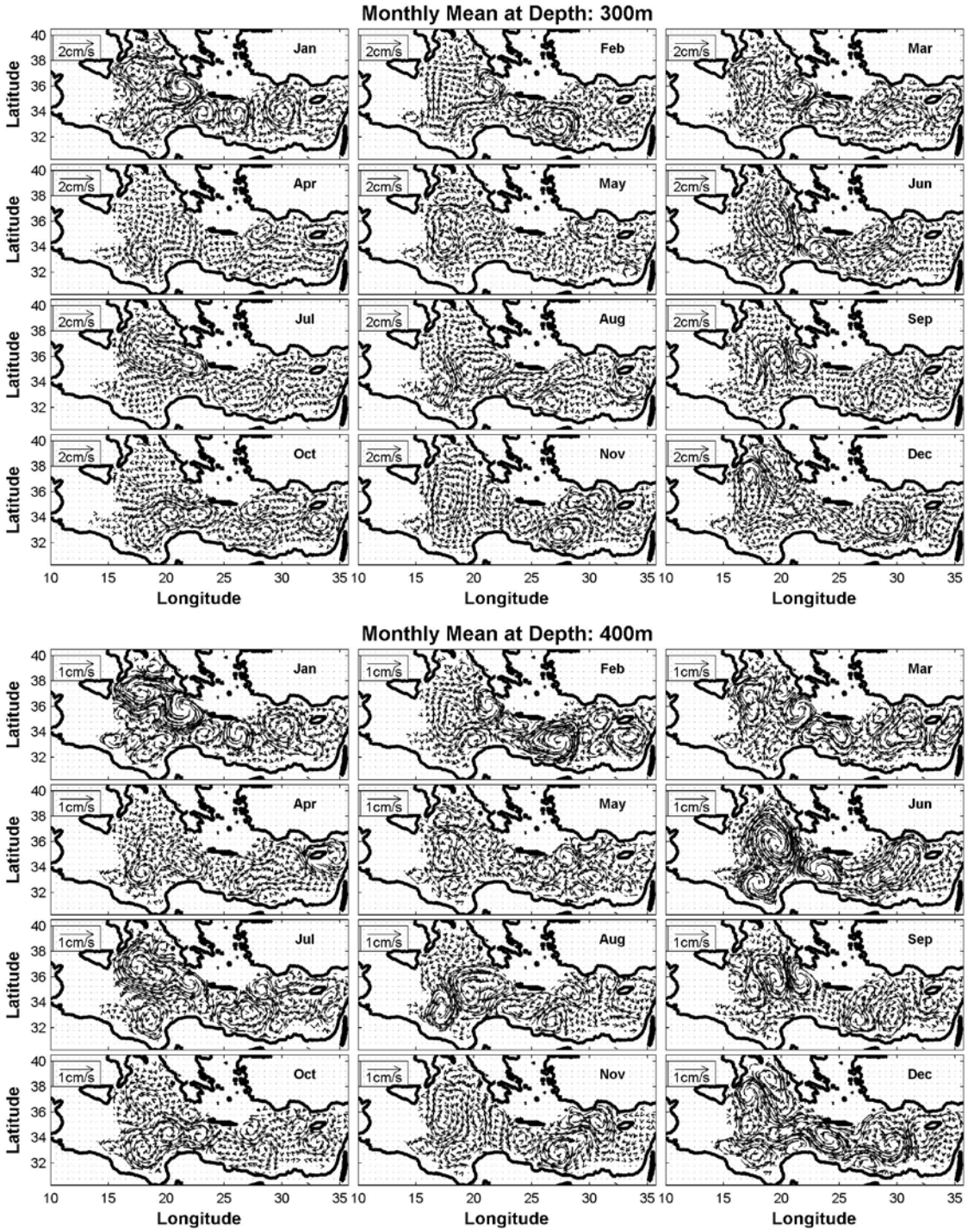
Monthly Mean at Depth: 300m
Jan
Feb
Mar
Apr
May
Jun
Jul
Aug
Sep
Oct
Nov
Dec
2cm/s
Latitude
Longitude
Monthly Mean at Depth: 400m
1cm/s

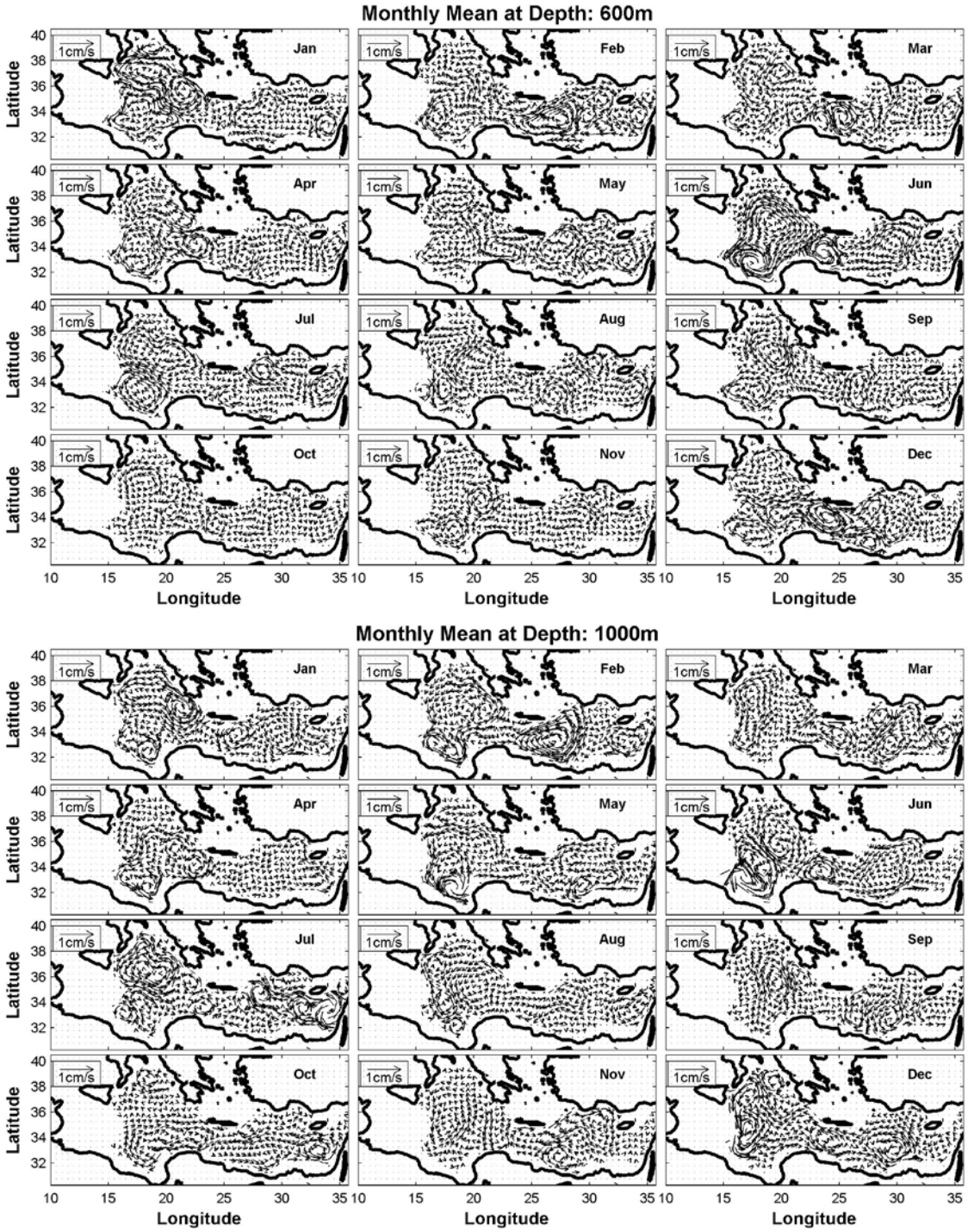
Monthly Mean at Depth: 600m
Jan
Feb
Mar
Apr
May
Jun
Jul
Aug
Sep
Oct
Nov
Dec
1cm/s
Latitude
Longitude
Monthly Mean at Depth: 1000m
Jan
Feb
Mar
Apr
May
Jun
Jul
Aug
Sep
Oct
Nov
Dec
1cm/s
Latitude
Longitude

APPENDIX D. FIRST FIVE EOF MODES OF HEAT CONTENT

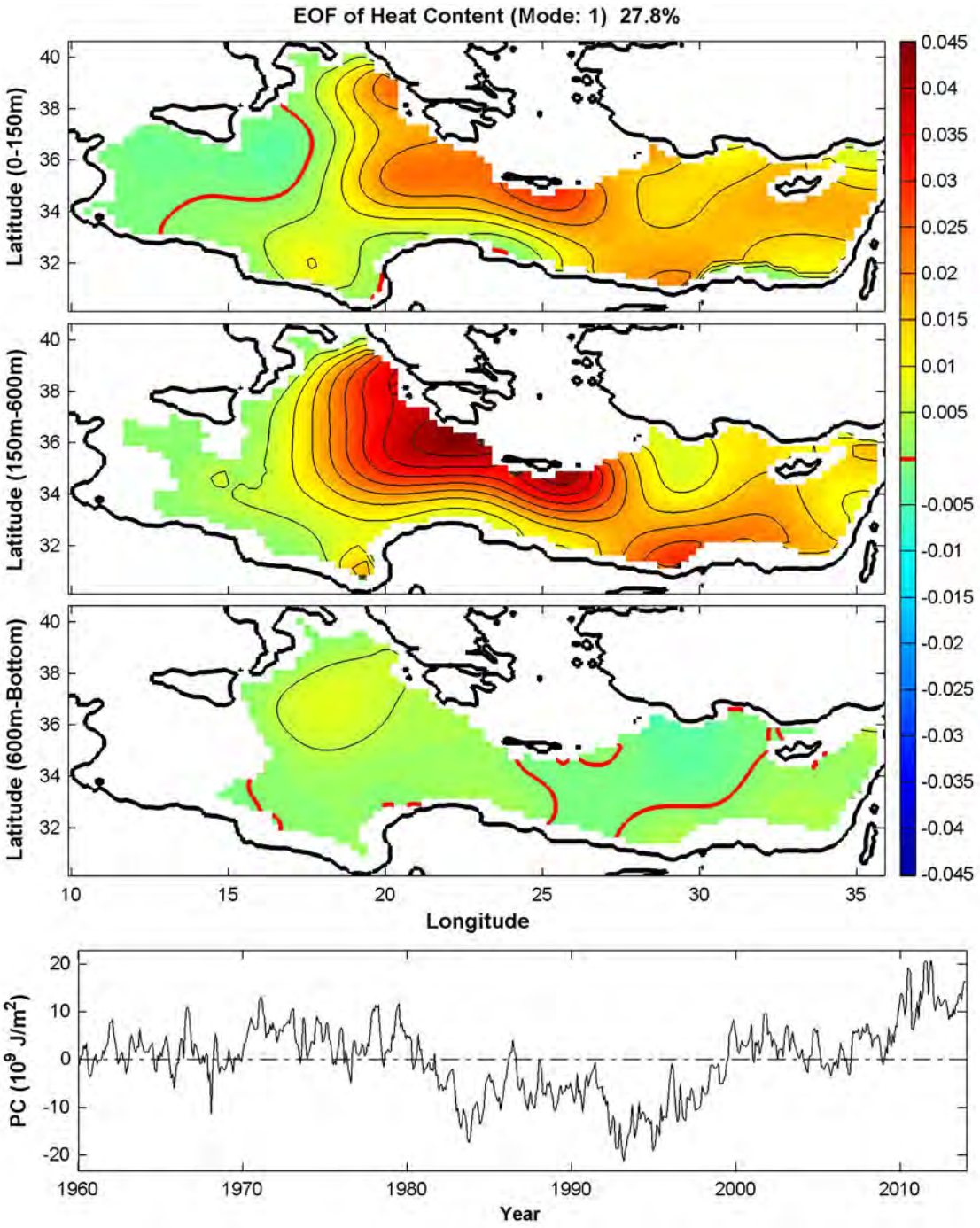

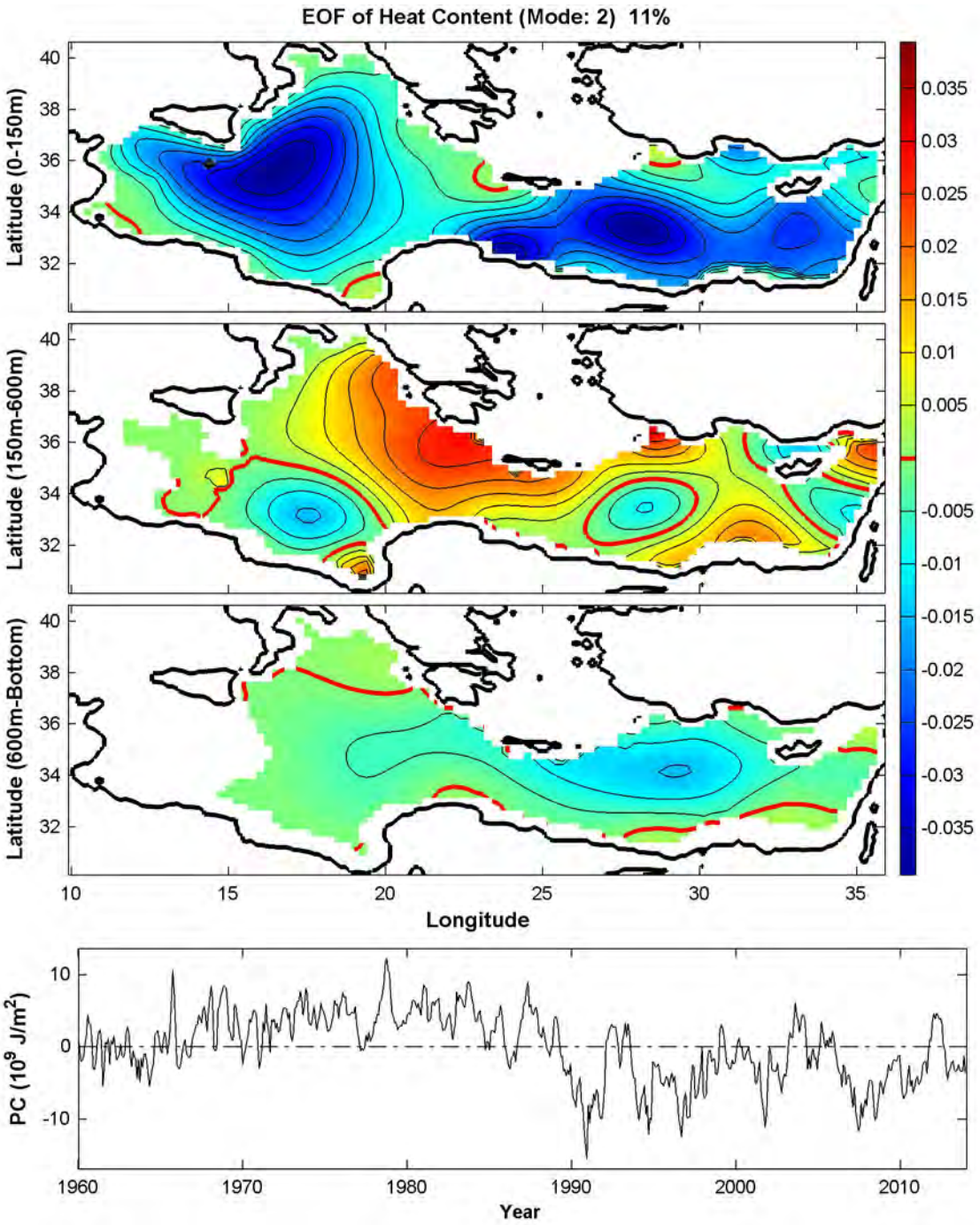
EOF of Heat Content (Mode: 2) 11%
Latitude (0-150m)
Latitude (150m-600m)
Latitude (600m-Bottom)
40
38
36
34
32
10
15
20
25
30
35
Longitude
0.035
0.03
0.025
0.02
0.015
0.01
0.005
-0.005
-0.01
-0.015
-0.02
-0.025
-0.03
-0.035
PC (10^9 J/m^2)
10
0
-10
1960
1970
1980
1990
2000
2010
Year

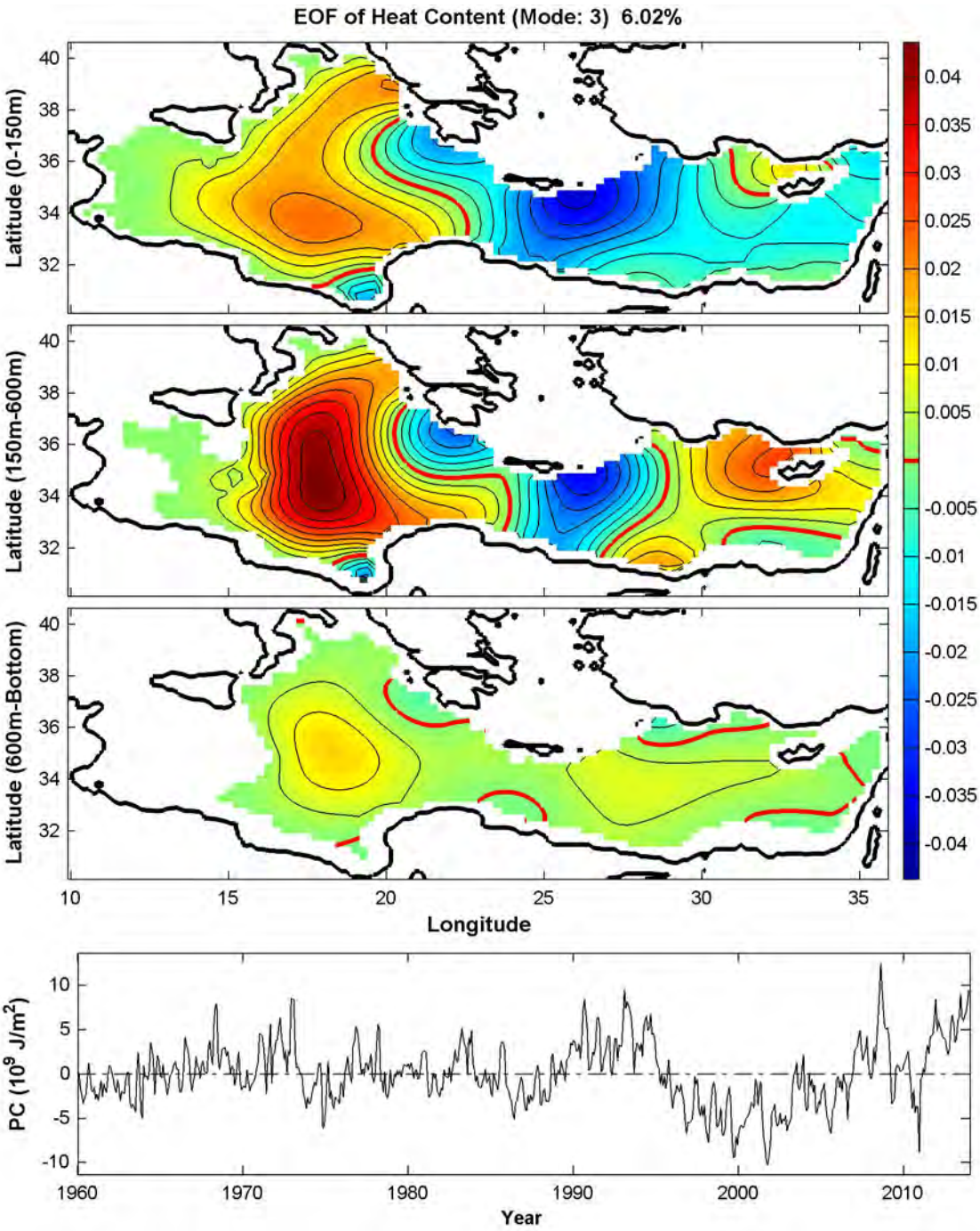
EOF of Heat Content (Mode: 3) 6.02%
Latitude (0-150m)
Latitude (150m-600m)
Latitude (600m-Bottom)
40
38
36
34
32
0.04
0.035
0.03
0.025
0.02
0.015
0.01
0.005
-0.005
-0.01
-0.015
-0.02
-0.025
-0.03
-0.035
-0.04
10
15
20
25
30
35
Longitude
PC (10^9 J/m^2)
10
5
0
-5
-10
1960
1970
1980
1990
2000
2010
Year

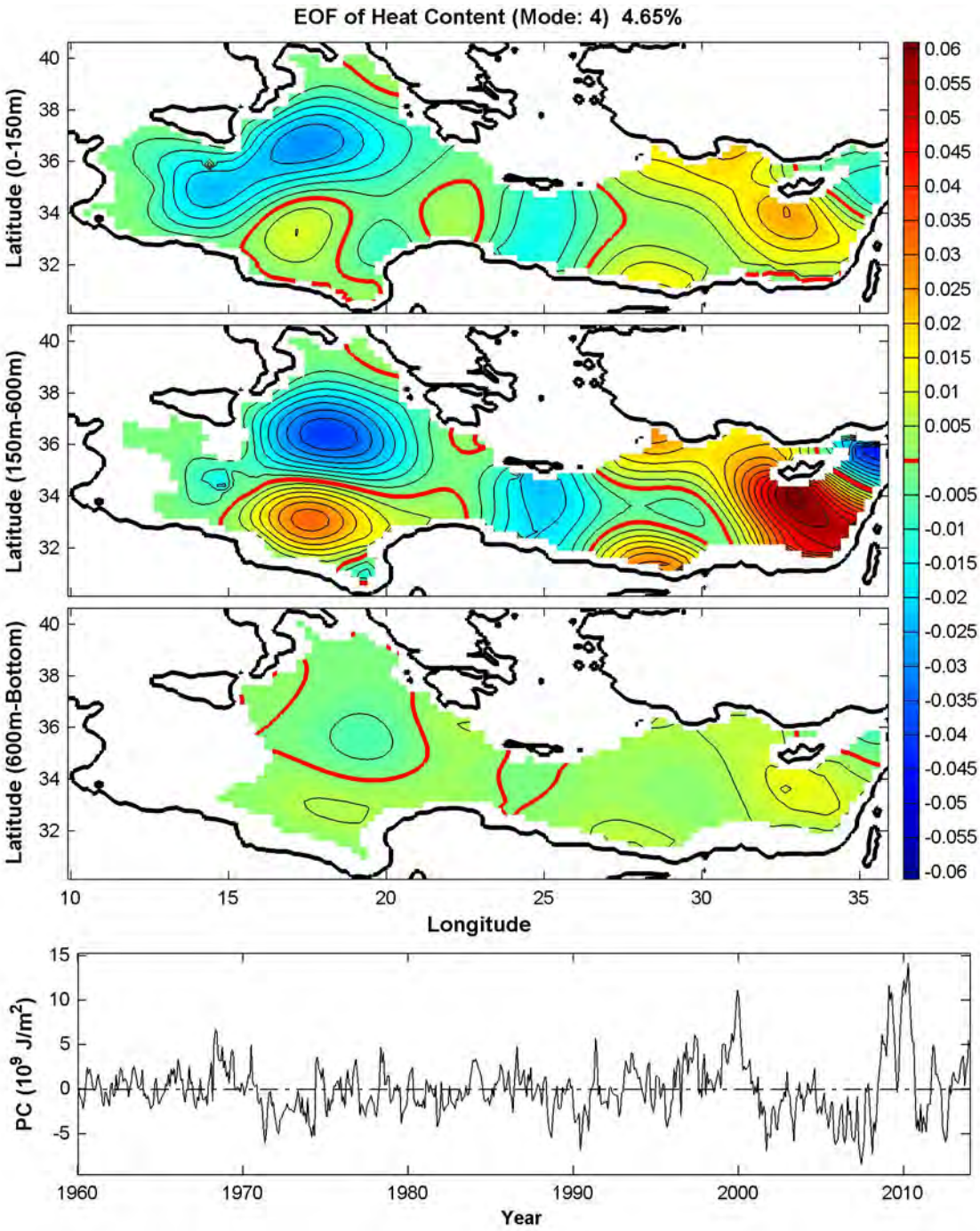
EOF of Heat Content (Mode: 4) 4.65%
Latitude (0-150m)
Latitude (150m-600m)
Latitude (600m-Bottom)
40
38
36
34
32
10
15
20
25
30
35
Longitude
0.06
0.055
0.05
0.045
0.04
0.035
0.03
0.025
0.02
0.015
0.01
0.005
-0.005
-0.01
-0.015
-0.02
-0.025
-0.03
-0.035
-0.04
-0.045
-0.05
-0.055
-0.06
PC (10^9 J/m^2)
15
10
5
0
-5
1960
1970
1980
1990
2000
2010
Year

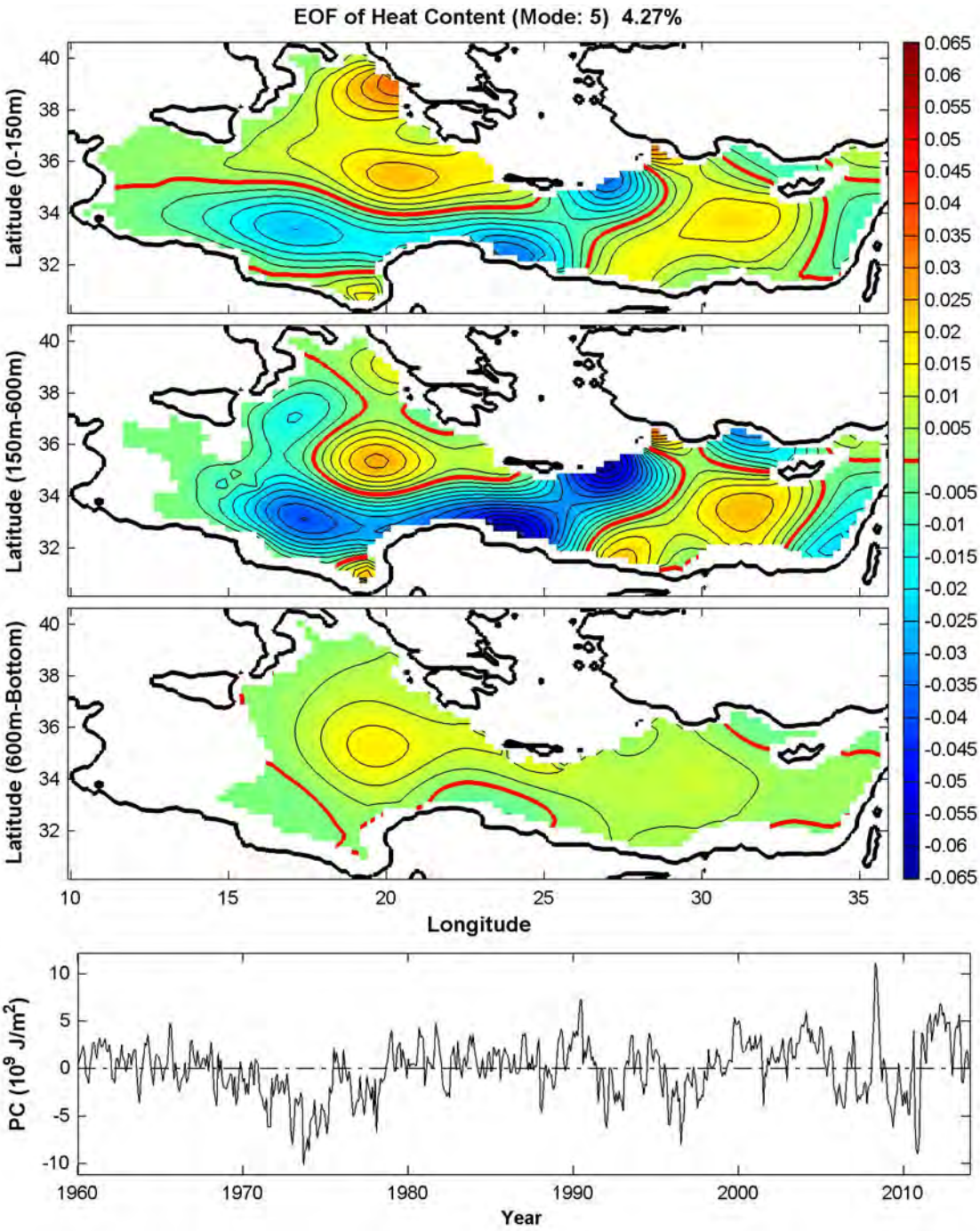
EOF of Heat Content (Mode: 5) 4.27%
Latitude (0-150m)
Latitude (150m-600m)
Latitude (600m-Bottom)
40
38
36
34
32
10
15
20
25
30
35
Longitude
0.065
0.06
0.055
0.05
0.045
0.04
0.035
0.03
0.025
0.02
0.015
0.01
0.005
-0.005
-0.01
-0.015
-0.02
-0.025
-0.03
-0.035
-0.04
-0.045
-0.05
-0.055
-0.06
-0.065
PC (10^9 J/m^2)
10
5
0
-5
-10
1960
1970
1980
1990
2000
2010
Year

THIS PAGE INTENTIONALLY LEFT BLANK

APPENDIX E. FIRST FIVE EOF MODES OF FRESHWATER CONTENT

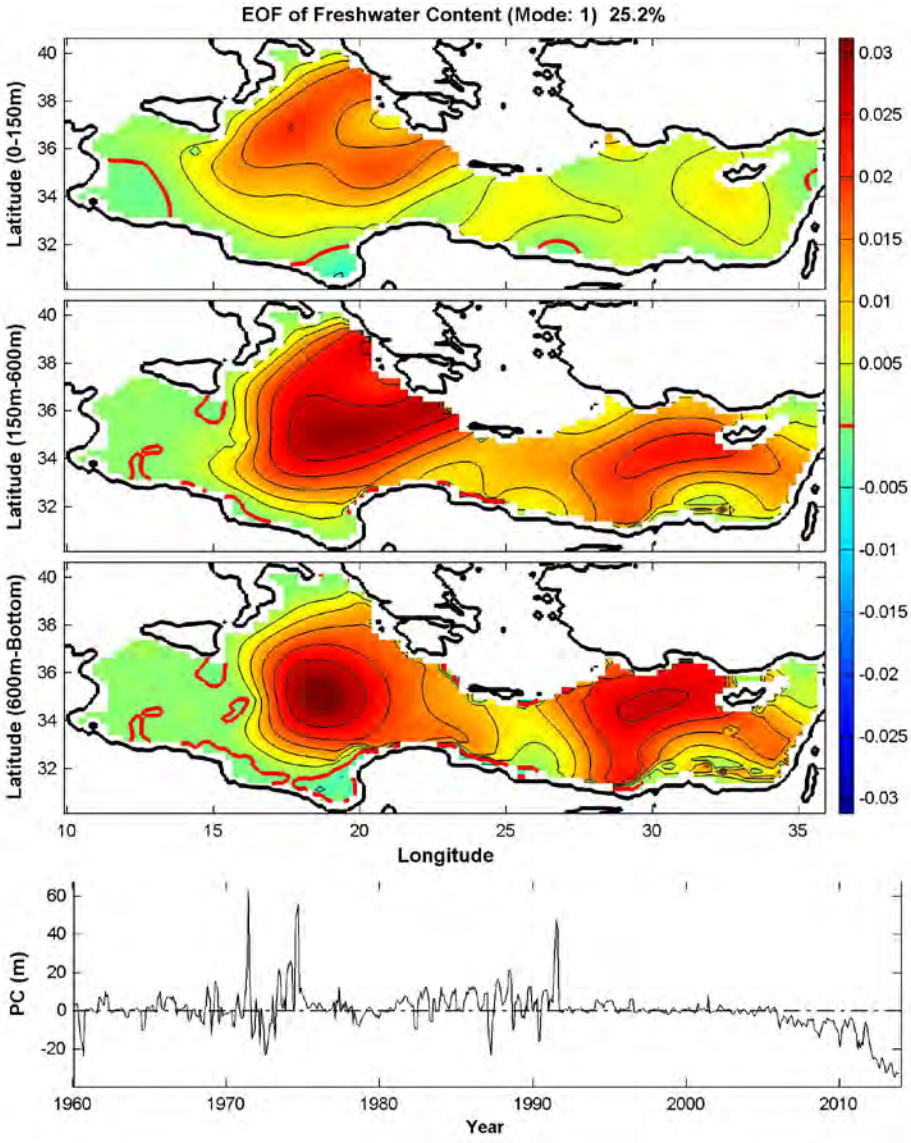

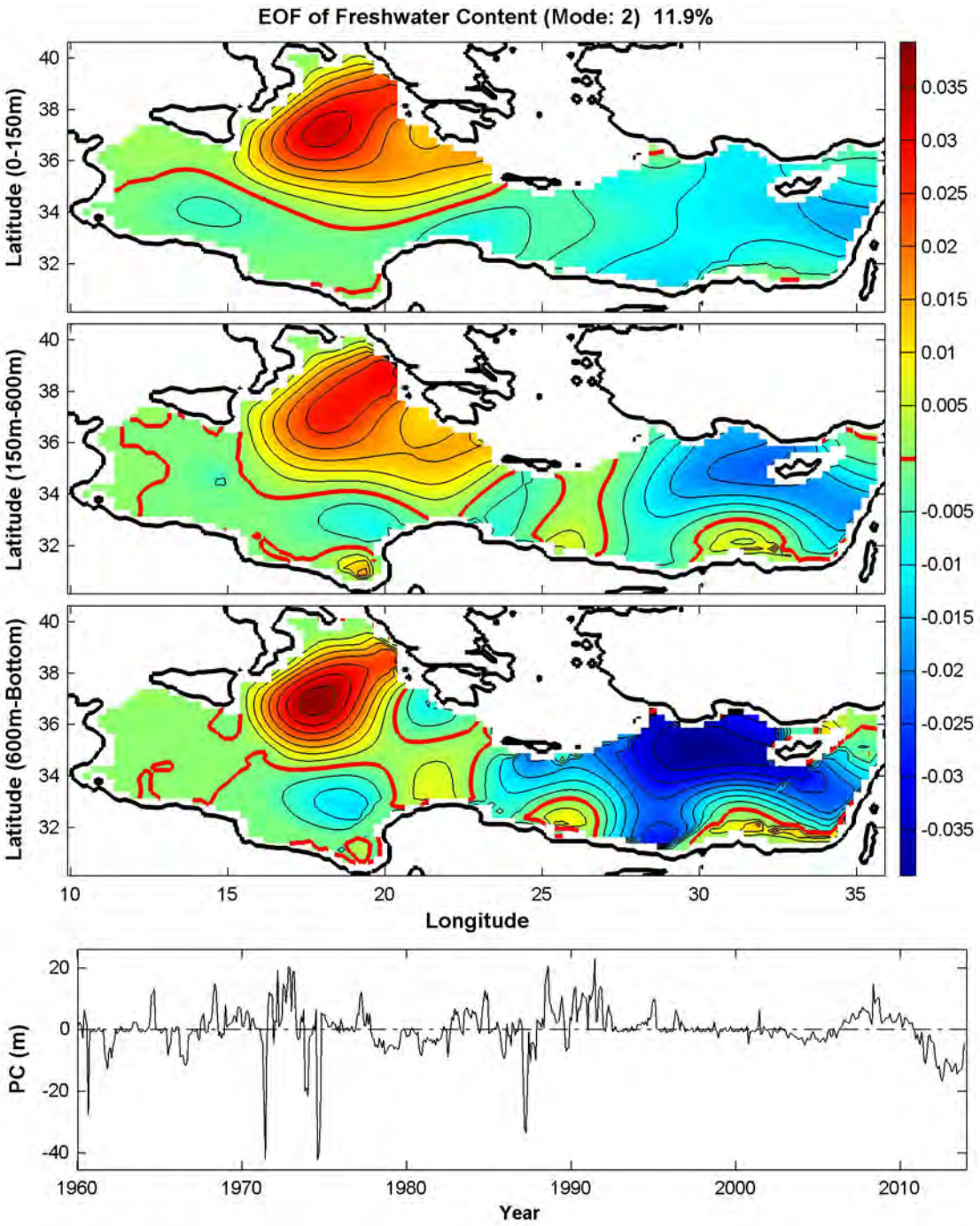
EOF of Freshwater Content (Mode: 2) 11.9%
Latitude (0-150m)
Latitude (150m-600m)
Latitude (600m-Bottom)
40
38
36
34
32
10
15
20
25
30
35
Longitude
0.035
0.03
0.025
0.02
0.015
0.01
0.005
-0.005
-0.01
-0.015
-0.02
-0.025
-0.03
-0.035
PC (m)
20
0
-20
-40
1960
1970
1980
1990
2000
2010
Year

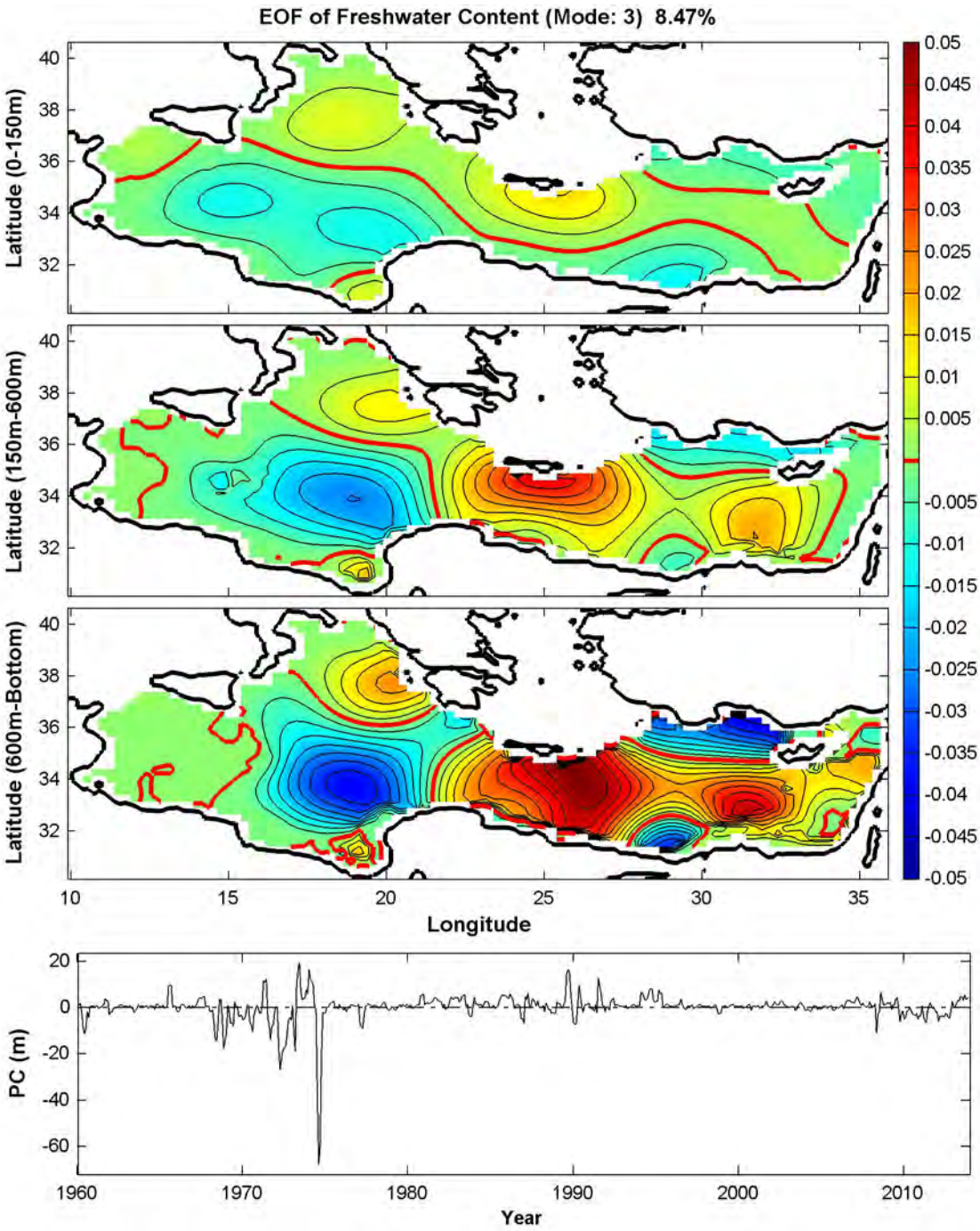
EOF of Freshwater Content (Mode: 3) 8.47%
Latitude (0-150m)
Latitude (150m-600m)
Latitude (600m-Bottom)
40
38
36
34
32
10
15
20
25
30
35
Longitude
0.05
0.045
0.04
0.035
0.03
0.025
0.02
0.015
0.01
0.005
-0.005
-0.01
-0.015
-0.02
-0.025
-0.03
-0.035
-0.04
-0.045
-0.05
PC (m)
20
0
-20
-40
-60
1960
1970
1980
1990
2000
2010
Year

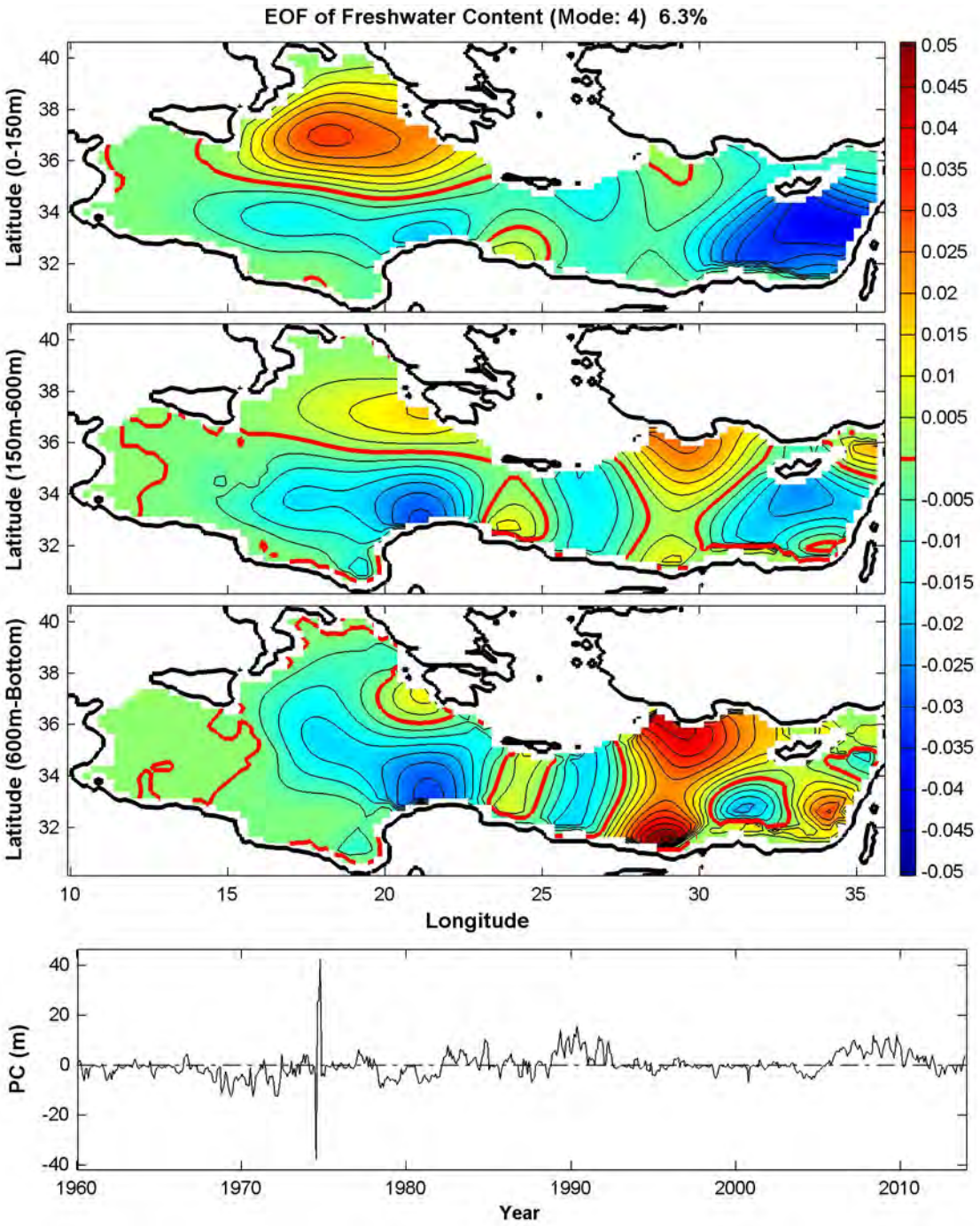
EOF of Freshwater Content (Mode: 4) 6.3%
Latitude (0-150m)
Latitude (150m-600m)
Latitude (600m-Bottom)
40
38
36
34
32
10
15
20
25
30
35
Longitude
0.05
0.045
0.04
0.035
0.03
0.025
0.02
0.015
0.01
0.005
-0.005
-0.01
-0.015
-0.02
-0.025
-0.03
-0.035
-0.04
-0.045
-0.05
PC (m)
40
20
0
-20
-40
1960
1970
1980
1990
2000
2010
Year

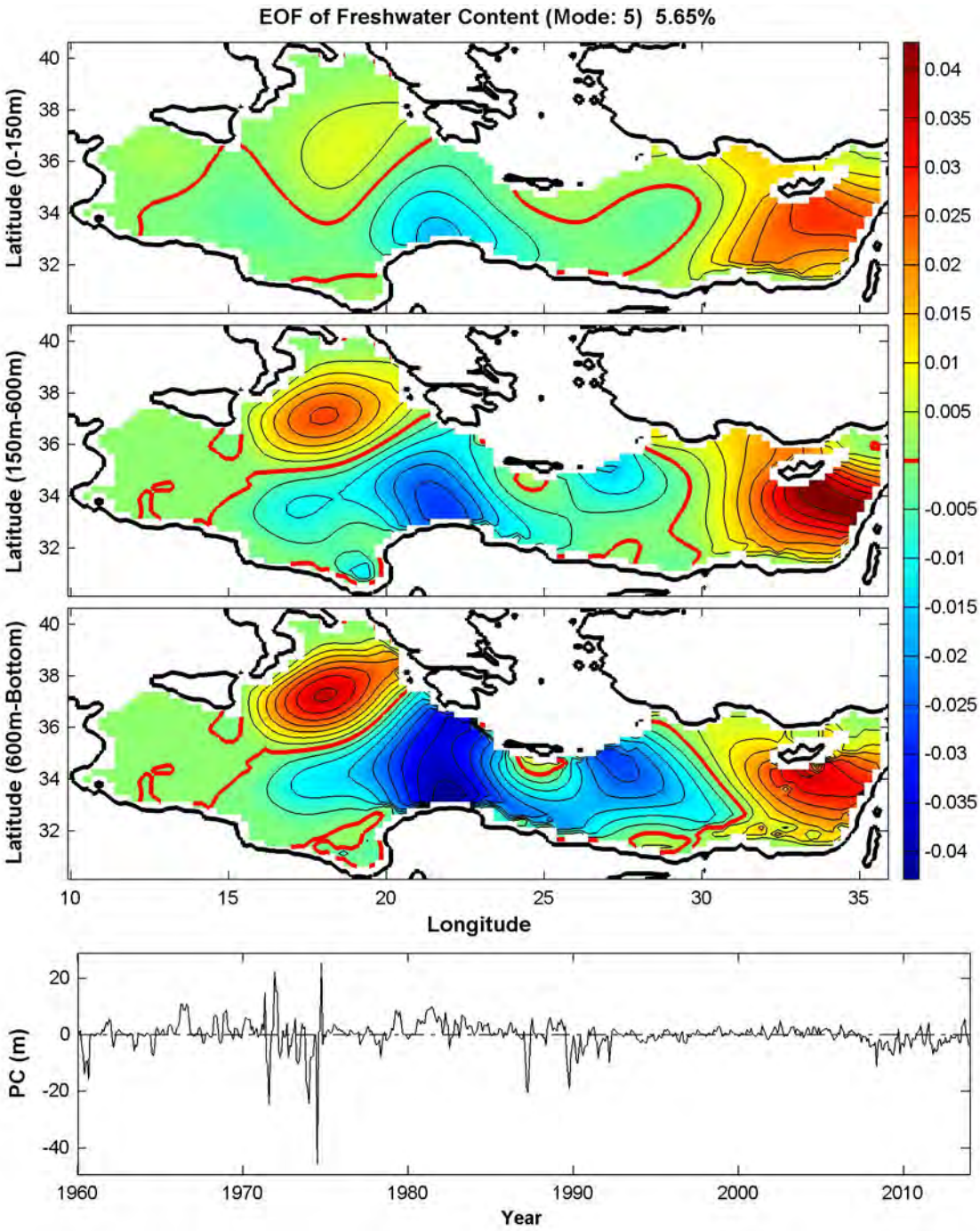
EOF of Freshwater Content (Mode: 5) 5.65%
Latitude (0-150m)
Latitude (150m-600m)
Latitude (600m-Bottom)
40
38
36
34
32
10
15
20
25
30
35
Longitude
0.04
0.035
0.03
0.025
0.02
0.015
0.01
0.005
-0.005
-0.01
-0.015
-0.02
-0.025
-0.03
-0.035
-0.04
PC (m)
20
0
-20
-40
1960
1970
1980
1990
2000
2010
Year

THIS PAGE INTENTIONALLY LEFT BLANK

LIST OF REFERENCES

Alhammoud, B., K. Béranger, L. Mortier, M. Crépon, and I. Dekeyser, 2005: Surface circulation of the Levantine Basin: comparison of model results with observations. *Prog.Oceanogr.,* **66**, 299–320.

Ancient Ports, 2015: Design waves for coastal structures on the Mediterranean coasts. Accessed 11 October 2015. [Available online at http://www.ancientportsantiques.com/ancient-port-structures/design-waves/]

Boxer, B., 2014: Mediterranean Sea. Accessed 14 September 2015. [Available online at http://www.britannica.com/place/Mediterranean-Sea]

Boyer, T. P., and Coauthors, 2013: World Ocean Database 2013. NOAA Atlas NESDIS 72, 209 pp, [Available online at http://www.nodc.noaa.gov/OC5/WOD13/ docwod13.html]

Chu, P. C., C. Fan, and W. Cai, 1998: P-vector inverse method evaluated using the Modular Ocean Model (MOM). *J.Oceanogr.,* **54**, 185–198.

Chu, P. C., R. T. Tokmakian, C. Fan, and L. C. Sun, 2015: Optimal Spectral Decomposition (OSD) for Ocean Data Assimilation. *J.Atmos.Ocean.Technol.,* **32**, 828–841.

Demirov, E. K., and N. Pinardi, 2007: On the relationship between the water mass pathways and eddy variability in the Western Mediterranean Sea. *Journal of Geophysical Research,* **112,** 1–21, doi:10.1029/2005JC003174.

Drago, A., R. Sorgente, and A. Olita, 2010: Sea temperature, salinity and total velocity climatological fields for the south-central Mediterranean Sea. GCP/RER/010/ITA/ MSM-TD-14. MedSudMed Technical Documents, 14, 35 pp.

Gaillard, P., and Coauthors, 2004: Wind and wave atlas of the Mediterranean Sea. Accessed 15 October 2015. [Available online at http://users.ntua.gr/mathan/pdf/ Pages_from%20_WIND_WAVE_ATLAS_MEDITERRANEAN_SEA_2004.pdf]

GRID-Arendal, 2013: Mediterranean Sea water masses: vertical distribution. Accessed 08 October 2015. [Available online at http://www.grida.no/graphicslib/detail/ mediterranean-sea-water-masses-vertical-distribution_d84b]

Group, T. M., and Coauthors, 2011: Marine ecosystems' responses to climatic and anthropogenic forcings in the Mediterranean. *Prog.Oceanogr.,* **91**, 97–166.

Heidorn, K. C., 2007: The Mediterranean: Birthplace of the Winds. Accessed 24 October 2015. [Available online at http://www.islandnet.com/~see/weather/almanac/arc2007/alm07mar.htm]

Integrated Ocean Observing System, 2014: Gliders/Autonomous Underwater Vehicles. Accessed 15 November 2015. [Available online at http://www.ioos.noaa.gov/glider/welcome.html]

Johnson, D., T. Boyer, H. Garcia, R. Locarnini, O. Baranova, and M. Zweng, 2013: *World Ocean Database 2013 User's Manual.* NODC Internal Report 22, 163 pp, [Available online at http://www.nodc.noaa.gov/OC5/WOD13/docwod13.html]

Kaihatu, J. M., R. A. Handler, G. O. Marmorino, and L. K. Shay, 1998: Empirical Orthogonal Function Analysis of Ocean Surface Currents Using Complex and Real-Vector Methods. *J.Atmos.Ocean.Technol.,* **15**, 927–941.

Krom, M., N. Kress, I. Berman-Frank, and E. Rahav, 2014: Past, Present and Future Patterns in the Nutrient Chemistry of the Eastern Mediterranean. *The Mediterranean Sea Its history and present challenges,* S. Goffredo, and Z. Dubinsky, Eds., Springer, 49–68.

Lascaratos, A., W. Roether, K. Nittis, and B. Klein, 1999: Recent changes in deep water formation and spreading in the eastern Mediterranean Sea: a review. *Prog.Oceanogr.,* **44**, 5–36.

Manca, B., M. Burca, A. Giorgetti, C. Coatanoan, M. Garcia, and A. Iona, 2004: Physical and biochemical averaged vertical profiles in the Mediterranean regions: an important tool to trace the climatology of water masses and to validate incoming data from operational oceanography. *J.Mar.Syst.,* **48**, 83–116.

Met Office, 2015: Winds of the world. Accessed 12 November 2015. [Available online at http://www.metoffice.gov.uk/learning/wind/wind-names]

National Geospatial-Intelligence Agency, 2011: North Atlantic Ocean and Adjacent Seas. Sailing Directions 140, 625 pp, [Available online at http://msi.nga.mil/MSISiteContent/StaticFiles/NAV_PUBS/SD/Pub140/Pub140bk.pdf]

The National Oceanography Centre Southampton, 2015: Mediterranean Outflow Sill. Accessed 04 October 2015. [Available online at http://www.euroargo-edu.org/img/med_outfl_sill.png]

Papadopoulou, K. N., V. Markantonatou, and C. J. Smith, 2011: Options for Delivering Ecosystem-based Marine Management. The Mediterranean Sea: Additional information on status of threatened ecological characteristics relevant to the Marine Strategy Framework Directive, 30 pp, [Available online at https://www.liverpool.ac.uk/media/livacuk/odemm/images/Mediterranean_Sea_Background.pdf]

Pinardi, N., E. Masetti, 2000: Variability of the large scale general circulation of the Mediterranean Sea from observations and modelling: a review. *Palaeogeogr., Palaeoclimatol., Palaeoecol.,* **158**, 153–173.

Robinson, A. R., W. G. Leslie, A. Theocharis, and A. Lascaratos, 2001: Mediterranean sea circulation. *Ocean Currents: A Derivative of the Encyclopedia of Ocean Sciences,* , 1689–1705, doi:10.1006/rwos.2001.0376.

Robinson, A. R., and Coauthors, 1992: General circulation of the Eastern Mediterranean. *Earth-Sci.Rev.,* **32**, 285–309.

Soto-Navarro, F. J., F. Criado-Aldeanueva, 2012: Model thermohaline trends in the Mediterranean Sea during the last years: a change with respect to the last decades? *The Scientific World Journal,* **2012**, 1–8, doi:10.1100/2012/365698.

Tanhua, T., D. Hainbucher, K. Schroeder, V. Cardin, M. Álvarez, and G. Civitarese, 2013: The Mediterranean Sea system: a review and an introduction to the special issue. *Ocean Science,* **9**, 789–803.

Tanabe, R., 2013: Mediterranean Sea. Accessed 22 August 2015. [Available online at http://www.newworldencyclopedia.org/ p/index.php?title=Mediterranean_Sea&oldid=971160]

Theocharis, A., M. Gacic, and H. Kontoyiannis, 1998: Physical and dynamical processes in the coastal and shelf areas of the Mediterranean. *The sea,* A. R. Robinson, K. H. Brink, Eds., John Wiley & Sons Inc., 863–887.

Università degli Studi di Pavia, 2005: The Mediterranean Sea. Accessed 02 September 2015. [Available online at http://www-3.unipv.it/cibra/edu_Mediterraneo_uk]

WeatherOnline, 2015: Etesian Winds. Accessed 12 November 2015. [Available online at http://www.weatheronline.co.uk/reports/wind/The-Etesian-Winds.htm]

WeatherOnline, 2015: Khamsin. Accessed 12 November 2015. [Available online at http://www.weatheronline.co.uk/reports/wind/The-Khamsin.htm]

Wikipedia contributors, 2015: Mediterranean Sea. Accessed 25 August 2015. [Available online at https://en.wikipedia.org/w/index.php?title= Mediterranean_Sea&oldid=695192772]

WorldAtlas, 2015: Map of the Mediterranean Sea. Accessed 24 August 2015. [Available online at http://www.worldatlas.com/aatlas/infopage/medsea.htm]

Zecchetto, S., F. De Biasio, 2007: Sea surface winds over the Mediterranean basin from satellite data (2000-04): Meso-and local-scale features on annual and seasonal time scales. *J. Appl. Meteor. Climatol.,* **46**, 814–827.

THIS PAGE INTENTIONALLY LEFT BLANK

INITIAL DISTRIBUTION LIST

1. Defense Technical Information Center
   Ft. Belvoir, Virginia

2. Dudley Knox Library
   Naval Postgraduate School
   Monterey, California